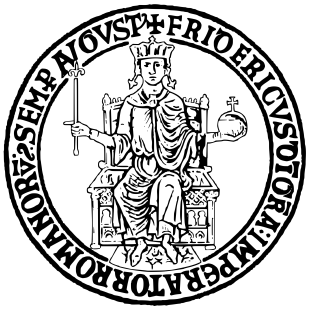

UNIVERSITY OF NAPLES FEDERICO II
DEPARTMENT OF INDUSTRIAL ENGINEERING
- MECHANIC AND ENERGETIC SECTION -

PH.D. SCHOOL IN INDUSTRIAL ENGINEERING –XXXVI CYCLE

The paths towards the decarbonisation of the transport sector: a multi-level analysis of electrified vehicles

Doctoral thesis

Ph.D. School Coordinator

Prof. Michele Grassi

Tutor

Prof. Alfredo Gimelli

Dr. Ing. Gabriele Di Blasio

Ing. Francesco De Nola

Ph.D. Candidate

Michele Pipicelli

To my family

II

Contents

Acknowledgment

I want to express my gratitude to several people that have provided me with immense technical and moral support throughout this project. I would like to thank my supervisors Prof. Alfredo Gimelli, Dr. Gabriele Di Blasio, and Eng. Francesco De Nola which gave me the opportunity to conduct my research at Institute of Sciences and Technologies for Sustainable Energy and Mobility (STEMS) giving intellectual freedom. I am particularly thankful for its mentoring and guidance in this PhD three-years journey to Dr. Gabriele Di Blasio. I would also like to thank all fellow colleagues at STEMS, in particular, Dr. Roberto Ianiello and Eng. Giuseppe Di Luca. Gratitude also to Teoresi Group which has contributed to fund the PhD, and to their team, and in particular Eng. Bernardo Sessa and Eng. Gianluca Toscano. I would like to acknowledge and give my warmest thanks to Prof. David Sedarksy which have given me the opportunity to spend a semester at Chalmers University of Technology, and all the people encountered at ECaPS, and in particular Prof. Lucien Koopmans, Mohammad Nikouei and my nakama Andreas "Andy" B. Ofner. Most importantly, I wish to extend thanks to my family, for their continuous support throughout all my life and for encouraging me to follow my dreams. A special merit to my brother Claudio, which between love and war, surely had a relevant role in my scientific journey. I thank Lucia for her unconditioned love, great patience, and for accompanying me on this path as well as in life.

Abstract

Climate change is a present and real problem on a global scale, which requires fast actions to mitigate it. Different solutions can help to achieve this objective, with the reduction of CO_2 as one of the most promising. Indeed, international policies have been proposed to address this issue, reducing the carbon intensity of modern technological society. Specifically, this work aims to analyze different vehicle technologies that can reduce the carbon footprint of the transport sector. Electrification, renewable liquid fuels, hydrogen, and driving automation systems are all technologies that can effectively contribute to higher energy efficiency and lower carbon emissions. Assessing all those technologies in a unique global and comprehensive study on the transport sector is somewhat complicated. For this reason, the work is structured in two main parts: the assessment of powertrain technology and the assessment of driving automation systems for different vehicle classes. Instead, the technology combinations are proposed to be analyzed with a specific case study. Regarding powertrains, the impact of different propulsion systems has been analyzed through a properly developed simulation framework evaluating different key performance indicators, including total cost of ownership, operational expenditures, wheel-to-wheel greenhouse gases, energy consumption, recharging time, and vehicle range. The analysis has involved passenger, light commercial, medium-duty, and heavy-duty vehicles. The methodology adopted has allowed us to define thresholds for fuel, electricity, and powertrain costs for which particular vehicular solutions offer better economic indicators. Sensitivity analysis on fuel and electricity emissions factors has allowed the definition of optimal powertrain for each scenario to decarbonize the fleets efficiently. Regarding driving automation systems, autonomous vehicles are promoted to reduce road accidents and improve road safety with a relevant impact on society. Besides social aspects, the driving automation system, exploiting the data gathered by their sensor and intelligent infrastructures, can be used to improve

the energy management of the vehicles. This optimization can be made at the single vehicle or fleet levels. Many works have addressed the potential benefits of driving automation systems on vehicle energy efficiency. However, those works usually neglect the energy consumption of the DAS system, focusing only on the powertrain. Through statistical methods and a case study, this work evaluates the net energy efficiency of autonomous vehicles compared to human-driving operated twin vehicles. Statistical results show that for light-duty vehicles, the energy demands of the driving automation system are relevant, and concur to a net worsening of the vehicle energy consumption. The scenario changes, looking to more energy-demanding vehicles, such as medium and heavy-duty trucks, for which no or slight improvement can be expected, respectively. A detailed case studio analysis with a detailed vehicle model has also partially confirmed the light-duty results.

List of Figures

List of Tables

Acronym list

ADAS	Advanced Driving Assistance System
AEC	Automotive Electronics Council
AFF	Alternative Fuel Feeding
ATS	After Treatment System
ASIC	Application Specific Integrated Circuit
ASIL	Automotive Safety Integrity Level
AV	Autonomous Vehicle
BaP	Battery Pack
BEV	Battery Electric Vehicle
BMS	Battery management system
BoP	Balance of Plant
BP	Bipolar Plate
CAN	Controller Area Network
CAV	Connected and Autonomous Vehicle
CCD	Charge-Coupled Device
CH2	Compressed Hydrogen Systems
CI	Compression Ignition
CL	Catalyst Layer
CMOS	Complementary Metal Oxide Semiconductor

CN Cetane Number

CNG Compressed Natural Gas

COP21 Conference of parties

CPU Central Processing Units

DAS Drive Autonomous Systems

DC Direct Current

DoD Deep-of-Discharge

DEA Dead-Endend Anode

DI Direct Injection

DOA Direction Of Arrival

DSP Digital Signal Processor

DSRC Dedicated Short Range Communication

EDLC Electrochemical double layer capaciter

EM Electric Motor

ESS Energy Storage System

EU Europe Union

EV Electric vehicle

FAME Fatty Acid Methyl Ester

FC Fuel Cell

FCEV Fuel Cell Eletric Vehicle

FCHEV Fuel Cell Hybrid Electric Vehicle

FFV Flex-Fuel Vehicles

FMCW Frequency Modulated Continuous Wave

FoV Field of View

FPGA Field Programmable Gate Array

GaN Gallium Nitride

GDL Gas Diffusion Layer

GHG Green Houses Gas

GLOSA Green Light Optimal Speed Advisory

GMSL Gigabit Multimedia Serial Link

GNSS Global Navigation Satellite System

GPS Global Positioning System

GPU Graphical Processing Unit

GWP Global Warming Potential

H2ICEV H_2-fueled Internal Combustion Engine Vehicles

HD Heavy Duty

HDV Heavy Duty Vehicle

HESS Hybrid Energy Storage Systems

HEV Hybrid Electric Vehicle

HiL Hardware in the Loop

HPC High Performance Computing

HVO Hydrotreated Vegetable Oils

ICCT International Council on Clean Transportation

ICE Internal Combustion Engine

ICEV Internal Combustion Engine Vehicle

ICT Information Comunication Technology

IEA International Energy Agency

IMU Inertial Measurement Unit

LCA Life Cycle Assessment

LCO Lithium Cobalt Oxide

LCOH Levelized Cost Of Hydrogen

LCV Light Commercial Vehicle

LD Light Duty

LDV Light Duty Vehicle

LH2 Liquid Hydrogen

LFP Lithium Iron Phosphate

LHV Lower Heating Values

LIDAR LIght Detection And Ranging

LMO Lithium Manganese Oxide

LNG Liquefied Natural Gas

LPG Liquefied Petroleum Gas

LQR Linear Quadratic Regulator

LRR Long Range Radar

KPI Key Performance Indicator

MDV Medium Duty Vehicle

MEA Membrane Electrode Assembly

MEMS Micro Electro-Mechanical Systems

MIMO Multi Input Multi Output

MMIC Monolithic Microwave Integrated Circuit

MPC Model Predictive Control

MPLW Maximum Permissible Laden Weight

MRR Medium Range Radar

MSRP Manufacturer Suggested Retail Price

MTBF Mean Time Between Failures

NCA Lithium Nickel Cobalt Aluminum Oxide

NExBTL Next Generation Bio to Liquid

NG Natural Gas

NHTSA National Highway Traffic Safety Administration

NIR Near InfraRed

NMC Lithium Nickel Manganese Cobalt Oxide

OCDMA Optical Code Division Multiple Access

OCV Open Circuit Voltage

OEM Original Equipment Manufacturer

OODA Observe Orient Decide and Act

OPA Optical Phased Array

ORR Oxygen Reduction Reaction

PCD Point Cloud Data

PEM Polymer Electrolyte Membrane

PEMFC Polymer Electrolyte Membrane Fuel Cell

PM Particular Matter

PFAD Palm Fatty Acid Distillate

PFI Port Fuel Injection

PGM Platinum Group Material

PID Proportional Integral Derivative

PMSM Permanent Magnet Synchronous Machine

PTFE Polytetrafluoroethylene

PU Processing Unit

RADAR RAdio Detection And Ranging

RM Reluctance Motor

SAE Society of Automotive Engineers

SC Supercapacitors

SCR Selective Catalytic Reduction

SDG Sustainable development goals

SI Spark Ignition

SiC Silicon Carbide

SLAM Simultaneous Localization And Mapping

SMR Steam Methane Reforming

SNR Signal to Noise Ratio

SoC State of Charge

SoH State of Health

SONAR Sound detection and Ranging

STP Standard Temperature and pressure

SRM Switching Reluctance Motor

SRR Short Range Radar

SWIR Short-Wave InfraRed

TCO Total Cost of Ownership

ToF Time of Flight

TOPS Trillion of Operations Per Second

TRL Technological Readiness Level

TTW Tank to Wheel

UOP Universal Oil Products

US-DOE United States Department of Energy

UVW Unladen Vehicle Weight

V2G Vehicle to Grid

V2I Vehicle to Infrastructure

V2N Vehicle to Network

V2P Vehicle to Pedestrian

V2V Vehicle to Vehicle

V2x Vehicle to Everything

VPI Vehicle Performance Indicator

VECTO Vehicle Energy Consumption calculation TOol

WBG Wide BandGap

WLTC Worldwide harmonized Light vehicles Test Cycle

WLTP Worldwide harmonized Light-duty Test Procedures

WTW Well-to-Wheel

Candidate's declaration

I hereby declare that this thesis submitted to obtain the academic degree of Philosophiæ Doctor (Ph.D.) in Ingegneria Industriale is my own unaided work, that have not used other than the sources indicated, and that all direct and indirect sources are acknowledged as references. Parts of this dissertation have been published in international journals and/or conference proceedings.
Napoli, January 31, 2024

Chapter 1

Introduction

Background

The anthropogenic environmental impact and the consequent climate change are among the most relevant issues of the XXI century worldwide. Pollutant and greenhouse gas emissions can be distinguished. The first is usually more relevant on a local scale (towns and cities), while the latter, due to their long life in the atmosphere, produces changes on a global scale (Earth). Pollutants have a direct effect on the air quality and the health and wellness state of living beings. Instead, the impact of greenhouse gases on health is indirect and linked to environmental changes and extreme natural events. Nowadays, the main attention is directed toward the reduction of carbon emissions to achieve the net zero goal (i.e., the emitted carbon emissions are compensated for by removing the same quantity from the atmosphere). Many countries have set carbon neutrality targets by 2050, except China, responsible for about 25% of worldwide carbon emissions, which has set its objective by 2060. Energy production is the main responsible for worldwide carbon emissions ($\approx 40\%$), followed by industry ($\approx 25\%$) and the transport sector ($\approx 22\%$). This work focuses on the road transport. Research and regulatory efforts have generated innovation in recent years, combining engine and fuel technologies and After Treatment System (ATS) improvements, substantially reducing vehicle pollutants emissions. Euro VId and future EURO VII vehicles are considered to have ultra-low emissions standards, ensuring low environmental impact. For Light Duty (LD) sector, including passenger cars and vans, the Fit for 55 packages have set that all the new vehicles from 2035 should have zero emissions. For Heavy Duty (HD) sector, a target reduction of 15% and 30% was set by 2025 and 2030,

respectively, compared to the 2019-2020 reference period. To reach those targets effectively, all the technology that can influence the transport sector should be analyzed, not only powertrains. A major trend in the transport sector is the development of driving automation systems, looking toward fully autonomous vehicles. The main motivations behind autonomous vehicles are related to improving safety, as road accidents cause about 1.2e6 deaths per year, with human errors as the primary cause. Besides, additional social benefits arise, such as ensuring ease of movement for the elderly or people with reduced mobility. Moreover, autonomous systems open the possibility of novel mobility scenarios, such as mobility as a service and robo-taxies. This can potentially reduce the number of vehicles in the circulating fleets, maximizing their usage and lowering the environmental impact.

Motivation and Objectives

Decarbonization is a complex research theme that requires holistic assessment. Regarding the transport sector, this work presents a technology-neutral analysis of the possible powertrains and driving automation systems. It is important to highlight that the optimal solutions depend on various geographical, political and economic factors (available feedstocks, profitability, vehicle usage, policies,...). The search for optimal solution within a particular scenario requires reliable methodologies able to estimate a vehicle performance by analyzing various Key Performance Indicators (KPIs). To this aim, a simulation framework has been developed and presented in the following, to analyze various powertrain solutions for different road vehicle classes. This work is based on bibliographic searches, numerical analysis and experimental activities. In this way, a ”multi-level” analysis has been proposed involving different methods and looking at different aspects of vehicles and their decarbonization. The combination of different techniques has been required by the complexity and extension of the research theme. The literature study has allowed to delineate the major research lines, define a picture of the state-of-art technology, and create an extensive dataset, employed in the following work phases. The main activity core is represented by numerical modelling, employing ad-hoc developed codes. Then, experimental activities has allowed to better tune the models, and check the consistency of the results.

Specifically, the main objectives of this work can be summarized as in the following.

I. Assessment of the most promising Green Houses Gass (GHGs) reduction strategies as

fuels, powertrains, and vehicle technologies

II. Development of a method for the comparison of different powertrain architectures and vehicle classes

III. Assessment of driving automation systems in terms of vehicle efficiency

Thesis outline and short summary

To achieve the objectives defined in the previous section, the study and the thesis work have been organized as schematically reported in figure 1.1.

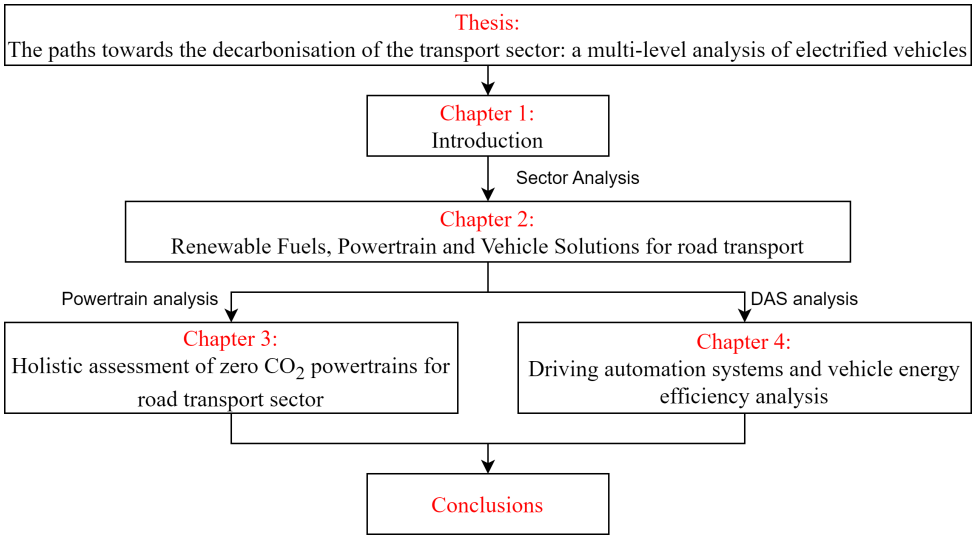

Figure 1.1: Thesis outline.

In particular, Chapter 2 contains the results of a comprehensive study on the decarbonization of the transport sector, namely renewable fuels, powertrain architectures and vehicle solutions. More in detail, chapter 2 analyzes the ever-demanding regulations on CO_2 emissions, which require efforts from a technology and infrastructure point of view. In this context renewable fuels can significantly reduce the environmental impact on the transport sector. Hydrogen fuel is an interesting solution compatible with both Internal Combustion Engine (ICE) and Fuel Cell (FC) based vehicles. A broader powertrain portfolio will likely be available in the next future to exploit optimally available energy vectors (electricity, hydrogen, etc.) and depending on the vehicle application domain. Hydrogen-based powertrains can play an important role. Additionally, vehicle technologies toward a greater connectivity and autonomy are the major trends.

In chapter 3, a proper methodology was developed to assess various powertrain options, all of which comply with future regulations. The analysis is based on data gathered from the extensive literature study and activities conducted in cooperation with industrial partners. The methodology allows assessing various performance indicators such as Total Cost of Ownership (TCO), GHGs emissions, energy consumption and recharging times. A comprehensive analysis of light, medium and heavy-duty vehicles showed that the optimal solutions in each application domain strongly depend on vehicle class and mission profile. Chapter 4 deals with the impact of driving automation systems on vehicle efficiency. Hardware architecture, data processing, and management solutions have been handled with the scope of improving vehicle energy efficiency. Extensive datasets have been generated, containing quantitative and qualitative information regarding sensors, computing units, and power consumption. The data were elaborated with proper statistical distributions and used as input in a Monte Carlo simulation to estimate Vehicle energy efficiency. The main outcomes are that, autonomous vehicles consumption improvements are not obvious compared to conventional human-driven vehicles. The conclusions summarize the main outcomes of the study and offer recommendations for further improvements.

Chapter 2

Renewable Fuels, Powertrain and Vehicle Solutions for road transport

The transport sector is undergoing a renewal process involving various actors, such as academics, research institutions, industry and customers. The process is complex as it depends on political, economic, technological and social aspects. This chapter discusses the major trend of this renewal process and mainly focuses on the technological aspects within the regulatory framework. In particular, section 2.1 deals with decarbonization policies and rules, section 2.2 discusses renewable fuels, and section 2.3 discusses their application in future ICE-based powertrains and alternative powertrains. In the end, section 2.4 presents an overview of vehicular technologies.

2.1 Trends in regulations toward the net zero carbon emission in 2050

At the international level, the United Nations Member States in 2015 adopted the 2030 Agenda for Sustainable Development, defining 17 Sustainable development goals (SDG) facing with main aspects to ensure a future better global and shared world for the whole humankind. In this context, in the same year, the Paris Agreement, the main legally binding international treaty to fight climate change, was adopted by 196 Parties at the United Nation Climate Change Conference Conference of parties (COP21) and ratified in the 2016. The main goal defined by the

COP21 is to limit the global average temperature increase to 2 °C above pre-industrial levels. To this aim, it is required to reach the peak of greenhouse gas emissions before 2025 and reduce it by at least of about 43 % by 2030. Huge investment and effort is needed to develop viable strategies and technical solutions. Successively, Europe Union (EU) in 2019 with the Green Deal has posed the net-zero goal by 2050. An overview of the country with different net-zero goal time frames is reported in table 2.1. In this context, novel technologies can help to improve

Year	**Country**
2030	Uruguay
2035	Finland
2040	Austria, Iceland
2045	Germany, Sweden
2050	Globally shared goal
2060	China, Kazakhstan, Ucraine
$>$ 2050	Australia, Singapore

Table 2.1: Overview of the net zero goals

conversion process efficiencies reducing the primary energy needs, and contribute to increase the renewable share. More specifically, for the transport sector, the US set an CO_2 reduction goal in the range 80% and 100% by 2050. The EU regulation 2019/631 set an average CO_2 reduction of 37.5% for passenger cars (w.r.t 91 g/km in 2021) and 31% for vans (w.r.t 147 g/km in 2021) by 2030. In 2035, all new vehicles should ensure a reduction of 100 % for both passenger cars and vans. However, there are some exceptions for manufacturers producing less than 10000 vehicles (by 2029) or 1000 (by 2030 and after). Then, the EU Regulation 2019/1242, for heavy-duty vehicles, set fleet-level limits on average CO_2 emission. In particular, it set a 15% limit from 2025 and a 30% from 2030 with respect to a 1-year reference period (from 1 July 2019 to 30 June 2020). In 2020 the "Fit for 55", was presented as a package of regulations to achieve a 55% reduction of EU greenhouse gases emissions. In 2021 a proposal for stricter emission limits was proposed for passenger cars (-25% by 2025, -45% by 2027 and -75% by 2030) and vans (-20% by 2025, -40% by 2027 and -70% by 2030). In 2023 the "Fit for 55" regulation posed a -55% and -50% reduction target for cars and vans respectively. New CO_2

emission standards for heavy duty vehicles are under discussion, proposing reductions of 45% by 2030, 65% by 2035 and 90% by 2040. Therefore, the need to urgently develop new powertrain solutions, energy carriers and storage to meet those targets. Even if electric powertrains will surely play a major role in the following years, optimal vehicle and powertrain solutions strongly depend on the end user application. A technology-neutral approach to face the problem should be adopted to define the application domain in which a particular solution prevails over others.

2.2 Trends in renewable fuels

The transition should consider using fuels based on renewable feedstocks, which are capable of reducing up to 80-90% the carbon footprint on Well-to-Wheel (WTW) basis. Therefore, this section presents a comprehensive discussion of the most attractive renewable fuels. The main focus is on alcohol, HVO and hydrogen fuels. The possible production pathways and feedstocks are various and the CO_2 impact can vary significantly. Different generations of biofuels are distinguished based on production methods, feedstocks and resource requirements. Figure 2.1 shows a raw classification over time. Currently, 2nd generation renewable fuels, such as the HVO, bio-methanol and bio-ethanol, are commercially available, while the 3rd and 4th generation are actually under investigation.

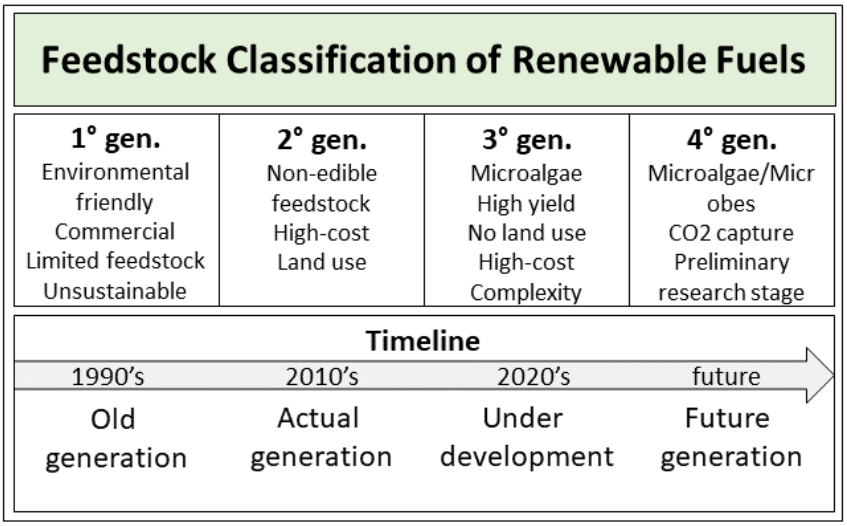

Figure 2.1: Overview on renewable biofuels generations.

Another critical factor for fuels is the energy density for their application on vehicles. Figure 2.2 compares specific energy on both volume and mass bases. For the sake of comparison, also energy densities of batteries have been included.

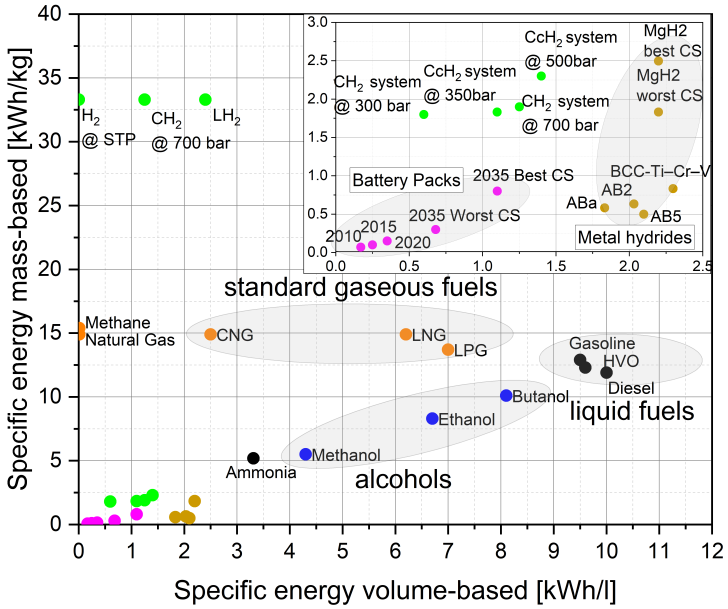

Figure 2.2: Overview on specific energy, on volume and mass basis, of different fuels

Conventional fossil fuels such as gasoline and diesel, or 2nd generation fuels HVO, offer the best trade-off, and around 44 MJ/kg and 36 MJ/dm^3. Alcohols have a lower energy density, while hydrogen offers the highest Lower Heating Values (LHV) (33.3 kWh/kg or 120 MJ/kg), but the lowest volume-based specific energy. In comparison to other gaseous fuels as Natural Gas (NG) and Liquefied Petroleum Gas (LPG), compression and liquefaction stages are more energy-demanding, requiring higher pressures (350 or 700 bar) and lower temperatures (about 20K). For the sake of comparison, the LPG requires lower pressure (approximately 2-8 bar) to be liquefied, while Compressed Natural Gas (CNG) is stored at around 220 bar, and Liquefied Natural Gas (LNG) at 110 K. The following subsections deepen the discussion of alcohols, HVO and hydrogen regarding characteristics and applications, highlighting main pros and cons.

2.2.1 Alcohols

Alcohol fuels can be produced from different feedstocks and pathways and are suitable for use in internal combustion engines. They are characterized by a lower carbon content, as for

methanol (C1) and ethanol (C2). In Table 2.2 are reported the alcohols properties and compared to the conventional diesel and gasoline fuels.

Property	**Diesel**	**Gasoline**	**Methanol**	**Ethanol**
Research Octane Number [-]	n/a	≥ 95	107-109	108-109
Cetane Number [-]	≥ 51	8-14	3.8-5	5-8
Molar mass [g/mol]	≈ 170	≈ 110	32	46.1
Carbon Number [-]	12-20	4-12	1	2
H/C [-]	1.8	1.9	4.0	3.0
O/C [-]	0	0	1	0.5
Lower Heating Value [Mj/kg]	43.0	42.6	20.0	27.0
Stochiometric Air-Fuel ratio	14.5	14.6	6.4	9.0
Viscosity (@40 °C) [cSt]	2.72	0.6	0.58	1.13
Density (@15 °C) [kg/m^3]	820-845	720-775	796	794
Heat of Vaporization [kJ/kg]	270	307	1160	920
Specific CO_2 emissions [g/MJ]	72.2	75.1	68.8	70.7

Table 2.2: Alcohols fuel properties. Data source: [1–6]

The hydroxyl group makes alcohol fuels, especially the short-chained ones, hydrophilic and give a dipole moment at their molecular structures [7]. The polarity generates a strong inter-molecular hydrogen bond raising the boiling point and the heat of vaporization H_{vap} (about 3-4 times higher than fossil fuels, see Table 2.2). Then, the miscibility characteristics with strong molecular polarity substances, such as water [8] rise. The higher heat of vaporization promotes the cooling effect of the air-fuel mixture and then of the in-cylinder temperature [9]. The cooling effect can in Port Fuel Injection (PFI) engine lead to an increase of volumetric efficiency. The presence of the carbon–oxygen bond tends to reduce the LHV, compared to the corresponding alkanes (e.g., 20 MJ/kg of methanol respect to 50 MJ/kg of methane), with a consequence raise of the fuel consumption [10]. The presence of oxygen lowers the stoichiometric air-to-fuel ratio, improve the combustion, and likely improve the engine global efficiency [11].

Due to their high-octane number rating (about 108 for both methanol and ethanol), both ethanol and methanol are well suited for Spark Ignition (SI) engines [12]. For a reliable and

effective application of alcohols in engines, safety, toxicity, lubricity, storage, and distribution characteristics should also be considered.

As the heat of vaporization (H_{vap}) of alcohols is slightly higher than conventional fuels, it strongly affects the engine cold start phase.

The lower emission factor of alcohols , see Table 2.2, leads to additional $_2$ benefits on well-to-wheel basis compared to the gasoline baseline. Regarding engine performances, benefits in efficiency can be obtained while on HC, CO and NOx trends are not obvious as they depend on various engine configuration and calibration factors.

Nowadays, alcohol fuels are blended with gasoline, and rarely with diesel fuels. For the commercial gasoline fuel, the directive 2009/30/EC and the EN 288 regulation limit alcohol blending volume to 5 and 10%, respectively. Moreover, they also limit to 3.7% v/v the oxygen content and this is to guarantee the maximum fuel compatibility for as many cars as possible. The above mentioned directive and regulation do not treat alcohol and oxygen limits in diesel rather they report for maximum level of biofuel (e.g. Fatty Acid Methyl Ester (FAME) up to 7% v/v in diesel), and this is justified by the lower interest in using diesel in the future. The most commercialized gasoline-ethanol blend is the E10, characterized by 10% ethanol and 90% gasoline on a volume basis. It is commonly used in the US [13], and similarly, the EU Directive 2009/30/EC limit the ethanol fraction in gasoline to 10% v/v. Limited fractions do not require engine modifications, while neat ethanol requires specific materials to avoid corrosion. In this regard, Flex-Fuel Vehicles (FFV) are usually capable to run with ethanol-gasoline or methanol-gasoline blends. Brazil and the USA have the greatest number of ethanol-gasoline FFV, while experimentation in California are being carried out on M85 FFV.

In merit to the life cycle assessment of green house gases emissions, the data gathered are reported in Figure 2.3.

The figure summarizes the CO_2 values for methanol and ethanol compared to conventional fuels. Mean values (square symbol) with standard deviation bars are reported. The methanol shows an higher deviation since its values strongly relate to the feedstock and production process (coal, biomasses, etc.). The highest value, $\approx 250 gCO_2/MJ$, is for methanol produced from coal. Thus, attention should be posed on the entire production path, rather then its use only. Gasoline and diesel production processes are more standardized (lower variability). It can be

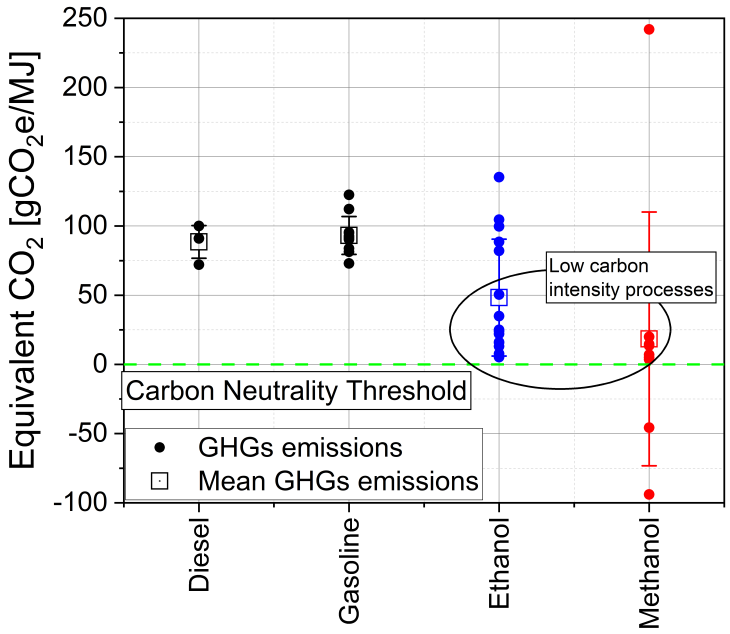

Figure 2.3: Equivalent CO_2 on Life Cycle Assesment for alcohols and fossil fuels. Data source: [14–27]

drawn that, alcohol produced from renewable feedstock, can drastically reduce the Well-To-Wheel CO_2, and in the range 25-75% compared to fossil fuels.

2.2.2 Hydrotreated Vegetable Oils

The term HVO emerged in the last decade when only vegetable oils (e.g. rapeseed, soybean, and corn oil) were used as feedstocks. Nowadays, non-edible feedstocks are preferred and mandatory for HVO production, as industrial waste (tall oil and fats) used cooking oils. It is common to identify HVO as "renewable diesel" and/or "green diesel". Several petrol companies are involved in HVO production around the world, such as Universal Oil Products (UOP)/Eni (UK, Italy), Neste Oil (Finland), Syntroleum (United States), SK energy (Korea), ConocoPhillips (United States, Ireland), and Nippon Oil (Japan), and they use different commercial name, e.g. the Next Generation Bio to Liquid (NExBTL) by Neste Oil Corporation [28], or "Green Diesel" by UOP/Eni Ecofining.

As a final product, HVO can be used as pure or blended in diesel and is fully compatible with modern Compression Ignition (CI) engines due to its characteristics. As paraffinic fuel, HVO

meets the EN 15940:2016 standard. For HVO-diesel blend, the final composition have to meet the diesel fuel regulations, such as EN590 and ASTM D975. Blend of up to 30% of HVO can meet the EN 590 requirements [29]. Since 2011, with an update of ASTM D7566-14, the HVO has also been approved for the aviation sector, allowing up to 50% of HVO in conventional jet fuel (ETIP Bioenergy—European Technology and Innovation Platform 2020). It demonstrates the potential of HVO also in the non-road transport sector.

Table 2.3 depicts the main characteristic of HVO compared to conventional diesel fuel. From a chemical point of view, the HVO is a bio-based liquid fuel composed mainly of paraffin and ISO-paraffin in the range C15–C18 and is free of sulfur and aromatic compounds, precursors of soot [30].

Property	**Diesel**	**HVO**
Cetane Number	≥ 51	75
Molar mass [g/mol]	≈ 170	≈ 225
Carbon number range [-]	12-20	15-18
H/C [-]	1.8	2.17
O/C [-]	0	0
Lower Heating Value [MJ/kg]	43.0	44.35
Stochiometric Air-Fuel Ratio [-]	14.5	15.2
Viscosity (@40 °C) [cSt]	2.72	2-4.5
Density (@15 °C) [kg/m^3]	820-845	770-795
Aromatics [%]	23	0
Sulfur content [mg/kg]	6.5	¡5

Table 2.3: HVO properties. Source data: [2, 5, 31]

The increased amount of paraffinic components in HVO fuel and the absence of aromatics lead to a high Cetane Number (CN), 75 versus 51 of diesel, as indicator of a superior fuel ignition quality [32]. In addition, HVO has high oxidation stability (no chemical oxygen), resulting in excellent storage behavior and similar to standard diesel and better than B7 diesel with FAME [33].

The lower boiling point promotes better evaporation of HVO, a reduced spray liquid length

[34], and then lower Particular Matter (PM).HVO has a higher H/C ratio, an higher LHV but lower density, and therefore characterized by a lower volumetric energy content.

The lubricity of HVO is at the limit of regulated interval ($< 460\mu m$), which assure adequate lubrication of the fuel injection system components [35]. Material compatibility is similar to fossil diesel and requires no particular attention [36].

HVO fuel has the potential to become an important player in the near future to support the transition timeframe toward carbon-neutral fuels in the transport sector. In internal engine application, generally, no differences in spray evolution are observed to diesel; droplet sizes for HVO are slightly smaller, due to the lower evaporation temperature, viscosity, and surface tension compared to diesel. This demonstrates that HVO can potentially replace diesel directly without any modification to CI engines. Several studies are published in the literature which demonstrate as HVO generally over perform diesel in terms of particulate matter, HC, CO, and thermal efficiency for CI engines. Slight increments NOx emissions can be expected. In general, the HVO assures a reduction in the range of 4–8% [37, 38] of tank-to-wheel GHG and up to 80% on WTW basis. There are different patented production methods and from different feedstocks. An analysis of literature data is presented to evaluate the environmental impact of HVO analyzing Life Cycle Assessment (LCA) and well-to-wheel studies. In particular, the section focuses on GHG and Global Warming Potential (GWP), as one of the most relevant issue faced by regulations as described in section 2.1. The LCArequires defining the process, in terms of inputs, outputs, and system boundaries. The main input for the process is the feedstock which can be classified in on-purpose and residual. The latter usually shows lower GHG emissions because neglect the cultivation phase [39]. A further classification could be based on edible and not-edible feedstock. The use of edible feedstock such as rapeseed and palm oil is of great concern, possibly leading to socio-economic implications [40]. Non-edible sources, such as jatropha oils, are of increasing interested [41]. A schematic of the production process of HVO is depicted in Fig. 2.4. In case of residual feedstock, the production part is neglected in the LCA analysis. System boundaries are of fundamental importance and should be carefully assessed since they can significantly influence the LCAresults. The inclusion or exclusion of some subprocess is sometimes subjective and can lead to significative differences among the analyses [42].

In this context, the discussion focuses only on climate change as a measure of equivalent car-

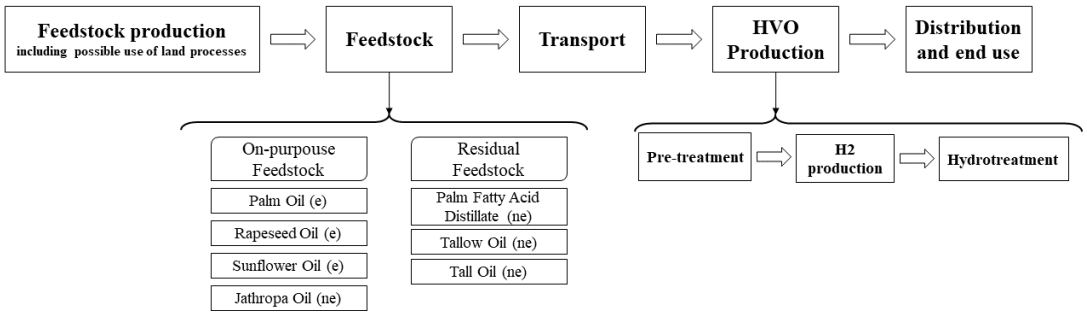

Figure 2.4: Typical process flow diagram for LCA of HVO. Typical feedstocks are reported, indicating with (e) the edible ones while with (ne) the non-edible ones

bon dioxide emissions for the functional unit of the product. For fuels, the functional units usually chosen are the mass of fuel burned, the energy released by combustion, brake energy, and vehicular distance traveled. All the available data reported have been converted in $gCO_{2,eq}$/MJ of fuel chemical energy of the fuel to avoid dependency on assumed vehicle efficiency, test driving cycle, combustion efficiency, or lower heating value (LHV). These data are shown in Fig. 2.5, where the diesel fuel was added as sake of comparison.

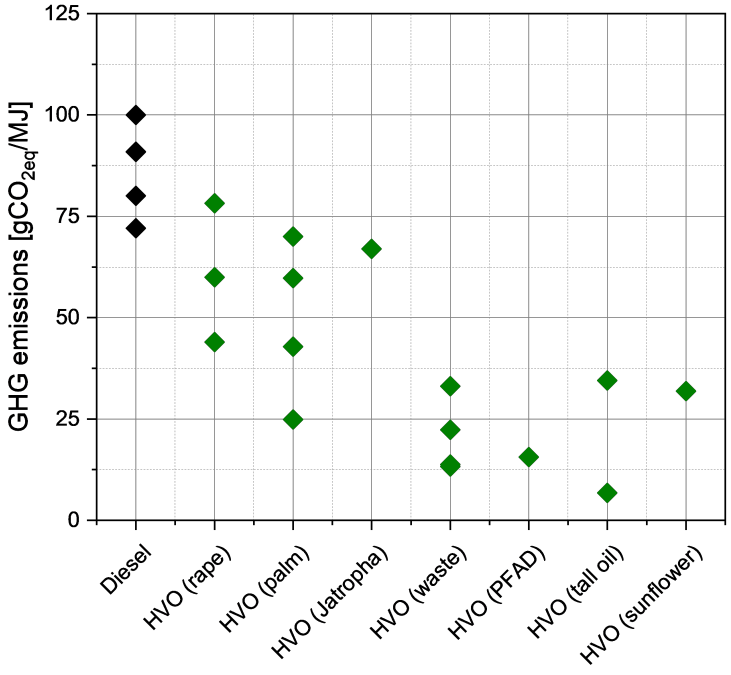

Figure 2.5: GHG emissions on well-to-wheel for diesel and HVO.

The standard diesel fuel GHG emissions vary between 75 and 100 $gCO_{2,eq}$/MJ, while the

HVO shows a significant variation ranging between 5 and 80 $gCO_{2,eq}$/MJ. Residual feedstocks such as Palm Fatty Acid Distillate (Palm Fatty Acid Distillate (PFAD)), waste and tall oil assure the lowest GHG. The HVO from residual feedstocks assures a reduction of about 75% of GHG emissions compared to fossil diesel. However, the availability of the feedstocks is not obvious and to seriously considered for a fair and balanced analysis about the use of renewable fuels to decarbonize the transport sector.

2.2.3 Hydrogen

Hydrogen (H2) can be theoretically produced in a renewable manner and has the potential to replace fossil fuels in the transport sector. To deepen the discussion, the main characteristics of the hydrogen are reported in Table 2.4.

Property	**Value**	**Ref**
Molecular weight [g/mol]	2.016	-
Normal Boiling Point (NBP) [K]	20.3	[43]
Lower Heating Value [MJ/kg]	120	[43]
Higher Heating Values [MJ/kg]	142	[43]
Density @ STP (gas) [kg/m^3]	0.083	[43]
Density @ NBP (liquid) [kg/m^3]	70.78	[44]
Triple point temperature [K]	13.803	[44]
Triple point pressure [bar]	0.07	[44]
Critical point temperature [K]	32.976	[44]
Critical point pressure [bar]	12.93	[44]
Stochiometric Air-Fuel ratio	34.3	[45]
Flammability limits in air [%]	4-75	[45]
Minimum Ignition Energy [mJ]	0.017	[45]
Auto-ignition temperature [K]	858	[45]

Table 2.4: Hydrogen fuel properties

Hydrogen is characterized by a very high lower heating value (120 MJ/kg), is carbon-free and ensures an almost clean combustion. It offers wide application potential as it can be used

to fuel both ICE and PEMFC [46]. On the other hand, hydrogen volume-based specific energy is very poor (around 0.01 MJ/litre at Standard Temperature and pressure (STP) conditions) and about three orders of magnitude less than traditional fossil fuels. Hydrogen shows extremely wide flammability conditions, spreading between 4% and 75% when mixed with air at STP conditions, and it also requires low ignition energy, increasing the safety concerns. Indeed, the minimum ignition energy of about 0.02 mJ can also be generated by static electricity from the human body [47]. Hydrogen is a non-toxic, odorless, stable and asphyxiating gas [48]. Material compatibility requires special attention, especially for the high-pressure lines, for which the embrittlement phenomenon can cause damage.

The low hydrogen density @STP requires specific storage solutions to increase the stored energy onboard. There are physical and chemical storage solutions. Physical storage systems demonstrate certain technological maturity. Chemical storage is still under investigation and development. Physical storage can be classified as Liquid Hydrogen (LH2), Compressed Hydrogen Systems (CH2) and Cryo-Compressed Hydrogen (CcH2). For a better understanding, the density of the hydrogen, reported in Figure 2.6, is a function of the temperature and storage pressures. CH2 offers density ranging between 30-50 kg/m^3. As sake of comparison, the LH2 offers density around 70 kg/m^3 and CcH2 offers around 90 kg/m^3.

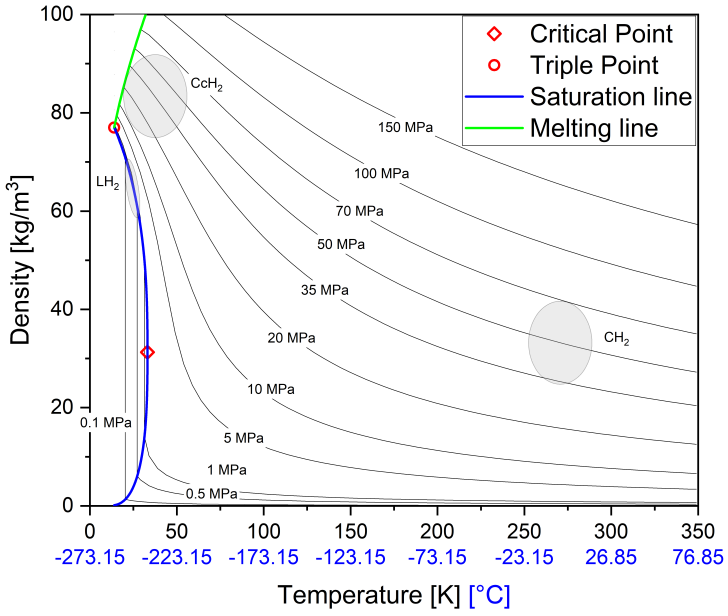

Figure 2.6: Hydrogen density as function of pressure and temperature. Source data: [49]

LH2 usually refers to liquefied hydrogen stored at low pressure, in the range of 1 to 5 bar. It is characterized by high hydrogen density and stored at cryogenic temperature. The LH2 vessel design is mainly designed for facing thermal insulation and the venting system issues. The liquefaction process requires high amount of energy, which can reach the 40% of the fuel one LHV. Due to the extremely low temperature, around 25 K, and to the boil-off losses, the LH2 are not suited to road vehicle on-board storage. In general boil-off losses become of lower entity increasing the volume of the vessels, being acceptable for some large-scale applications [50]. These include among all the use on aircraft and intercontinental hydrogen transport. Likely in the near future, only CH2 at 350 and 700 bar storage systems will be available. There are 144 fuelling station for CH2 in the European territory (2021), and will likely increasing according to forecasts [51]. The vessel can be classified starting from type I which is all made of metal to V by increasing composite materials. Commercially available systems for hydrogen storage are of type IV, with composite wrap and polymer liner.

Hydrogen can be produced in different manners. Based on the emission of the hydrogen production process, it is usually classified as grey, blue and green hydrogen, from the most pollutant to the cleanest [52]. Recently, some additional colours have been proposed but not fully accepted and adopted yet. H2 from electrolysis of water powered actual energy-mix or nuclear power, are named yellow and pink respectively. The brown colour relates to the gasification of lignite and turquoise to the methane pyrolysis. The last, is gaining increasing attention due to the side production in the process of carbon black instead of carbon dioxide, which can be easily stored and used in other industries [53]. The two most common hydrogen production processes are the Steam Methane Reforming (SMR) and the electrolysis. Pinksy et al. [54] have analyzed the technology readiness level of various hydrogen production processes. The results show that only the SMR and alkaline electrolysis process are at operational system level, the PEMFC electrolysis is at Technological Readiness Level (TRL) 6 (i.e., preliminary design and prototype validation), while the others ones are all at lower TRL levels. Different implementations are available for water electrolysis classified on electrolyte type as the common alkaline cells and the polymer electrolyte membrane Polymer Electrolyte Membrane (PEM) [55]. Alkaline electrolyzer can achieve 60-70% of HHV-based efficiency and are the most mature technology, with further margin of improvement regarding electrodes, electrocatalyst and electrolytes [56].

PEM is still not a mature production method but has the potential to reach similar efficiency of Alkaline solutions, high current density, faster response, capable to operate at partial loads and produce pure hydrogen [57].

In regard to hydrogen combustion, it is zero-soot and CO_2 emission. Figure 2.7 reports the environmental impact for producing a kg of hydrogen in terms of equivalent CO_2.

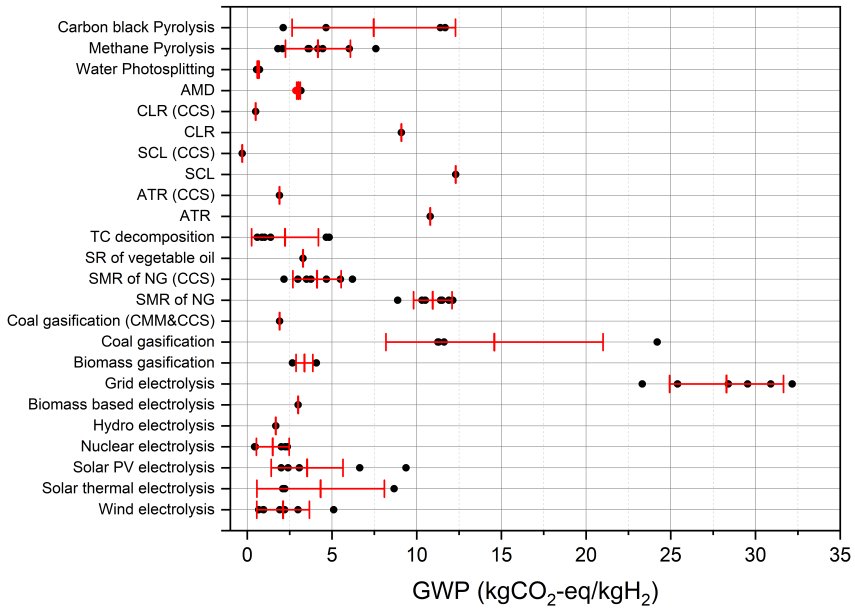

Figure 2.7: GHG emissions from LCA for hydrogen production. Source data: [58–66]

The emissions factors vary of more than one order of magnitude among various methods. SMR has a mean value of about 11 $kg_{CO2,eq}/kg_{H2}$, which lowers to 4.5 $kg_{CO2,eq}/kg_{H2}$ if carbon capture system are employed. Water electrolysis show greatest variation ranging from less than 1 $kg_{CO2,eq}/kg_{H2}$ to over 30 $kg_{CO2,eq}/kg_{H2}$, depending on the energy source of the electricity. Grid electrolysis have the highest environmental impact. Electrolysis from renewable energy source ("Green Hydrogen") have values lower than 5 $kg_{CO2,eq}/kg_{H2}$. .

The application and impact of hydrogen as fuel in vehicles is discussed in more details in the following sections.

2.3 Trends in powertrain technologies

Research and development of new powertrain technologies have recently focused on producing more efficient and cleaner solutions. Electrified powertrains have been developed with many powertrain layouts, especially for light-duty vehicles, such as city and passenger cars.

The ICE has received several technological upgrades to improve its efficiency and reduce harmful emissions without significantly reducing carbon dioxide emissions. On a global WTW scale, carbon dioxide reduction is much easier by applying renewable fuels as HVO and alcohols (already discussed in previous subsections). Compression ignition engines have been optimized in terms of combustion architecture, injection systems and aftertreatment systems. Regarding spark ignition engines, the gasoline direct injection, turbo-charging, downsizing, and variable valve timings are commonly optimized to improve cycle efficiency. Global ICE efficiencies are around 40-45 % for CI engines and 35-40 % for SI engines). Two thirds of fuel energy is wasted as heat in exhaust gases, cooling and lubricating fluids, thus, the interest toward waste heat recovery system (WHR). On the other hand, electric-based powertrains are more efficient. In fact, a typical efficiency ranges from 60 to 80 %. The energy storage system represents the major limits in terms of volumes and weight of battery packs at acceptable vehicle range autonomy. To face with this limit, various hybrid solutions have been proposed. Hybrid configurations can be classified in parallel and series. In parallel, the engine and electric motor can power the transmission simultaneously. In series configuration, the transmission is powered by the electric motor and a thermal engine is used to charge the batteries. The advantage of this second configuration is the opportunity to adopt a smaller engine that works at a fixed operating point and has optimal efficiency.

In the following section, the most relevant powertrain technologies are discussed. Specifically, hydrogen internal combustion engines, electric motors, fuel cells, and electrical energy storage systems are discussed.

2.3.1 Hydrogen Internal Combustion Engines

The use of hydrogen in CI engines is viable through the diesel pilot injection to ignite the mixture. However the dual fuel solution do not complies with upcoming regulations. For SI engines,

both PFI and DI injection strategies are possible for hydrogen. Due to the low hydrogen density, PFI engines reduce the volumetric efficiency of up to 30% [67]. The low quenching distance, low ignition energy, high flame speed and wide flammability limits, makes hydrogen particularly subject to abnormal combustion phenomena such as pre-ignition, knock and backfire. The backfire is typical for PFI engines, in which the air-hydrogen mixture burns into the intake manifold due to pre-ignition or to backflow of hot exhaust gases [68] during the scavenging phase. Injection, valve timings, hotspots, and crevice volume are the main factors to be optimized to control backfire. Thus, DI strategy is preferable, but still not mature because of the reliable DI injectors unavailability. Prototype engine with DI injector are under development. The high injection timings require early injection strategies and a knocking tendency. On the other hand, for late injections, the air-fuel mixture is poorer and unburnt hydrogen higher [69]. Higher DI pressure improve the air-mixture while reducing injection timing, but they will be available only in a few years. Both PFI and DI SI H2 engines requires an adoption of cold-type spark plugs. Spark plug can be a source of hot spot promoting the ignition of the air-fuel mixture [70]. Cold-rated spark mitigate this phenomenon. Moreover, platinum-based electrodes should be avoided due to the possible catalytic effect in the oxygen reduction reaction [71].

The hydrogen fueled ICE produce nitrogen oxides and possible particles mainly derived from lubricant oil. Most hydrogen ICEs will likely operate in ultra-lean conditions to achieve higher efficiencies and lower NOx emissions. Suitable ATS are lean nox trap or Selective Catalytic Reduction (SCR) systems. The SCR need the injection of urea (commercially AdBlue) with the formula $(NH_2)_2CO$. The urea solution produce, trough thermolysis, ammonia and isocyanic acid.

$$(\mathrm{NH_2})_2\mathrm{CO} \longrightarrow \mathrm{NH_3} + \mathrm{HNCO} \tag{2.1}$$

Then the isocyanic acid trough hydrolysis reacts to produce ammonia and carbon dioxide.

$$\mathrm{HNCO} \longrightarrow \mathrm{NH_3} + \mathrm{CO_2} \tag{2.2}$$

In the SCR the ammonia react trough three main reactions to reduce the nitrogen oxides to molecular nitrogen (equations 2.3,2.4,2.5).

$$4\,\mathrm{NO} + 4\,\mathrm{NH_3} + \mathrm{O_2} \longrightarrow 4\,\mathrm{N_2} + 6\,\mathrm{H_2O} \tag{2.3}$$

$$\mathrm{NO} + \mathrm{NO_2} + 2\,\mathrm{NH_3} \longrightarrow 2\,\mathrm{N_2} + 3\,\mathrm{H_2O} \tag{2.4}$$

$$6\,NO_2 + 8\,NH_3 \longrightarrow 7\,N_2 + 12\,H_2O \tag{2.5}$$

Thus, urea utilization lead to carbon dioxide production and will also be limited by carbon reduction regulations. Heavy-duty vehicles with zero emissions are those with less than 1 g/kWh of emitted CO_2 with limited quantity of urea [72].

Due to their development stage, hydrogen ICE requires the development of a combustion system and control strategies to optimize their working condition, offering stable combustion with low emissions levels. The safe operation of a hydrogen engine requires a proper design of crevice volume, piston rings, and sealing to avoid hydrogen leakage. The hydrogen absorption by lubricating oil and the blow-by effect introduce hydrogen in the crankcase, which requires proper ventilation to keep hydrogen concentration below the flammability limits. The application of hydrogen in internal combustion engines will increase the global hydrogen demand, pushing the production and delivery infrastructure development to be useful also for industry.

2.3.2 Electric Motors

Electric motors are a fundamental technology in the pursuit of a more sustainable mobility. Recent developments in the last decades have allowed to reduce their weight and size, improving operating range and specific power, making it suitable for the transport sector. There are many possible classifications of electric motor. Alternate current and direct current motors can be distinguished, as well as synchronous and asynchronous machines or brushed or brushless motors. The most relevant electric motors used for propulsion are the following [73].

- Direct current motors (DC): low cost and simple to control, characterized by relatively low efficiency $< 85\%$ and low power density. The commutator adopts coal brushes, which are subject to wear and are usually adopted for small electric vehicles for which they offer sufficient lifetime.

- Induction Motors (IM): simple and low cost motor; rotor made of laminated steel and short-circuited aluminum bars. AC current on the stator creates a rotating magnetic field that drags the rotor. Due to the difference between the rotor and magnetic field speed, there is a slip between the rotor and stator, and the machine is of asynchronous type. Efficiency vary between 75 % (for small motors) to 95 % (for stationary application).

- Synchronous Permanent Magnet (SPM): sometimes referred to also as Permanent Magnet Synchronous Machine (PMSM). The rotor has a fixed magnetic field due to the permanent magnet, resulting in high power density and very high efficiency. They are expensive due to the use of permanent magnet made of rare earth material, and high environmental impact. Brittle and an adequate cooling is of primary importance for motor durability. The control system are particularly complex and costly. The possibility of building them with reduced packaging and high specific powers makes them suitable for mounting in wheel hubs.

- Reluctance Motor (RM): also referred to as Switching Reluctance Motor (SRM), not adopted actually in automotive applications. Characterized by high efficiency and up to 95 %, but the high ripple torque lead to high noise and vibration levels. The RM rotor is a simple rotor of ferromagnetic materials without the use neither of permanent magnet nor windings. The development of more advanced power controller and control strategies can limit their drawbacks with possible applications in the transport sector.

The power controller of electric motor is a crucial part to exploit the maximum performance. Automotive power controller are able to use the electric machine both as generator and motor, enabling the regenerative braking. This is a great advantage of electric vehicle, which recovering part of their kinetic energy during braking allows to improve the energy consumption. Standard power controller are based on insulated-gate bipolar transistor (IGBT) technology, which have enabled the use of PMSM due to their high frequency switching capability and power ratings. However state-of-art and future controller are exploiting Wide BandGap (WBG) power device made by Silicon Carbide (SiC) and Gallium Nitride (GaN). These materials enable higher switching frequencies in power electronics, reducing energy losses and improving overall motor performance at the expense of higher costs [74].

2.3.3 Fuel Cells

The fuel cells are electrochemical conversion systems capable of converting chemical energy from a fuel and oxidizer into electricity. Core part of an FC is the electrolyte, placed between the electrodes, which separate fuel and oxidizer while allowing the flowing of ions. FC typical

classification is based on the type of electrolyte adopted. According to this criteria, Phosphoric acid FC, Polymer electrolyte membrane FC, Alkaline FC, Molten Carbonate FC and Solid-oxide FC can be distinguished [75]. Each FC is characterized by different fuels, catalysts, cell components and operating temperatures. In the transport sector PEMFC has been widely adopted for its characteristics, such as low operating temperatures and high power density [76]. Table 2.5 presents typical characteristics of a PEMFC.

Property	**Value**
Thermodynamic voltage @ STP [V]	+1.23V
Operating temperature [°C]	80
Catalyst Material	Platinum Group
Cell component material	Carbon based
Electrolyte	Polymer membrane (e.g., NafionTM)
Fuel	H_2
Oxidiser	O_2
Exhaust Product	H_2O

Table 2.5: Typical properties of an H2 - O2 PEMFC. Source: [75]

In the following, the PEMFC and the Balance of Plant (BoP) systems are discussed highlighting most relevant issues and concerns. Excluding hydrogen storage and supply, the PEMFC suffer of high cost and low durability which limits its diffusion. A typical PEMFC schematic drawing is reported in Figure 2.8. In the following, the single parts of the PEMFC are discussed, highlighting limitations and actual research focus.

Usually, the PEM, the CL and the GDL, with the requested seal gasket, are packed together in the form of Membrane Electrode Assembly (MEA). This represents the smaller functional part, which usually offers high current and low voltage currents. The cells are stacked to increase the global power and reach adequate output voltage. The bipolar plates have a crucial role in FC since they are responsible for electron flow, distribution of reactant gases to single cells, while ensuring mechanical strength and heat transfer capability [77]. In the transport sector usually metallic Bipolar Plate (BP) are adopted thanks to cost effectiveness, material strength, shock resistance, electric conductivity and heat transfer with the major drawback to be exposed to

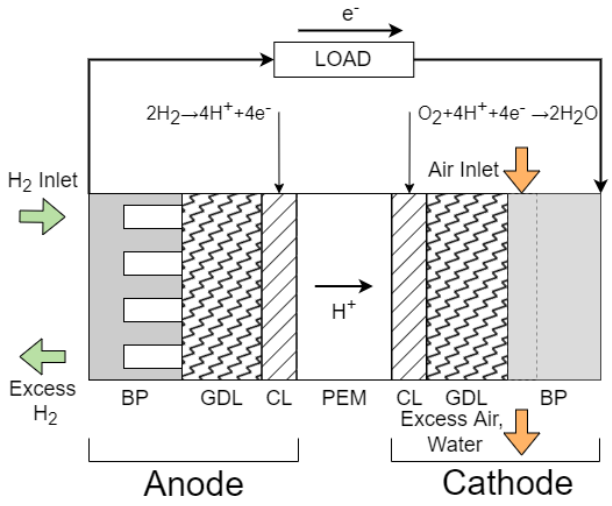

Figure 2.8: Typical PEMFC. BP: Bipolar Plate; GDL: Gas Diffusion Layer; CL: Catalyst Layer; PEM: Proton Exchange Membrane;

corrosion due to the electrolyte [78]. New coating for metallic materials to improve corrosion resistance and electrical conductivity are under investigation. [79]. Then, the GDL should distribute gases from channel to the catalyst/electrolyte interfaces [80]. The GDL have to offer gas and vapour permeability and diffusion capability, while ensuring flush out of excess water [81]. Usually carbon paper is adopted, due to their low cost, and to increase the hydrophobicity it is charged with a Polytetrafluoroethylene (PTFE) loading [82]. The CL, usually made by Platinum Group Material (PGM) represents the location where the electrochemical reactions take place [83], and have to reduce the required activation voltage with special regard to Oxygen Reduction Reaction (ORR) [84]. The use of PGM leads to high cost, which can represent up to 80% of the cost of an FC stack [85]. The PEM, the central part of the MEA allows proton to flow from anode to cathode while maintaining the mechanical strength to support the reactant gas pressure. The standard choice is a sulfonated poly-tetrafluoro-ethylene membrane with the commercial name of Nafion™ [86]. The PEM ensure high proton conductivity with very low resistance and zero electronic conductivity in a wide range of temperature and humidity levels. The it ensure electrochemical and thermal stability, mechanical strength and high durability [87]. To keep high conductivity levels of the Nafion™, the membrane is hydrated requiring the humidification of reactant gas streams [88]. Research is currently being conducted on alternative PEM to

reduce cost and improve temperature operation capability, resulting in higher catalyst activity, reduced catalyst contamination and higher exhaust heat quality [89]. Additionally, actual FC CL has durability issues due to the degradation of their properties with time. In particular, two main degradation processes can be highlighted: particle growth, reducing the electro-chemichal surface area, and transition metal leaching, which is used in Pt alloy to improve ORR mass activity [90]. Current research activities focus on alternative PEM materials, the reduction of PGM-catalyst loading, the development of non-PGM catalyst materials and strategies for high current density operation to reduce cost and improve efficiency and durability [91]. Typical efficiency value at stack level ranges frin 50% to 60% [92]. However, the overall system efficiency is usually lower as it requires a complex management system. In Figure 2.9 is reported a typical PEMFC system layout, which includes the auxiliaries to operate the FC system.

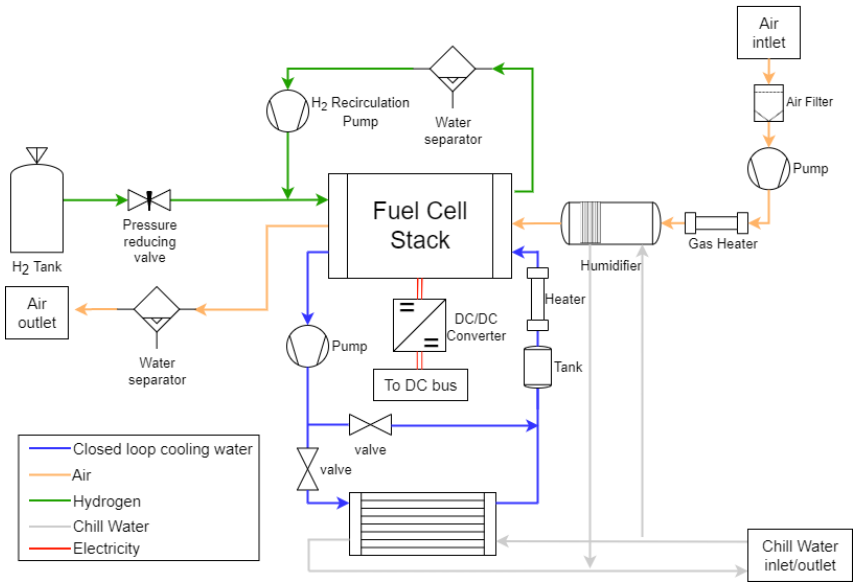

Figure 2.9: PEMFC typical system layout.

The main subsystem are reported in the following.

- **Fuel system**. Hydrogen is fed to the FC at a pressure level between 2 and 4 bar [93]. The choice of operating pressures is linked to reach a balance among thermochemical, kinetic, and mass transport performance. An injector usually provide the fuel into the

stack. Toyota Mirai adopts a design with three injectors, in which the third is only in case of high demanding power and speed [94]. A hydrogen recirculation system allows to maximize the stack efficiency, recovering the hydrogen not reacting on CL-PEM interface [95]. However, the hydrogen recirculation pump requires additional load, and alternative solutions are possible as Dead-Endend Anode (DEA) and Alternative Fuel Feeding (AFF). The DEA relies on pressure regulation of the fuel gas supply without a fuel exhaust flow. However, some periodic purge operations are needed because of the accumulation of nitrogen and water, which causes voltage decay and corrosion due to hydrogen starvation [96]. The purging time and frequency should be adapted according to PEMFC operating conditions and power outputs [97]. AFF represent an evolution of the DEA concept, using two different inlet ports for hydrogen ensuring a better recirculation and homogenization of nitrogen and water separation avoiding cell flooding [98].

- **Air system**. The FC performance can be heavily affected, also in irreversible way, by poisoning of air contaminants. A proper air filtering is needed. A small quantity of sulfur dioxide (SO2) can reduce performance up to 30% with permanent efficiency losses [99]. A compressor is usually adopted to ensure higher air operating pressures.

- **Cooling system**. The material anisotropic nature, the non-uniform heat generation at the cathode require a proper FC stack cooling system [100]. The thermal management of FC is of primary relevance to allow cold start without damage, and control the temperature to assure optimal efficiency and good hydration, avoiding membrane damage, flooding and material delamination and deterioration [101]. For PEMFC power higher than 10 kW liquid and phase change cooling are required [102]. The PEMFC has more demanding cooling needs than ICE applications [103] and they are complex with high exposed thermal exchanging surfaces [104] or increased fluid circulation with higher cooling power requirements [105]. Additionally, there is the need of two different cooling system, one for the stack itself, characterized by high-temperature ($>$60 °C) and one by lower temperature ($<$60 °C), adopted for all the electronics, especially the DC/DC converter [106]. In the end, to successfully guarantee the right cooling, maximizing the system efficiency and improving FC durability, a dedicated thermal management strategy should be adopted.

- **Water management system**. PEM requires to be humidified for optimal operation. usually Humidifier on inlet lines are the standard configuration. Toyota Mirai adopts thinner membrane, which promotes water diffusion, and a special counter flow cell, successfully removing the humidifier without compromising the mechanical properties of the electrolyte membrane and FC efficiency [[107]. The whole system layout should prevent water accumulation and promote drainage since when stored at sub-zero temperatures, the water becomes ice with an expansion that can cause damage to the MEA components [108].

- **DC/DC converter**. The FC output voltage is highly dependent by the current density. As a results the FC stack output shows high variation of the voltage output which can represent also 30& of the nominal value, which requires a

The complex FC system management and the number of auxiliaries required produce additional losses which lower the global system efficiency.

2.3.4 Electrical Energy Storage Systems

In this section the electrical energy systems are discussed focusing on secondary batteries and supercapacitors. Batteries are the main electrical energy storage systems in the road transport sector. Batteries are electro-chemical devices capable of store energy chemically, and release it through an electric current. For the transportation sector only secondary batteries (i.e., reversible chemistry, rechargeable) are of interest. The battery can be classified according different criteria, but the most common are based on definition of materials composing negative and positive current collectors, electrolyte, anode and cathode. There are different kind of chemistry available, but the ones based on lithium ion are the state-of-art in the transportation sectors [109]. Regarding lithium chemistry the most relevant families can be distinguished based on cathode material [110]:

- Lithium Cobalt Oxide (LCO)

- Lithium Iron Phosphate (LFP)

- Lithium Manganese Oxide (LMO)

- Lithium Nickel Manganese Cobalt Oxide (NMC)
- Lithium Nickel Cobalt Aluminum Oxide (NCA)

The main chemical reaction characterizing the different chemistry are reported in table 2.6.

Chemistry	**Electrode**	**Reaction**
LCO	Anode	$nLiC_6 \rightleftharpoons C_6 + nLi^+ + ne^-$
	Cathode	$Li_{m-n}CoO_2 + nLi^+ + ne^- \rightleftharpoons LiCoO_2$
	Overall	$Li_nC_6 + Li_{m-n}CoO_2 \rightleftharpoons Li_0C_6{}^+Li_CoO_2$
LFP	Anode	$Li_nC_6 \rightleftharpoons Li_0C_6 + nLi^+ + ne^-$
	Cathode	$Li_{m-n}FePO_4 + nLi^+ + ne^- \rightleftharpoons Li_mFePO_4$
	Overall	$Li_nC_6 + Li_{m-n}FePO_4 \rightleftharpoons Li_0C_6{}^+Li_mFePO_4$
LMO	Anode	$Li_nC_6 \rightleftharpoons Li_0C_6 + nLi^+ + ne^-$
	Cathode	$Li_{m-n}Mn_2O_4 + nLi^+ + ne^- \rightleftharpoons Li_mMn_2O_4$
	Overall	$Li_nC_6 + Li_{m-n}Mn_2O_4 \rightleftharpoons Li_0C_6 + Li_mMn_2O_4$
NMC	Anode	$Li_nC_6 \rightleftharpoons Li_0C_6 + nLi^+ + ne^-$
	Cathode	$Li_{m-n}(Ni_xMn_yCo_z)O_2 + nLi^+ + ne^- \rightleftharpoons Li_m(Ni_xMn_yCo_z)O_2$
	Overall	$Li_nC_6 + Li_{m-n}(Ni_xMn_yCo_z)O_2 \rightleftharpoons Li_0C_6 + Li_m(Ni_xMn_yCo_z)O_2$
NCA	Anode	$Li_nC_6 \rightleftharpoons Li_0C_6 + nLi^+ + ne^-$
	Cathode	$Li_{m-n}(Ni_xCo_yAl_z)O_2 + nLi^+ + ne^- \rightleftharpoons Li_m(Ni_xCo_yAl_z)O_2$
	Overall	$Li_nC_6 + Li_{m-n}(Ni_xCo_yAl_z)O_2 \rightleftharpoons Li_0C_6 + Li_m(Ni_xCo_yAl_z)O_2$

Table 2.6: Lithium chemistry battery comparison [111].

.

The most relevant parameters from a vehicle perspective are battery energy and power densities, safety costs and durability. The comparison of some characteristics offered by the various chemistry is reported in 2.7. As example NCA offers high energy density but lower cycle capability, reducing its lifetime durability, on the other hand, LFP has high cycling capability but low energy density.

In the last two decades, battery industries have greatly increased energy density from 100 to 200 Wh/kg and up to 250 Wh/kg for cylindrical cells. The practical limit is around 350-370

Chemistry	**Nominal Voltage [V]**	**Operating Voltage Range [V]**	**Energy density [Wh/kg]**	**Cobalt [y/n]**	**Thermal Runaway [°C]**	**Cycle life [-]**
LCO	3.60	2.00-4.2	150-240	y	150	500-1000
LFP	3.20	2.00-3.65	90-120	n	270	2000+
LMO	3.70	2.50-4.20		n	250	300-700
NMC	3.60	2.50-4.20	150-220	y	210	1000-2000
NCA	3.60	2.50-4.20	250-300	y	150	500

Table 2.7: Lithium battery key parameter comparison. Source data: [111].

.

Wh/kg. For higher density, novel battery chemistry and technology are required. Alternative chemistries are being investigated to reduce costs, improve energy and power density, ensure safe operation and storage and reduce environmental impact.

Lithium ion batteries suffers many factors which affects lifetime. Both high and low temperatures, State of Charge (SoC), high current rate, etc. affects deterioration or in some case, catastrophic event as thermal runaway. For those reason a supervisory system, namely Battery management system (BMS), is required to monitor, protect, and optimize the battery operations [112]. The BMS estimates the SoC, State of Health (SoH) employing different techniques, as direct or model based measurements, ensure cell balancing, thermal management, and safety systems [113].

According to Kawamoto et al. [114], the production impact of Battery Electric Vehicle (BEV) can be roughly double than that of Internal Combustion Engine Vehicle (ICEV)s in terms of the GWP, and mainly due to the Battery Pack (BaP). The BaP can reach up to 20% of the LCA, GHG emissions, morever it requires rare raw materials, resulting in high environmental impact. Therefore, battery recycling and re-manufacturing are mandatory as a long-term solution [115]. In this context, battery ageing plays a relevant role. The battery lifetime relates to the battery operating conditions such as the SoC, Deep-of-Discharge (DoD), current (Amperes or C-rating), and temperature [116].

The Geological Survey of Finland reports that besides energy production and management problems, there is not available known resources, in terms of Nickel, Cobalt, Lithium and

Graphite for the production of one full generation of Electric vehicle (EV) [117]. In this context, shared mobility, often referred to as “Mobility as a Service (Maas)”, can effectively reduce the number of new vehicles, decreasing production and disposal phase environmental impact and reducing the demand for rare material [118]. The use of a shared mobility assure a reduction in terms of GWP and other environmental indicators in the range from 20% to 40% with respect private mobility [119]. LCO batteries contains about 23 % of Cobalt, while NMC and NCA used 4 % and 2 % respectively, allowing a reduction of ore material requirements [120]. Alternative to the lithium chemistry as sodium ion batteries are under development and with the potential of higher performance and wide raw material availability [121]. Solid state batteries adopt solid electrolyte instead of organic solutions, which improve the battery safety and stability, supporting higher currents, useful for fast charging, while allowing to overcome the theoretical energy and power density limits of actual technologies [122]. Many manufacturers are working on this technology but the availability is limited as the technology is not mature yet.

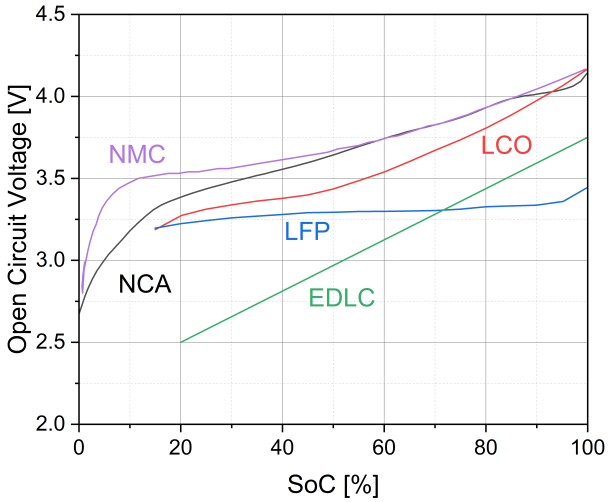

Figure 2.10: Lithium-ion batteries and supercapacitors open circuit voltage comparison. Data source: [123]

Another electrical energy storage system is the supercapacitor, also named ultracapacitor. There are three kind of supercapacitors: EDLC, pseudo capacitors and hybrid capacitors [124]. The name supercapacitors derive from their capability to offer high value of capacitance up to 10^3 Farads, while standard capacitors offers capacity of 10^{-6}-10^{-3} Farads. Thin dielectrics and high specific area electrode are adopted to reach high values of capacitance. Differently from

batteries the charge on electrode changes about linearly, resulting in near linear Open Circuit Voltage (OCV). Figure 2.10 shows a comparison of different lithium battery chemistry and a typical Electrochemical double layer capaciter (EDLC) -OCV. The linear OCV curve typical of supercapacitors, and the near flat OCV curve of LFP chemistry.

Supercapacitors (SC) are characterized by high power and low energy density. They are particularly suited for fast transient loads and are less prone to the ageing phenomenon due to the high currents. Because of their high cost and lo energy density they are usually adopted together with batteries. SC belong to the category of high-power density Energy Storage System (ESS), while lithium-based batteries to the high energy density ESS. This kind of system are usually called Hybrid Energy Storage Systems (HESS). A comparison of batteries and supercapacitors in terms of energy and power density at different integration levels (cell, module, and pack) is reported in figure 2.11. The data were collected from many manufacturers and technical resources. The mass-related specific power and energy decreased passing from the cell to the module and from this to the pack level. Comparing the BaP and SC modules, the first offered about a 35-times greater specific energy and 20-times lower specific power.

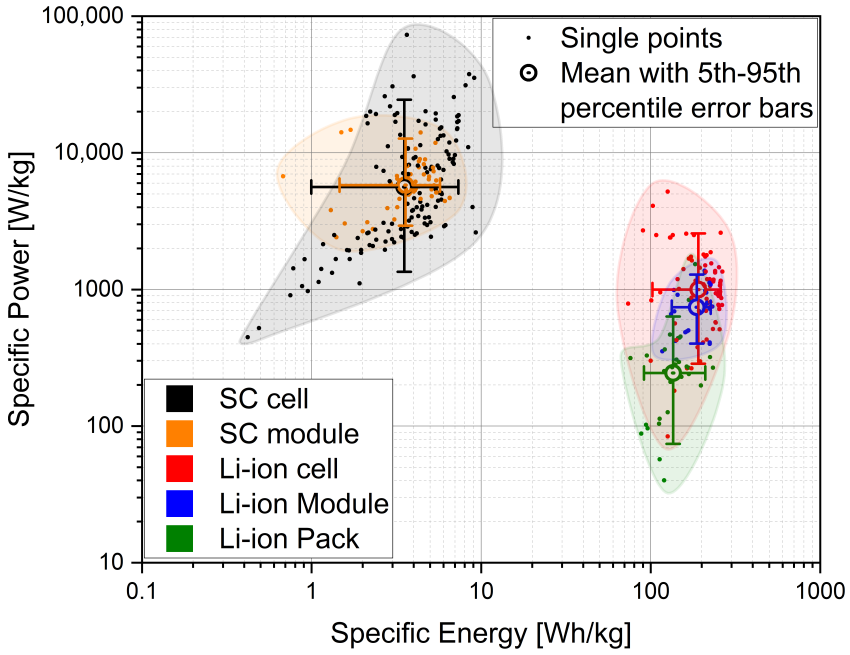

Figure 2.11: Lithium-ion batteries and supercapacitors comparison.

Many topologies can be designed to exploit the SC and BaP, such as passive, semi-active

HESS and full-active, function of the complexity and cost but with higher potential in terms of the operational performanmce. An overview of the configurations is reported in Figure 2.12.

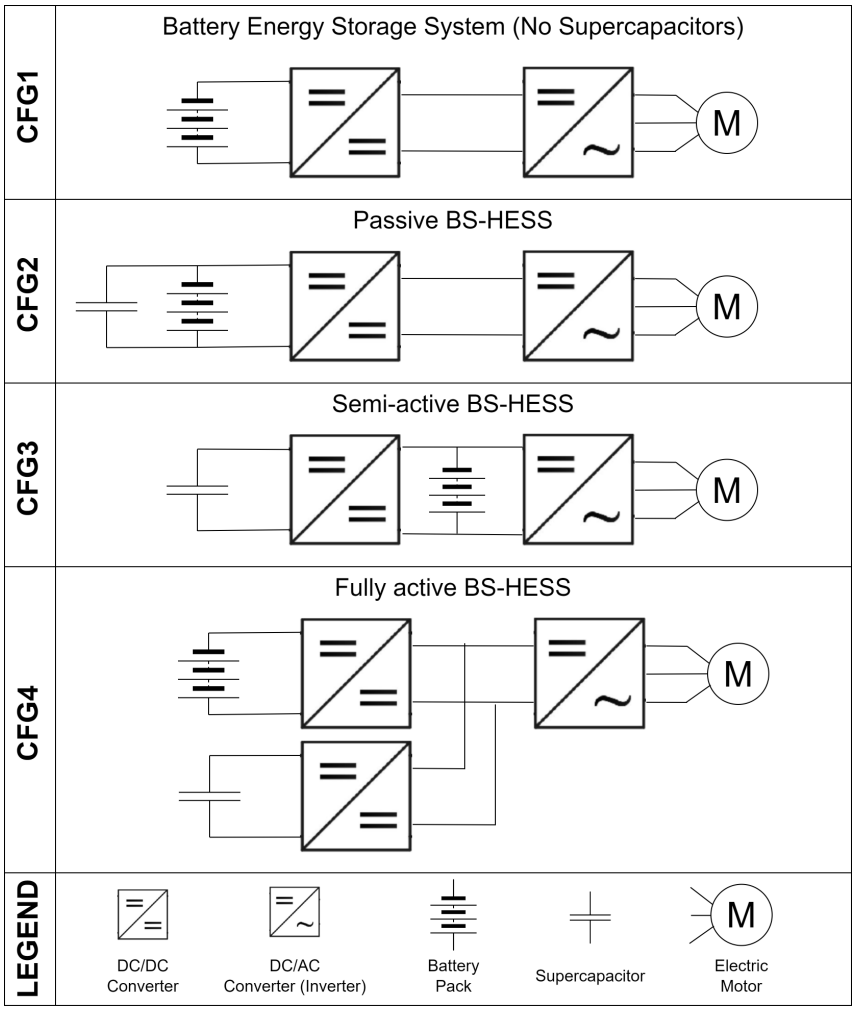

Figure 2.12: Battery pack and supercapacitors hybrid energy storage topologies.

The full-active control strategy requires two additional DC/DC converter with a dedicated control unit with increased inverter cost in case of smaller batteries (city cars) and in the same order of battery cost. The passive and semi-active topologies do not require additional converters, but requires dedicated EMS development. The passive topology does not require a control strategy since it is impossible to control its operation actively. In this case, the charging and discharging of the SC are dictated by the electrical characteristics of the BS-HESS as the battery internal resistance, and SC resistance and capacitance [125]. The SCs, acts as a low-pass filter. The BaPs and SCs are connected electrically in parallel, with resistive and capacitive char-

acteristics respectively (RC branch). The semi-active topology does not require an additional converter and can ensure better performance due to the additional degree of freedom in the management of the HESS [126] with high transient response (supercapacitors) and high energy density (batteries) improving the durability. Recent researches are aimed to improve supercapacitors durability, reduce the self discharging, enlarge their operating temperature range and reduce costs [127].

2.4 Trends in vehicles technologies

The road transport sector is currently evolving towards new emerging vehicular solutions driven by goals of air quality improvement, climate change mitigation, and vehicle safety enhancement. On one hand, from the vehicle architecture perspective, the first two points are strictly related to the fuels (section 2.2) and powertrain architecture (section 2.3) adopted. On the other hand emerging digital technologies, with the developing of autonomous systems and vehicle connectivity, are driving to possible revolution of the transport sector shifting to new mobility paradigms.

Electrification plays a crucial role, with conspicuous investment, in developing technology and infrastructures [128]. However, also the hydrogen have been chosen as one possible candidate to decarbonize the sector. In fact, different policies and objectives have been established to promote the diffusion of hydrogen production and technology. In particular, the EU in 2020 have established a European hydrogen roadmap to promote the production and use of clean hydrogen from renewable sources. In 2022, pushed by the natural gas crisis, the EU, with the REPowerEU plan, has further accelerated and promoted hydrogen as an alternative and clean energy source. In September 2022, the EU parliament claimed the intent to produce ten million tons of renewable hydrogen by 2030.

Besides, the vehicle connectivity among vehicles allow new opportunities in terms of fleet management, data production and new services. Green Light Optimal Speed Advisory (GLOSA) is an example of driving assistance system, whose working logic can be integrated in autonomous driving, to reduce vehicles travel times and improving fuel efficiency [129]. The connectivity opens new mobility paradigms creating the opportunity for novel technologies

gathering and exploiting the available information. As sake of example, the weather conditions, can be monitored in real-time by Connected and Autonomous Vehicle (CAV) sensors and transmitted to cloud-based database and services, which allow almost real-time data acquisition to improve weather changes tracking and forecasts [130].

In the following the connectivity is discussed more technically, while the driving automation system and autonomous vehicles are discusses more in chapter 4.

Vehicle connectivity is under development and will play a crucial role in future intelligent transport systems. Various taxonomy are adopted to define various relationship between vehicles and other actors. The most common name are reported in the following.

- **Vehicle to Everything (V2x)**
- **Vehicle to Vehicle (V2V)**
- **Vehicle to Infrastructure (V2I)**
- **Vehicle to Grid (V2G)**
- **Vehicle to Network (V2N)**
- **Vehicle to Pedestrian (V2P)**

To deploy a efficient connectivity the standardization is the most relevant point. The Dedicated Short Range Communication (DSRC), with standards 802.11p (US) and ITS-GT (EU), and Cellullar V2x (C-V2x) are the most relevant in transport [131]. C-V2x can in different operating mode: i) with a direct sidelink (PS5 mode) with a communication established directly between the two vehicles; ii) with the intervehicular communication passing trough a base station (uu mode); or iii) communication trough cellular network [132]. Obviously, the performance, in terms of latency and bandwidth but also range varies among the modes. Table 2.8 provides a comparison of some characteristics of those protocols.

Other than physical layer, standardization is required also to the message level (i.e., how the information are transmitted) to ensure the universal exchange of information among various vehicles, systems and infrastructures. Examples of standard can be the SAE J2735 or European ETSI EN 302 637-2. Those standard define the information to be transmitted, as vehicle position and attitude, wheel encoders, path and road information, and how they should be send.

Parameter	DSRC	4G-V2x	5G NR-V2x
Standard	IEEE 802.11p/bd	4G LTE	5G LTE
Frequency	5.9Ghz (p) 60 Ghz (bd)	sub 6 Ghz	sub 5.9-60 Ghz
Range [m]	< 250	100 (PS5) few km (uu mode) some tens km (cellular)	1000(6Ghz)-100(60Ghz)
Latency [ms]	< 5	50	1
Max Datarate [Mbps]	27	50	300

Table 2.8: Vehicle connectivity comparison.

.

Future intelligent transport systems will likely to be dependent by connectivity. However, the connectivity raises additional concerns about vehicle cybersecurity, which should be considered to ensure a safe vehicle operations, avoiding cyberattacks and neglecting altered injected data [133]. This is a topic of great concern in the development of autonomus vehicles but relies more on the information and communication technology experts than system engineers. For this reason is not deepened in this thesis.

The pursuit of enhancing road safety is pushing for the development of Drive Autonomous Systems (DAS), with positive repercussions on social, economic, and efficiency aspects [134]. DAS can range from assisted to fully autonomous driving systems. Different classifications have been recently proposed for a standardized framework, the National Highway Traffic Safety Administration (NHTSA) 5-level system or BASt 5-degrees of automation [135]. However, the most common classification is the SAE J3016, which defines six classes from L0 to L5 representing vehicles without any assistance and fully autonomous, respectively [136]. Mercedes-Benz recently introduced the first production car equipped with the first L3 system into the market. Many pilot projects at L4 have already been deployed, while L5 vehicles are expected to be available only in several years. L4 pilot vehicles are able to drive autonomously but with some limitations on vehicle speed, take-over manoeuvre, and operation in the absence of a Global Navigation Satellite System (GNSS) signal or under severe weather conditions [137]. The importance of those pilot projects relies on understanding the main obstacles encountered and limiting the diffusion of autonomous solutions and on the definition of possible solutions [138].

The social aspects are crucial for the wide acceptance of self-driving cars and are strictly related to the technical level reached by Autonomous Vehicle (AV). In a recent statistical study on a simulator, manual drivers in scenarios with autonomous vehicles have experienced safety concerns, average speed reduction, and more safety issues during specific manoeuvres [139]. Most AV designs include V2x communication systems. They are usually named as AVs or as CAV, since they likely will all be connected in the future. Thereby in the manuscript the CAVs include also the AV. In general, connectivity allows for improving the safety, performance, and reliability of CAVs. The communication of ego-vehicle position and future actions to surrounding vehicles provide fundamental information on crash avoidance strategies [140]. A critical aspect of AV is the interaction with human-driven vehicles and the surrounding environment [141]. The interaction among vehicles, pedestrians, cyclists and other actors can result in frequent stops [142], and deploying autonomous vehicles in real-life scenarios is challenging to achieve safe, reliable, and comfortable operations [143].

The autonomous system, with its sensor, and the connectivity allows the access to large dataset, regarding many aspects as vehicle surrounding, traffic conditions, real-time monitoring, weather conditions, surrounding actors (pedestrian and other vehicles) future path. Those information can be used by a network or distributed controller for optimal fleet management in terms of traffic and energy consumption, while ensuring safe operation and reduce incidents [144]. On the other hand, advanced sensors, high computational power, and novel technologies can improve energy efficiency and comfort [145]. However, studies often neglect the increment of vehicle power consumption due to the DAS systems. This rise the research question if a vehicle equipped by a driving automation system can improve the vehicle efficiency considering their increased hardware power consumption. The question is faced and deepened in Chapter 4.

Bibliography

[1] Magín Lapuerta, José Rodríguez-Fernández, and Octavio Armas. "Correlation for the estimation of the density of fatty acid esters fuels and its implications. A proposed Biodiesel Cetane Index". en. In: *Chemistry and Physics of Lipids* 163.7 (Sept. 2010), pp. 720–727. ISSN: 0009-3084. DOI: 10.1016/j.chemphyslip.2010.06.004.

[2] Michele Pipicelli et al. "Alcohol Fuels in Compression Ignition Engines". In: *Application of Clean Fuels in Combustion Engines*. Ed. by Gabriele Di Blasio et al. Singapore: Springer Singapore, 2022, pp. 9–31. ISBN: 978-981-16-8751-8. DOI: 10.1007/978-981-16-8751-8_2.

[3] Giuseppe Di Luca et al. "Alcohol Fuels in Spark Ignition Engines". In: *Application of Clean Fuels in Combustion Engines*. Ed. by Gabriele Di Blasio et al. Singapore: Springer Singapore, 2022, pp. 33–54. ISBN: 978-981-16-8751-8. DOI: 10.1007/978-981-16-8751-8_3.

[4] Qianqian Li, Wu Jin, and Zuohua Huang. "Laminar Flame Characteristics of C1–C5 Primary Alcohol-Isooctane Blends at Elevated Temperature". en. In: *Energies* 9.7 (July 2016). Number: 7 Publisher: Multidisciplinary Digital Publishing Institute, p. 511. DOI: 10.3390/en9070511.

[5] Wei Dan Ping, Stefan Korcek, and Hugh Spikes. "Comparison of the Lubricity of Gasoline and Diesel Fuels". In: *1996 SAE International Fall Fuels and Lubricants Meeting and Exhibition*. ISSN: 0148-7191. SAE International, Oct. 1996. DOI: https://doi.org/10.4271/962010.

[6] B. Rajesh Kumar and S. Saravanan. “Use of higher alcohol biofuels in diesel engines: A review”. en. In: *Renewable and Sustainable Energy Reviews* 60 (July 2016), pp. 84–115. ISSN: 1364-0321. DOI: 10.1016/j.rser.2016.01.085.

[7] Choongsik Bae and Jaeheun Kim. “Alternative fuels for internal combustion engines”. en. In: *Proceedings of the Combustion Institute* 36.3 (Jan. 2017), pp. 3389–3413. ISSN: 1540-7489. DOI: 10.1016/j.proci.2016.09.009.

[8] R. J. Pearson and J. W. G. Turner. “Renewable fuels: An automotive perspective”. English (US). In: *Comprehensive Renewable Energy* (Jan. 2012). Publisher: Elsevier Ltd, pp. 305–342. DOI: 10.1016/B978-0-08-087872-0.00522-9.

[9] Sam Shamun, Giacomo Belgiorno, and Gabriele Di Blasio. “Engine Parameters Assessment for Alcohols Fuels Application in Compression Ignition Engines”. In: *Alternative Fuels and Their Utilization Strategies in Internal Combustion Engines*. Ed. by Akhilendra Pratap Singh et al. Singapore: Springer Singapore, 2020, pp. 125–139. ISBN: 978-981-15-0418-1. DOI: 10.1007/978-981-15-0418-1_8.

[10] Yahya Çelebi and Hüseyin Aydın. “An overview on the light alcohol fuels in diesel engines”. en. In: *Fuel* 236 (Jan. 2019), pp. 890–911. ISSN: 0016-2361. DOI: 10.1016/j.fuel.2018.08.138.

[11] Vikram Kumar, Akhilendra Pratap Singh, and Avinash Kumar Agarwal. “Gaseous emissions (regulated and unregulated) and particulate characteristics of a medium-duty CRDI transportation diesel engine fueled with diesel-alcohol blends”. en. In: *Fuel* 278 (Oct. 2020), p. 118269. ISSN: 0016-2361. DOI: 10.1016/j.fuel.2020.118269.

[12] Ho Young Kim, Jun Cong Ge, and Nag Jung Choi. “Effects of Ethanol–Diesel on the Combustion and Emissions from a Diesel Engine at a Low Idle Speed”. en. In: *Applied Sciences* 10.12 (Jan. 2020). Number: 12 Publisher: Multidisciplinary Digital Publishing Institute, p. 4153. DOI: 10.3390/app10124153.

[13] Omar I. Awad et al. “Alcohol and ether as alternative fuels in spark ignition engine: A review”. en. In: *Renewable and Sustainable Energy Reviews* 82 (Feb. 2018), pp. 2586–2605. ISSN: 1364-0321. DOI: 10.1016/j.rser.2017.09.074.

[14] Aleksander Marek et al. “Assessment of the Logistic System of Fuel Life Cycle Using the LCA Method”. en. In: *Agricultural Engineering* 20.3 (Sept. 2016), pp. 125–134. DOI: 10.1515/agriceng-2016-0050.

[15] Gloria Zhi Fu, Albert W. Chan, and David E. Minns. “Life Cycle assessment of bio-ethanol derived from cellulose”. en. In: *The International Journal of Life Cycle Assessment* 8.3 (May 2003), pp. 137–141. ISSN: 1614-7502. DOI: 10.1007/BF02978458.

[16] Aiduan Li Borrion, Marcelle C. McManus, and Geoffrey P. Hammond. “Environmental life cycle assessment of bioethanol production from wheat straw”. en. In: *Biomass and Bioenergy* 47 (Dec. 2012), pp. 9–19. ISSN: 0961-9534. DOI: 10.1016/j.biombioe.2012.10.017.

[17] Marjorie Morales et al. “Life cycle assessment of gasoline production and use in Chile”. eng. In: *The Science of the Total Environment* 505 (Feb. 2015), pp. 833–843. ISSN: 1879-1026. DOI: 10.1016/j.scitotenv.2014.10.067.

[18] Otávio Cavalett et al. “Comparative LCA of ethanol versus gasoline in Brazil using different LCIA methods”. en. In: *The International Journal of Life Cycle Assessment* 18.3 (Mar. 2013), pp. 647–658. ISSN: 1614-7502. DOI: 10.1007/s11367-012-0465-0.

[19] Sara González-García et al. “Comparative life cycle assessment of ethanol production from fast-growing wood crops (black locust, eucalyptus and poplar)”. en. In: *Biomass and Bioenergy*. Biorefinery 39 (Apr. 2012), pp. 378–388. ISSN: 0961-9534. DOI: 10.1016/j.biombioe.2012.01.028.

[20] Loan T. Le et al. “Energy and greenhouse gas balances of cassava-based ethanol”. en. In: *Biomass and Bioenergy* 51 (Apr. 2013), pp. 125–135. ISSN: 0961-9534. DOI: 10.1016/j.biombioe.2013.01.011.

[21] Yuda Yulisa Restianti and Shabbir H. Gheewala. “Life cycle assessment of gasoline in Indonesia”. en. In: *The International Journal of Life Cycle Assessment* 17.4 (May 2012), pp. 402–408. ISSN: 1614-7502. DOI: 10.1007/s11367-011-0372-9.

[22] Pahola Thathiana Benavides et al. “Life-cycle analysis of fuels from post-use non-recycled plastics”. en. In: *Fuel* 203 (Sept. 2017), pp. 11–22. ISSN: 0016-2361. DOI: 10.1016/j.fuel.2017.04.070.

[23] B. Daylan and N. Ciliz. “Life cycle assessment and environmental life cycle costing analysis of lignocellulosic bioethanol as an alternative transportation fuel”. en. In: *Renewable Energy* 89 (Apr. 2016), pp. 578–587. ISSN: 0960-1481. DOI: 10.1016/j.renene.2015.11.059.

[24] Annie Levasseur et al. “Assessing butanol from integrated forest biorefinery: A combined techno-economic and life cycle approach”. en. In: *Applied Energy* 198 (July 2017), pp. 440–452. ISSN: 0306-2619. DOI: 10.1016/j.apenergy.2017.04.040.

[25] Yigang Liu et al. “Comprehensive analysis of environmental impacts and energy consumption of biomass-to-methanol and coal-to-methanol via life cycle assessment”. en. In: *Energy* 204 (Aug. 2020), p. 117961. ISSN: 0360-5442. DOI: 10.1016/j.energy.2020.117961.

[26] Jegannathan Kenthorai Raman and Edgard Gnansounou. “LCA of bioethanol and furfural production from vetiver”. eng. In: *Bioresource Technology* 185 (June 2015), pp. 202–210. ISSN: 1873-2976. DOI: 10.1016/j.biortech.2015.02.096.

[27] Nathalie Becker, Lovisa Björnsson, and Pål Börjesson. *Greenhouse gas savings for Swedish emerging lignocellulose-based biofuels - using the EU renewable energy directive calculation methodology*. English. Vol. Report 104. Miljö- och energisystem, LTH, Lunds universitet, Oct. 2017. ISBN: 978-91-86961-30-5.

[28] Ari Engman et al. “Neste renewable diesel handbook”. In: *Neste Proprietary Publication, Espoo* (2016).

[29] Thomas Bohl et al. “Particulate number and NOx trade-off comparisons between HVO and mineral diesel in HD applications”. en. In: *Fuel* 215 (Mar. 2018), pp. 90–101. ISSN: 0016-2361. DOI: 10.1016/j.fuel.2017.11.023.

[30] Marius Zubel et al. “Advanced Fuel Formulation Approach using Blends of Paraffinic and Oxygenated Biofuels: Analysis of Emission Reduction Potential in a High Efficiency Diesel Combustion System”. en. In: *SAE International Journal of Fuels and Lubricants* 9.3 (Oct. 2016), pp. 481–492. ISSN: 1946-3960. DOI: 10.4271/2016-01-2179.

[31] Jacek Hunicz et al. “Efficient hydrotreated vegetable oil combustion under partially premixed conditions with heavy exhaust gas recirculation”. en. In: *Fuel* 268 (May 2020), p. 117350. ISSN: 0016-2361. DOI: 10.1016/j.fuel.2020.117350.

[32] Om Parkash Bhardwaj et al. “Potential of Hydrogenated Vegetable Oil (HVO) in Future High Efficiency Combustion System”. In: *SAE International Journal of Fuels and Lubricants* 6.1 (Apr. 2013), pp. 157–169. ISSN: 1946-3952. DOI: https://doi.org/10.4271/2013-01-1677.

[33] Athanasios Dimitriadis et al. “Evaluation of a Hydrotreated Vegetable Oil (HVO) and Effects on Emissions of a Passenger Car Diesel Engine”. In: *Frontiers in Mechanical Engineering* 4 (2018). ISSN: 2297-3079.

[34] Hamidreza Fajri et al. “Mixture Formation Analysis for Diesel, n-Dodecane, RME, and HVO in Large-Scale Injector Nozzles”. In: *CO2 Reduction for Transportation Systems Conference*. ISSN: 0148-7191. SAE International, June 2022.

[35] R. H. Barbour, D. J. Rickeard, and N. G. Elliott. “Understanding Diesel Lubricity”. In: June 2000, pp. 2000–01–1918. DOI: 10.4271/2000-01-1918.

[36] Leonardo Pellegrini, Carlo Beatrice, and Gabriele Di Blasio. *Investigation of the Effect of Compression Ratio on the Combustion Behavior and Emission Performance of HVO Blended Diesel Fuels in a Single-Cylinder Light-Duty Diesel Engine*. English. SAE Technical Paper 2015-01-0898. ISSN: 0148-7191, 2688-3627. Warrendale, PA: SAE International, Apr. 2015. DOI: 10.4271/2015-01-0898.

[37] T. Murtonen et al. “Emissions with Heavy-duty Diesel Engines and Vehicles using FAME, HVO and GTL Fuels with and without DOC+POC Aftertreatment”. en. In: *SAE International Journal of Fuels and Lubricants* 2.2 (Nov. 2009), pp. 147–166. ISSN: 1946-3960. DOI: 10.4271/2009-01-2693.

[38] Gabriele Di Blasio, Roberto Ianniello, and Carlo Beatrice. “Hydrotreated vegetable oil as enabler for high-efficient and ultra-low emission vehicles in the view of 2030 targets”. en. In: *Fuel* 310 (Feb. 2022), p. 122206. ISSN: 0016-2361. DOI: 10.1016/j.fuel.2021.122206.

[39] Shveta Soam and Karl Hillman. “Factors influencing the environmental sustainability and growth of hydrotreated vegetable oil (HVO) in Sweden”. en. In: *Bioresource Technology Reports* 7 (Sept. 2019), p. 100244. ISSN: 2589-014X. DOI: 10.1016/j.biteb.2019.100244.

[40] Mustafa Balat. “Potential alternatives to edible oils for biodiesel production – A review of current work”. en. In: *Energy Conversion and Management* 52.2 (Feb. 2011), pp. 1479–1492. ISSN: 0196-8904. DOI: 10.1016/j.enconman.2010.10.011.

[41] Rickard Arvidsson et al. “Life cycle assessment of hydrotreated vegetable oil from rape, oil palm and Jatropha”. en. In: *Journal of Cleaner Production* 19.2 (Jan. 2011), pp. 129–137. ISSN: 0959-6526. DOI: 10.1016/j.jclepro.2010.02.008.

[42] Sangwon Suh et al. “System Boundary Selection in Life-Cycle Inventories Using Hybrid Approaches”. In: *Environmental Science & Technology* 38.3 (Feb. 2004). Publisher: American Chemical Society, pp. 657–664. ISSN: 0013-936X. DOI: 10.1021/es0263745.

[43] N. T. Stetson, S. McWhorter, and C. C. Ahn. “1 - Introduction to hydrogen storage”. en. In: *Compendium of Hydrogen Energy*. Ed. by Ram B. Gupta, Angelo Basile, and T. Nejat Veziroğlu. Woodhead Publishing Series in Energy. Woodhead Publishing, Jan. 2016, pp. 3–25. ISBN: 978-1-78242-362-1. DOI: 10.1016/B978-1-78242-362-1.00001-8.

[44] Federico Ustolin, Nicola Paltrinieri, and Filippo Berto. “Loss of integrity of hydrogen technologies: A critical review”. en. In: *International Journal of Hydrogen Energy* 45.43 (Sept. 2020), pp. 23809–23840. ISSN: 0360-3199. DOI: 10.1016/j.ijhydene.2020.06.021.

[45] P. V. Elumalai et al. “Hydrogen in Spark Ignition Engines”. en. In: *Application of Clean Fuels in Combustion Engines*. Ed. by Gabriele Di Blasio et al. Energy, Environment, and Sustainability. Singapore: Springer Nature, 2022, pp. 195–213. ISBN: 9789811687518. DOI: 10.1007/978-981-16-8751-8_10.

[46] Janusz Nowotny and T. Nejat Veziroglu. “Impact of hydrogen on the environment”. en. In: *International Journal of Hydrogen Energy*. 3rd Iranian Fuel Cell Seminar 36.20 (Oct. 2011), pp. 13218–13224. ISSN: 0360-3199. DOI: 10.1016/j.ijhydene.2011.07.071.

[47] Ryosuke Kurokawa et al. “Preventing explosions of hydrogen gas inhalers”. In: *Medical Gas Research* 9.3 (Sept. 2019), pp. 160–162. ISSN: 2045-9912. DOI: 10.4103/2045-9912.266996.

[48] Selma Atilhan et al. “Green hydrogen as an alternative fuel for the shipping industry”. en. In: *Current Opinion in Chemical Engineering* 31 (Mar. 2021), p. 100668. ISSN: 2211-3398. DOI: 10.1016/j.coche.2020.100668.

[49] E. W. Lemmon et al. *NIST Standard Reference Database 23: Reference Fluid Thermodynamic and Transport Properties-REFPROP, Version 10.0, National Institute of Standards and Technology*. 2018. DOI: https://doi.org/10.18434/T4/1502528.

[50] Ram R. Ratnakar et al. “Hydrogen supply chain and challenges in large-scale LH2 storage and transportation”. en. In: *International Journal of Hydrogen Energy* 46.47 (July 2021), pp. 24149–24168. ISSN: 0360-3199. DOI: 10.1016/j.ijhydene.2021.05.025.

[51] Gregor ERBACH and LISELOTTE JENSEN. “EU hydrogen policy: Hydrogen as an energy carrier for a climate-neutral economy”. In: (2021). Publisher: EPRS: European Parliamentary Research Service.

[52] Carla B. Robledo et al. “Integrating a hydrogen fuel cell electric vehicle with vehicle-to-grid technology, photovoltaic power and a residential building”. en. In: *Applied Energy* 215 (Apr. 2018), pp. 615–629. ISSN: 0306-2619. DOI: 10.1016/j.apenergy.2018.02.038.

[53] Nuria Sánchez-Bastardo, Robert Schlögl, and Holger Ruland. “Methane Pyrolysis for Zero-Emission Hydrogen Production: A Potential Bridge Technology from Fossil Fuels to a Renewable and Sustainable Hydrogen Economy”. In: *Industrial & Engineering Chemistry Research* 60.32 (Aug. 2021). Publisher: American Chemical Society, pp. 11855–11881. ISSN: 0888-5885. DOI: 10.1021/acs.iecr.1c01679.

[54] Roxanne Pinsky et al. “Comparative review of hydrogen production technologies for nuclear hybrid energy systems”. en. In: *Progress in Nuclear Energy* 123 (May 2020), p. 103317. ISSN: 0149-1970. DOI: 10.1016/j.pnucene.2020.103317.

[55] Alfredo Ursua, Luis M. Gandia, and Pablo Sanchis. “Hydrogen Production From Water Electrolysis: Current Status and Future Trends”. In: *Proceedings of the IEEE* 100.2

(Feb. 2012). Conference Name: Proceedings of the IEEE, pp. 410–426. ISSN: 1558-2256. DOI: 10.1109/JPROC.2011.2156750.

[56] Kai Zeng and Dongke Zhang. "Recent progress in alkaline water electrolysis for hydrogen production and applications". en. In: *Progress in Energy and Combustion Science* 36.3 (June 2010), pp. 307–326. ISSN: 0360-1285. DOI: 10.1016/j.pecs.2009.11.002.

[57] S. Shiva Kumar and V. Himabindu. "Hydrogen production by PEM water electrolysis – A review". en. In: *Materials Science for Energy Technologies* 2.3 (Dec. 2019), pp. 442–454. ISSN: 2589-2991. DOI: 10.1016/j.mset.2019.03.002.

[58] Ramchandra Bhandari, Clemens A. Trudewind, and Petra Zapp. "Life cycle assessment of hydrogen production via electrolysis – a review". en. In: *Journal of Cleaner Production*. Special Volume: Making Progress Towards More Sustainable Societies through Lean and Green Initiatives 85 (Dec. 2014), pp. 151–163. ISSN: 0959-6526. DOI: 10.1016/j.jclepro.2013.07.048.

[59] Shayan Sadeghi, Samane Ghandehariun, and Marc A. Rosen. "Comparative economic and life cycle assessment of solar-based hydrogen production for oil and gas industries". en. In: *Energy* 208 (Oct. 2020), p. 118347. ISSN: 0360-5442. DOI: 10.1016/j.energy.2020.118347.

[60] Yaser Khojasteh Salkuyeh, Bradley A. Saville, and Heather L. MacLean. "Techno-economic analysis and life cycle assessment of hydrogen production from natural gas using current and emerging technologies". en. In: *International Journal of Hydrogen Energy* 42.30 (July 2017), pp. 18894–18909. ISSN: 0360-3199. DOI: 10.1016/j.ijhydene.2017.05.219.

[61] Javier Dufour et al. "Life cycle assessment of alternatives for hydrogen production from renewable and fossil sources". en. In: *International Journal of Hydrogen Energy*. 10th International Conference on Clean Energy 2010 37.2 (Jan. 2012), pp. 1173–1183. ISSN: 0360-3199. DOI: 10.1016/j.ijhydene.2011.09.135.

[62] Samane Ghandehariun and Amit Kumar. "Life cycle assessment of wind-based hydrogen production in Western Canada". en. In: *International Journal of Hydrogen Energy*

41.22 (June 2016), pp. 9696–9704. ISSN: 0360-3199. DOI: 10.1016/j.ijhydene.2016.04.077.

[63] Ali Erdogan Karaca, Ibrahim Dincer, and Junjie Gu. “Life cycle assessment study on nuclear based sustainable hydrogen production options”. en. In: *International Journal of Hydrogen Energy* 45.41 (Aug. 2020), pp. 22148–22159. ISSN: 0360-3199. DOI: 10.1016/j.ijhydene.2020.06.030.

[64] Andi Mehmeti et al. “Life Cycle Assessment and Water Footprint of Hydrogen Production Methods: From Conventional to Emerging Technologies”. en. In: *Environments* 5.2 (Feb. 2018). Number: 2 Publisher: Multidisciplinary Digital Publishing Institute, p. 24. ISSN: 2076-3298. DOI: 10.3390/environments5020024.

[65] Jörg Burkhardt et al. “Hydrogen mobility from wind energy – A life cycle assessment focusing on the fuel supply”. en. In: *Applied Energy* 181 (Nov. 2016), pp. 54–64. ISSN: 0306-2619. DOI: 10.1016/j.apenergy.2016.07.104.

[66] E. Cetinkaya, I. Dincer, and G. F. Naterer. “Life cycle assessment of various hydrogen production methods”. en. In: *International Journal of Hydrogen Energy*. 2010 AIChE Annual Meeting Topical Conference on Hydrogen Production and Storage Special Issue 37.3 (Feb. 2012), pp. 2071–2080. ISSN: 0360-3199. DOI: 10.1016/j.ijhydene.2011.10.064.

[67] Gavin Dober et al. “Direct Injection Systems for Hydrogen Engines”. en. In: *MTZ worldwide* 82.12 (Dec. 2021), pp. 60–65. ISSN: 2192-9114. DOI: 10.1007/s38313-021-0720-5.

[68] Jianbing Gao et al. “Review of the backfire occurrences and control strategies for port hydrogen injection internal combustion engines”. en. In: *Fuel* 307 (Jan. 2022), p. 121553. ISSN: 0016-2361. DOI: 10.1016/j.fuel.2021.121553.

[69] Fabio Santi Mortellaro et al. “Effect of Start of Injection in a Hydrogen-Fueled DISI Engine: Experimental and Numerical Investigation”. en. In: Capri, Italy, Aug. 2023, pp. 2023–24–0015. DOI: 10.4271/2023-24-0015.

[70] L. M. Das. “7 - Hydrogen-fueled internal combustion engines”. en. In: *Compendium of Hydrogen Energy*. Ed. by Frano Barbir, Angelo Basile, and T. Nejat Veziroğlu. Woodhead Publishing Series in Energy. Oxford: Woodhead Publishing, Jan. 2016, pp. 177–217. ISBN: 978-1-78242-363-8. DOI: 10.1016/B978-1-78242-363-8.00007-4.

[71] Ho Lung Yip et al. “A Review of Hydrogen Direct Injection for Internal Combustion Engines: Towards Carbon-Free Combustion”. en. In: *Applied Sciences* 9.22 (Jan. 2019). Number: 22 Publisher: Multidisciplinary Digital Publishing Institute, p. 4842. ISSN: 2076-3417. DOI: 10.3390/app9224842.

[72] Sebastian Verhelst and James W. G. Turner. “Hydrogen-Fueled Spark Ignition Engines”. en. In: *Hydrogen for Future Thermal Engines*. Ed. by Efstathios-Al. Tingas. Green Energy and Technology. Cham: Springer International Publishing, 2023, pp. 329–351. ISBN: 978-3-031-28412-0. DOI: 10.1007/978-3-031-28412-0_8.

[73] Juan de Santiago et al. “Electrical Motor Drivelines in Commercial All-Electric Vehicles: A Review”. In: *IEEE Transactions on Vehicular Technology* 61.2 (Feb. 2012). Conference Name: IEEE Transactions on Vehicular Technology, pp. 475–484. ISSN: 1939-9359. DOI: 10.1109/TVT.2011.2177873.

[74] William Cai et al. “Review and Development of Electric Motor Systems and Electric Powertrains for New Energy Vehicles”. en. In: *Automotive Innovation* 4.1 (Feb. 2021), pp. 3–22. ISSN: 2522-8765. DOI: 10.1007/s42154-021-00139-z.

[75] Ryan O’hayre et al. *Fuel cell fundamentals*. John Wiley & Sons, 2016.

[76] Xueqin Lü et al. “A comprehensive review on hybrid power system for PEMFC-HEV: Issues and strategies”. en. In: *Energy Conversion and Management* 171 (Sept. 2018), pp. 1273–1291. ISSN: 0196-8904. DOI: 10.1016/j.enconman.2018.06.065.

[77] H. Tawfik, Y. Hung, and D. Mahajan. “Metal bipolar plates for PEM fuel cell—A review”. en. In: *Journal of Power Sources*. Selected Papers presented at the FUEL PROCESSING FOR HYDROGEN PRODUCTION SYMPOSIUM at the 230th American Chemical SocietyNational Meeting Washington, DC, USA, 28 August – 1 September 2005 163.2 (Jan. 2007), pp. 755–767. ISSN: 0378-7753. DOI: 10.1016/j.jpowsour.2006.09.088.

[78] Kangning Xiong et al. “Modeling, design, materials and fabrication of bipolar plates for proton exchange membrane fuel cell: A review”. en. In: *Applied Energy* 301 (Nov. 2021), p. 117443. ISSN: 0306-2619. DOI: 10.1016/j.apenergy.2021.117443.

[79] Yuxi Song et al. “Review on current research of materials, fabrication and application for bipolar plate in proton exchange membrane fuel cell”. en. In: *International Journal of Hydrogen Energy*. Progress in Fuel Cells 45.54 (Nov. 2020), pp. 29832–29847. ISSN: 0360-3199. DOI: 10.1016/j.ijhydene.2019.07.231.

[80] Mingchao Liang et al. “An analytical model for the transverse permeability of gas diffusion layer with electrical double layer effects in proton exchange membrane fuel cells”. en. In: *International Journal of Hydrogen Energy* 43.37 (Sept. 2018), pp. 17880–17888. ISSN: 0360-3199. DOI: 10.1016/j.ijhydene.2018.07.186.

[81] Reza Omrani and Bahman Shabani. “Review of gas diffusion layer for proton exchange membrane-based technologies with a focus on unitised regenerative fuel cells”. en. In: *International Journal of Hydrogen Energy* 44.7 (Feb. 2019), pp. 3834–3860. ISSN: 0360-3199. DOI: 10.1016/j.ijhydene.2018.12.120.

[82] Qin Chen et al. “Recent progress of gas diffusion layer in proton exchange membrane fuel cell: Two-phase flow and material properties”. en. In: *International Journal of Hydrogen Energy* 46.12 (Feb. 2021), pp. 8640–8671. ISSN: 0360-3199. DOI: 10.1016/j.ijhydene.2020.12.076.

[83] Wenbin Li, Rui Lin, and Yue Yang. “Investigation on the reaction area of PEMFC at different position in multiple catalyst layer”. en. In: *Electrochimica Acta* 302 (Apr. 2019), pp. 241–248. ISSN: 0013-4686. DOI: 10.1016/j.electacta.2019.02.003.

[84] Lishan Peng and Zidong Wei. “Catalyst Engineering for Electrochemical Energy Conversion from Water to Water: Water Electrolysis and the Hydrogen Fuel Cell”. en. In: *Engineering* 6.6 (June 2020), pp. 653–679. ISSN: 2095-8099. DOI: 10.1016/j.eng.2019.07.028.

[85] Slobodan Petrovic and Eklas Hossain. “Development of a Novel Technological Readiness Assessment Tool for Fuel Cell Technology”. In: *IEEE Access* 8 (2020). Conference

Name: IEEE Access, pp. 132237–132252. ISSN: 2169-3536. DOI: 10.1109/ACCESS.2020.3009193.

[86] S. J. Peighambardoust, S. Rowshanzamir, and M. Amjadi. "Review of the proton exchange membranes for fuel cell applications". en. In: *International Journal of Hydrogen Energy* 35.17 (Sept. 2010), pp. 9349–9384. ISSN: 0360-3199. DOI: 10.1016/j.ijhydene.2010.05.017.

[87] Y. Hu et al. "Improving the Overall Characteristics of Proton Exchange Membranes via Nanophase Separation Technologies: A Progress Review". en. In: *Fuel Cells* 17.1 (2017). _eprint: https://onlinelibrary.wiley.com/doi/pdf/10.1002/fuce.201600172, pp. 3–17. ISSN: 1615-6854. DOI: 10.1002/fuce.201600172.

[88] Steven J. Hamrock and Michael A. Yandrasits. "Proton Exchange Membranes for Fuel Cell Applications". In: *Journal of Macromolecular Science, Part C* 46.3 (Sept. 2006). Publisher: Taylor & Francis _eprint: https://doi.org/10.1080/15583720600796474, pp. 219–244. ISSN: 1532-1797. DOI: 10.1080/15583720600796474.

[89] Kenji Miyatake and Masahiro Watanabe. "Emerging membrane materials for high temperature polymer electrolyte fuel cells: durable hydrocarbon ionomers". en. In: *Journal of Materials Chemistry* 16.46 (Nov. 2006). Publisher: The Royal Society of Chemistry, pp. 4465–4467. ISSN: 1364-5501. DOI: 10.1039/B612153E.

[90] Rodney L. Borup et al. "Recent developments in catalyst-related PEM fuel cell durability". en. In: *Current Opinion in Electrochemistry*. Energy Storage • Energy Transformation 21 (June 2020), pp. 192–200. ISSN: 2451-9103. DOI: 10.1016/j.coelec.2020.02.007.

[91] Yun Wang et al. "PEM Fuel cell and electrolysis cell technologies and hydrogen infrastructure development – a review". en. In: *Energy & Environmental Science* 15.6 (June 2022). Publisher: The Royal Society of Chemistry, pp. 2288–2328. ISSN: 1754-5706. DOI: 10.1039/D2EE00790H.

[92] Tomas Tronstad et al. "Study on the use of fuel cells in shipping". In: *European Maritime Safety Agency* (2017).

[93] Johannes Hoeflinger and Peter Hofmann. “Air mass flow and pressure optimisation of a PEM fuel cell range extender system”. en. In: *International Journal of Hydrogen Energy* 45.53 (Oct. 2020), pp. 29246–29258. ISSN: 0360-3199. DOI: 10.1016/j.ijhydene.2020.07.176.

[94] I. Pielecha, W. Cieślik, and A. Szałek. “The use of electric drive in urban driving conditions using a hydrogen powered vehicle - Toyota Mirai”. EN. In: *Combustion Engines* R. 57, nr 1 (2018). ISSN: 2300-9896. DOI: 10.19206/CE-2018-106.

[95] Jiquan Han et al. “A review of key components of hydrogen recirculation subsystem for fuel cell vehicles”. en. In: *Energy Conversion and Management: X* 15 (Aug. 2022), p. 100265. ISSN: 2590-1745. DOI: 10.1016/j.ecmx.2022.100265.

[96] Toyoaki Matsuura et al. “Degradation phenomena in PEM fuel cell with dead-ended anode”. en. In: *International Journal of Hydrogen Energy* 38.26 (Aug. 2013), pp. 11346–11356. ISSN: 0360-3199. DOI: 10.1016/j.ijhydene.2013.06.096.

[97] Alberto Gomez, Agus P. Sasmito, and Tariq Shamim. “Investigation of the purging effect on a dead-end anode PEM fuel cell-powered vehicle during segments of a European driving cycle”. en. In: *Energy Conversion and Management* 106 (Dec. 2015), pp. 951–957. ISSN: 0196-8904. DOI: 10.1016/j.enconman.2015.10.025.

[98] S. Rodosik, J. -P. Poirot-Crouvezier, and Y. Bultel. “Simplified anode architecture for PEMFC systems based on alternative fuel feeding: Experimental characterization and optimization for automotive applications”. en. In: *International Journal of Hydrogen Energy* 45.38 (July 2020), pp. 19720–19732. ISSN: 0360-3199. DOI: 10.1016/j.ijhydene.2020.05.014.

[99] J. A. Prithi et al. “Studies on PEMFC Stack for SO2 Contamination at Air Cathode”. en. In: *Fuel Cells* 17.3 (2017), pp. 308–314. ISSN: 1615-6854. DOI: 10.1002/fuce.201600118.

[100] Satish G. Kandlikar and Zijie Lu. “Thermal management issues in a PEMFC stack – A brief review of current status”. en. In: *Applied Thermal Engineering*. Selected Papers from the 10th UK National Heat Transfer Conference, Edinburgh, Scotland, Septem-

ber 10-11, 2007 29.7 (May 2009), pp. 1276–1280. ISSN: 1359-4311. DOI: 10.1016/j.applthermaleng.2008.05.009.

[101] Qin Chen et al. “Thermal management of polymer electrolyte membrane fuel cells: A review of cooling methods, material properties, and durability”. en. In: *Applied Energy* 286 (Mar. 2021), p. 116496. ISSN: 0306-2619. DOI: 10.1016/j.apenergy.2021.116496.

[102] Mahdi Ramezanizadeh et al. “A review on the approaches applied for cooling fuel cells”. en. In: *International Journal of Heat and Mass Transfer* 139 (Aug. 2019), pp. 517–525. ISSN: 0017-9310. DOI: 10.1016/j.ijheatmasstransfer.2019.05.032.

[103] Satish G Kandlikar and Zijie Lu. “Fundamental research needs in combined water and thermal management within a proton exchange membrane fuel cell stack under normal and cold-start conditions”. In: *Journal of Fuel Cell Science and Technology* 6.4 (2009). Publisher: American Society of Mechanical Engineers Digital Collection.

[104] Rajesh K. Ahluwalia and Xiaohua. Wang. “Fuel cell systems for transportation: Status and trends”. en. In: *Journal of Power Sources* 177.1 (Feb. 2008), pp. 167–176. ISSN: 0378-7753. DOI: 10.1016/j.jpowsour.2007.10.026.

[105] S. Rogg et al. “Cooling Modules for Vehicles with a Fuel Cell Drive”. en. In: *Fuel Cells* 3.3 (2003). _eprint: https://onlinelibrary.wiley.com/doi/pdf/10.1002/fuce.200332108, pp. 153–158. ISSN: 1615-6854. DOI: 10.1002/fuce.200332108.

[106] Laurent Art, Matthias Jung, and Rainer Lutz. “Thermal Management Systems for Electrified Commercial Vehicles”. en. In: *MTZ worldwide* 83.12 (Dec. 2022), pp. 60–65. ISSN: 2192-9114. DOI: 10.1007/s38313-022-1401-8.

[107] Toshihiko Yoshida and Koichi Kojima. “Toyota MIRAI Fuel Cell Vehicle and Progress Toward a Future Hydrogen Society”. en. In: *The Electrochemical Society Interface* 24.2 (Jan. 2015). Publisher: IOP Publishing, p. 45. ISSN: 1944-8783. DOI: 10.1149/2.F03152if.

[108] Pengcheng Liu and Sichuan Xu. “A Progress Review on Heating Methods and Influence Factors of Cold Start for Automotive PEMFC System”. In: Apr. 2020, pp. 2020–01–0852. DOI: 10.4271/2020-01-0852.

[109] Adrian König et al. “An Overview of Parameter and Cost for Battery Electric Vehicles”. en. In: *World Electric Vehicle Journal* 12.1 (Mar. 2021). Number: 1 Publisher: Multidisciplinary Digital Publishing Institute, p. 21. ISSN: 2032-6653. DOI: 10.3390/wevj12010021.

[110] S. Panchal et al. “Cycling degradation testing and analysis of a LiFePO4 battery at actual conditions”. en. In: *International Journal of Energy Research* 41.15 (2017). _eprint: https://onlinelibrary.wiley.com/doi/pdf/10.1002/er.3837, pp. 2565–2575. ISSN: 1099-114X. DOI: 10.1002/er.3837.

[111] Manh-Kien Tran et al. “Comparative Study of Equivalent Circuit Models Performance in Four Common Lithium-Ion Batteries: LFP, NMC, LMO, NCA”. en. In: *Batteries* 7.3 (Sept. 2021). Number: 3 Publisher: Multidisciplinary Digital Publishing Institute, p. 51. ISSN: 2313-0105. DOI: 10.3390/batteries7030051.

[112] B. E. Lebrouhi et al. “Key challenges for a large-scale development of battery electric vehicles: A comprehensive review”. In: *Journal of Energy Storage* 44 (Dec. 2021), p. 103273. ISSN: 2352-152X. DOI: 10.1016/j.est.2021.103273.

[113] Giuseppe Di Luca et al. “Review on Battery State Estimation and Management Solutions for Next-Generation Connected Vehicles”. en. In: *Energies* 17.1 (Jan. 2024). Number: 1 Publisher: Multidisciplinary Digital Publishing Institute, p. 202. ISSN: 1996-1073. DOI: 10.3390/en17010202.

[114] Ryuji Kawamoto et al. “Estimation of CO2 Emissions of Internal Combustion Engine Vehicle and Battery Electric Vehicle Using LCA”. en. In: *Sustainability* 11.9 (Jan. 2019). Number: 9 Publisher: Multidisciplinary Digital Publishing Institute, p. 2690. ISSN: 2071-1050. DOI: 10.3390/su11092690.

[115] Xin Lai et al. “Critical review of life cycle assessment of lithium-ion batteries for electric vehicles: A lifespan perspective”. en. In: *eTransportation* 12 (May 2022), p. 100169. ISSN: 2590-1168. DOI: 10.1016/j.etran.2022.100169.

[116] Evelina Wikner and Torbjörn Thiringer. “Extending Battery Lifetime by Avoiding High SOC”. en. In: *Applied Sciences* 8.10 (Oct. 2018). Number: 10 Publisher: Multidisciplinary Digital Publishing Institute, p. 1825. ISSN: 2076-3417. DOI: 10.3390/app8101825.

[117] Annelis K. Breed, Daniel Speth, and Patrick Plötz. “CO2 fleet regulation and the future market diffusion of zero-emission trucks in Europe”. en. In: *Energy Policy* 159 (Dec. 2021), p. 112640. ISSN: 0301-4215. DOI: 10.1016/j.enpol.2021.112640.

[118] *COMMUNICATION FROM THE COMMISSION TO THE EUROPEAN PARLIAMENT, THE EUROPEAN COUNCIL, THE COUNCIL, THE EUROPEAN ECONOMIC AND SOCIAL COMMITTEE AND THE COMMITTEE OF THE REGIONS REPowerEU Plan*. en. 2022.

[119] *COMMUNICATION FROM THE COMMISSION TO THE EUROPEAN PARLIAMENT, THE COUNCIL, THE EUROPEAN ECONOMIC AND SOCIAL COMMITTEE AND THE COMMITTEE OF THE REGIONS A hydrogen strategy for a climate-neutral Europe*. en. 2020.

[120] European Commission et al. *Analysis of material efficiency aspects of personal computers product group*. Publications Office, 2018. DOI: doi/10.2788/89220.

[121] Jang-Yeon Hwang, Seung-Taek Myung, and Yang-Kook Sun. “Sodium-ion batteries: present and future”. en. In: *Chemical Society Reviews* 46.12 (2017). Publisher: Royal Society of Chemistry, pp. 3529–3614. DOI: 10.1039/C6CS00776G.

[122] Jürgen Janek and Wolfgang G. Zeier. “Challenges in speeding up solid-state battery development”. en. In: *Nature Energy* 8.3 (Mar. 2023). Number: 3 Publisher: Nature Publishing Group, pp. 230–240. ISSN: 2058-7546. DOI: 10.1038/s41560-023-01208-9.

[123] Yin Hua et al. “Estimation of State of Charge for Two Types of Lithium-Ion Batteries by Nonlinear Predictive Filter for Electric Vehicles”. en. In: *Energies* 8.5 (May 2015). Number: 5 Publisher: Multidisciplinary Digital Publishing Institute, pp. 3556–3577. ISSN: 1996-1073. DOI: 10.3390/en8053556.

[124] Niraj Kumar et al. “Recent Advanced Supercapacitor: A Review of Storage Mechanisms, Electrode Materials, Modification, and Perspectives”. In: *Nanomaterials* 12.20 (Oct. 2022), p. 3708. ISSN: 2079-4991. DOI: 10.3390/nano12203708.

[125] Ziyou Song et al. “A comparison study of different semi-active hybrid energy storage system topologies for electric vehicles”. en. In: *Journal of Power Sources* 274 (Jan. 2015), pp. 400–411. ISSN: 0378-7753. DOI: 10.1016/j.jpowsour.2014.10.061.

[126] Pratim Bhattacharyya et al. “A Modified Semi-Active Topology for Battery-Ultracapacitor Hybrid Energy Storage System for EV Applications”. In: *2020 IEEE International Conference on Power Electronics, Smart Grid and Renewable Energy (PESGRE2020)*. Jan. 2020, pp. 1–6. DOI: 10.1109/PESGRE45664.2020.9070531.

[127] Poonam et al. “Review of supercapacitors: Materials and devices”. In: *Journal of Energy Storage* 21 (Feb. 2019), pp. 801–825. ISSN: 2352-152X. DOI: 10.1016/j.est.2019.01.010.

[128] Emilia M. Szumska. “Electric Vehicle Charging Infrastructure along Highways in the EU”. en. In: *Energies* 16.2 (Jan. 2023). Number: 2 Publisher: Multidisciplinary Digital Publishing Institute, p. 895. ISSN: 1996-1073. DOI: 10.3390/en16020895.

[129] Simon Stebbins et al. “Characterising Green Light Optimal Speed Advisory trajectories for platoon-based optimisation”. In: *Transportation Research Part C: Emerging Technologies* 82 (Sept. 2017), pp. 43–62. ISSN: 0968-090X. DOI: 10.1016/j.trc.2017.06.014.

[130] Robert J. Lempert et al. “The societal benefits of vehicle connectivity”. In: *Transportation Research Part D: Transport and Environment* 93 (Apr. 2021), p. 102750. ISSN: 1361-9209. DOI: 10.1016/j.trd.2021.102750.

[131] Joshua E. Siegel, Dylan C. Erb, and Sanjay E. Sarma. “A Survey of the Connected Vehicle Landscape—Architectures, Enabling Technologies, Applications, and Development Areas”. In: *IEEE Transactions on Intelligent Transportation Systems* 19.8 (Aug. 2018). Conference Name: IEEE Transactions on Intelligent Transportation Systems, pp. 2391–2406. ISSN: 1558-0016. DOI: 10.1109/TITS.2017.2749459.

[132] Lili Miao, John Jethro Virtusio, and Kai-Lung Hua. “PC5-Based Cellular-V2X Evolution and Deployment”. en. In: *Sensors* 21.3 (Jan. 2021). Number: 3 Publisher: Multidisciplinary Digital Publishing Institute, p. 843. ISSN: 1424-8220. DOI: 10.3390/s21030843.

[133] Sasan Jafarnejad et al. “A Car Hacking Experiment: When Connectivity Meets Vulnerability”. In: *2015 IEEE Globecom Workshops (GC Wkshps)*. Dec. 2015, pp. 1–6. DOI: 10.1109/GLOCOMW.2015.7413993.

[134] Ilja Nastjuk et al. “What drives the acceptance of autonomous driving? An investigation of acceptance factors from an end-user’s perspective”. In: *Technological Forecasting and Social Change* 161 (Dec. 2020), p. 120319. ISSN: 0040-1625. DOI: 10.1016/j.techfore.2020.120319.

[135] William Payre, Stewart Birrell, and Andrew Martin Parkes. “Although autonomous cars are not yet manufactured, their acceptance already is”. In: *Theoretical Issues in Ergonomics Science* 22.5 (June 2021), pp. 567–580. ISSN: 1463-922X. DOI: 10.1080/1463922X.2020.1836284.

[136] “J3016C: Taxonomy and Definitions for Terms Related to Driving Automation Systems for On-Road Motor Vehicles - SAE International”. In: (June 2021).

[137] Anne Faxér et al. “Shared Shuttle Services S3–phase 2”. In: (2021).

[138] Eliane Horschutz Nemoto, Ines Jaroudi, and Guy Fournier. “Introducing Automated Shuttles in the Public Transport of European Cities: The Case of the AVENUE Project”. en. In: *Advances in Mobility-as-a-Service Systems*. Ed. by Eftihia G. Nathanail, Giannis Adamos, and Ioannis Karakikes. Advances in Intelligent Systems and Computing. Cham: Springer International Publishing, 2021, pp. 272–285. ISBN: 978-3-030-61075-3. DOI: 10.1007/978-3-030-61075-3_27.

[139] Vanessa Stange, Matthias Kühn, and Mark Vollrath. “Manual drivers’ experience and driving behavior in repeated interactions with automated Level 3 vehicles in mixed traffic on the highway”. In: *Transportation Research Part F: Traffic Psychology and Behaviour* 87 (May 2022), pp. 426–443. ISSN: 1369-8478. DOI: 10.1016/j.trf.2022.04.019.

[140] Akhil Shetty et al. “Safety challenges for autonomous vehicles in the absence of connectivity”. In: *Transportation Research Part C: Emerging Technologies* 128 (July 2021), p. 103133. ISSN: 0968-090X. DOI: 10.1016/j.trc.2021.103133.

[141] Panagiotis Papantoniou, V. Kalliga, and Constantinos Antoniou. “How Autonomous Vehicles May Affect Vehicle Emissions on Motorways”. en. In: *Advances in Mobility-as-a-Service Systems*. Ed. by Eftihia G. Nathanail, Giannis Adamos, and Ioannis Karakikes. Advances in Intelligent Systems and Computing. Cham: Springer International Publish-

ing, 2021, pp. 296–304. ISBN: 978-3-030-61075-3. DOI: 10.1007/978-3-030-61075-3_29.

[142] Hannah R.M. Pelikan. "Why Autonomous Driving Is So Hard: The Social Dimension of Traffic". In: *Companion of the 2021 ACM/IEEE International Conference on Human-Robot Interaction*. HRI '21 Companion. New York, NY, USA: Association for Computing Machinery, Mar. 2021, pp. 81–85. ISBN: 978-1-4503-8290-8. DOI: 10.1145/3434074.3447133.

[143] Manzoor Ahmed Khan et al. "A journey towards fully autonomous driving - fueled by a smart communication system". In: *Vehicular Communications* 36 (Aug. 2022), p. 100476. ISSN: 2214-2096. DOI: 10.1016/j.vehcom.2022.100476.

[144] Liuhui Zhao and Andreas A. Malikopoulos. "Enhanced Mobility With Connectivity and Automation: A Review of Shared Autonomous Vehicle Systems". In: *IEEE Intelligent Transportation Systems Magazine* 14.1 (Jan. 2022). Conference Name: IEEE Intelligent Transportation Systems Magazine, pp. 87–102. ISSN: 1941-1197. DOI: 10.1109/MITS.2019.2953526.

[145] A. Musa et al. "A review of model predictive controls applied to advanced driver-assistance systems". In: *Energies* 14.23 (2021). DOI: 10.3390/en14237974.

Chapter 3

Holistic assessment of zero CO_2 powertrains for road transport sector

According to the international regulation framework analyzed in chapter 2, future regulations will limit the CO_2 emissions to zero (or $<$1-2g/kWh) with different timeframes for light-duty and heavy-duty vehicles. Many future powertrain architectures can comply with those limits relying on electric drive, batteries, H2-ICE and FC. Electrification is often seen as the best overall solution. Very often H2 is criticized by its turn-around relatively low efficiency, but the decarbonization problem is complex and need an on holistic approach to evaluate the optimal solution. In this context, arises the need of a reliable methodology for the preliminary holistic assessment of different powertrain architectures. The single methods adopted in this chapter are not novel but their combination is unique and represent a novelty. In particular, the quasi-static approach to vehicle modeling is a well established method for fast analysis oriented to fuel and energy consumption assessments [1]. On the other side, numerous studies have been carried out analyzing various specific aspects, including techno-economical indicators [2] and life cycle assessment [3], comparing existing vehicles. On one side this choice allows to deepen the study and potentially obtain more reliable and accurate calculations as referring to an existing vehicle. On the other side often very different vehicle are compared as the choice is limited to market availability, resulting in a not fair comparison of vehicle with different range, cost or performance. Some studies exists, as [4], in which an holistic comparison is proposed adopting typical vehicle data and with some not clear working hypothesis. Within this

work a combination of known methodology (i.e., vehicle quasi-static modeling, performance indicator calculations,...) have been combined with a proper rationale to propose an holistic analysis methodology capable of analyze various vehicle solutions. With a such methodology it is possible to select a tailored solution for each use case scenario with the objective of a fast and effective transport sector decarbonization. Thus this chapter present the development of the methodology to cope with this goal and the coding in a simulation framework. The novelty of this work is the integration of a physics-based vehicle model in the framework which allows to make sensitivity analysis and capture variables of interest trends. The methodology can be further extended in the future to deal also with non-road vehicles. The novel simulation framework are then adopted to analyze four vehicle classes (light, medium and heavy duty and light commercial vehicles) and the results are reported and discussed in the following.

3.1 Methodology

In this section all the most relevant numerical methods, assumptions and adopted data are reported for clearly define how the reported results was obtained and ensure their reproducibility. A schematical representation of the main steps of the works is shown in Figure 3.1.

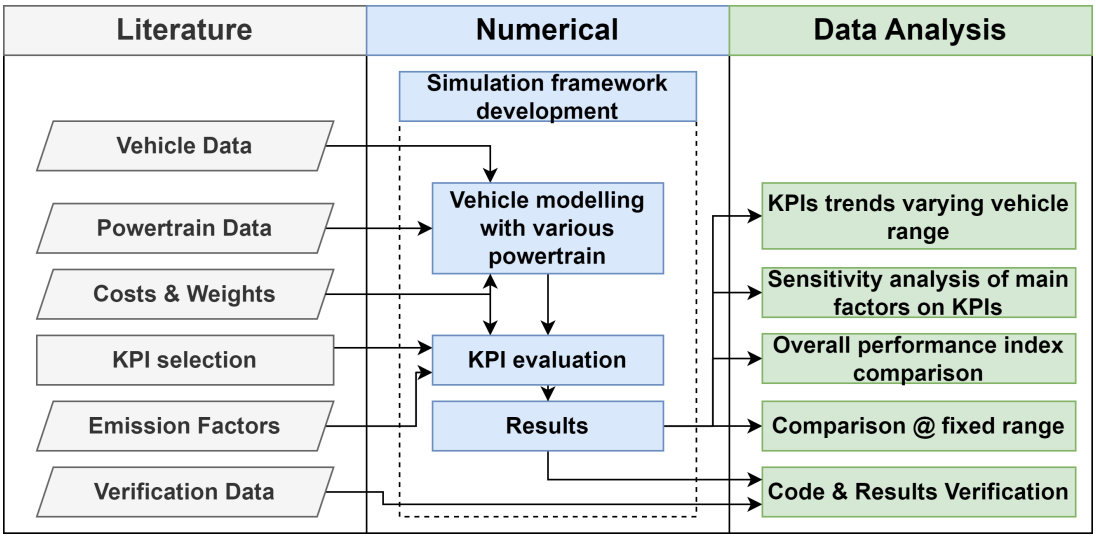

Figure 3.1: Investigation method workflow

The assessment proposed has required an intensive literature survey to gather all the request data. These, not exclusively, include state-of-art KPIs of the powertrain components, includ-

ing weight and cost data, together with vehicle data, reference scenarios, emission factors and process efficiencies. This phase is essential to fulfill the comparison proposed in a clearer and most precise manner. The researches has been carried out on the main scientific databases and Original Equipment Manufacturers (OEMs) and manufacturers technical resources. Exploiting those information, various parametric models have been developed each with a specific powertrain architecture. Those model has been integrated in ad-hoc developed simulation framework which includes algorithms for the estimation of some performance indicators such as TCO, WTW energy consumption, WTW GHGs emissions. The analysis for each vehicle class have been involved different powertrain architectures which are shown in Figure 3.2. These includes H_2-fueled Internal Combustion Engine Vehicles (H2ICEV), Fuel Cell Eletric Vehicle (FCEV), BEV and two hybrid series configurations, one exploiting H2-ICE and the other FC as range extender. In this context, FCEV referrers to a vehicle which electrical power request is demanded to FC, the battery act only has energy buffer in the transient phases, and it is characterized by low energy capacity. On the other side, all the other configurations, characterized by higher battery size and lower FC maximum power have been considered as Fuel Cell Hybrid Electric Vehicle (FCHEV).

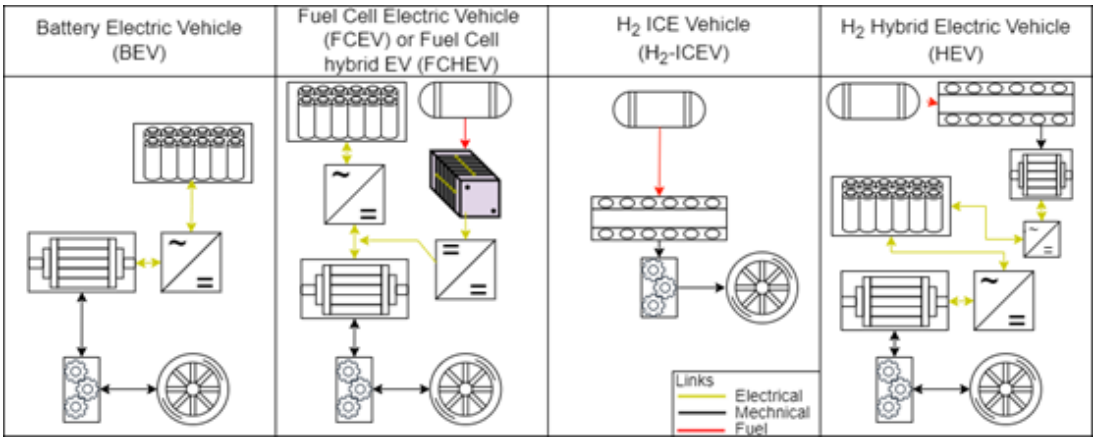

Figure 3.2: Vehicle architecture analysed

The hybrid powertrain architecture requires a control strategy. In this work a charge-sustaining approach is adopted, with FC and H2-ICE following with a slow dynamics the power demand of the vehicle while operating in optimal conditions thanks to off-line optimal map computation. The battery is used for high-power demanding driving conditions and braking energy recovery. In the following details on the simulation framework and algorithms (section

3.1), and the main assumption and data (3.2) are reported. In the end, in section 3.3, a code verification using literature data are reported.

3.1.1 Simulation Framework

For the numerical analyses of the different powertrain configurations and vehicle layouts the Quasi-Static-Simulation (QSS) Toolbox developed by the University of Zurich was adopted [5]. The toolbox, based on Simulink environment, offer energy-oriented vehicle modeling capability using traditional graphical object modeling with a backward approach. Modifications have been implemented in the toolbox block to fulfill the research objectives of this work. The main ones are synthetically reported in the following.

- Introduction of new driving cycles and its parametrization
- Modified vehicle model and driving cycle to introduce the road slope
- Additional controllers for fuel cell vehicle regenerative braking, hybrid vehicle range extender strategy, gear shift
- Modified ICE and EM model and data
- Parametric gear box with variable number of gears
- Minor modifications for additional outputs

Based on a backward approach and considering only longitudinal motions, the adopted toolbox has the advantage of extremely low computational time, making it ideal for optimisation, sizing, and sensitivity analysis regarding energy-related global aspects. It is well suited for build up around a simulation framework which includes the definition of all parameters and calculations of performance indicators with post-processing to further elaborate and collect all relevant data in a single output file. The framework has been developed in the MATLAB functions and it is an updated version of the one used in previous work by the authors [6]. The vehicle model expressed by means of equation 1, include the following terms: i) the traction force F_T; ii) the rolling resistance. $C_r mg\cos(\phi)$; iii) the aerodynamic force $0.5\rho V^2 AC_d$; and iv) the parallel component of gravitational force due to the slope $mg\sin(\phi)$.

$$m\dot{V} = F_T - C_r mg\cos(\phi) - 0.5\rho V^2 A C_d - mg\sin(\phi) \tag{3.1}$$

A schematic view of one developed model is reported in Figure 3.3. One part of the models, the one on the left in the figure, is the same for every type of vehicle, which is composed by a driving cycle block, which gives instantaneous information about speed, acceleration, and grade of the road. These are given to the vehicle block, in which the total traction force is calculated by the imposed driving cycle and adopting a standard formulation regarding the acting force on a vehicle [7]. Then for every powertrain configuration a gearbox with its controller is considered. The remaining part are dependent on the specific powertrain architecture considered, as it includes Electric Motor (EM), FC, ICE, BP and additional specific controllers.

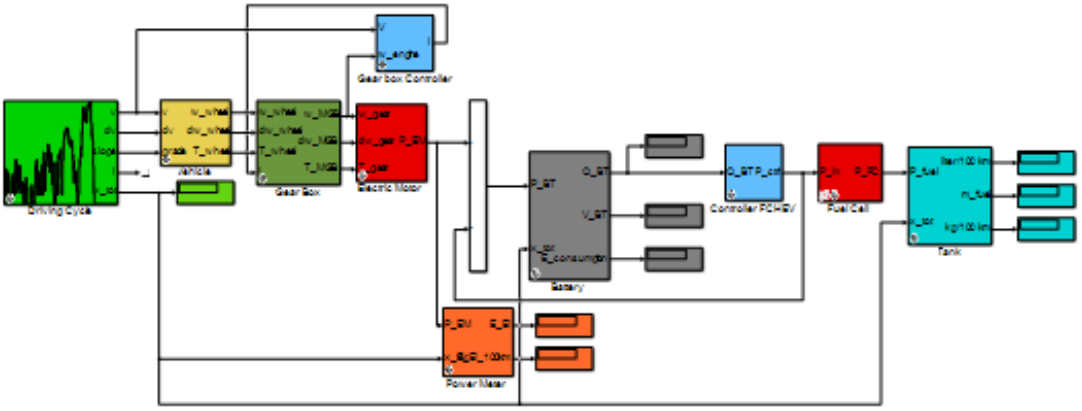

Figure 3.3: Schematic view of the FCHEV model

The model is included in a simulation framework including the various vehicle models developed and all the pre and post processing, which are synthetically reported in Figure 3.4. Given the input file, in pre-processing, the model evaluates according to a set of different driving cycle, using a point mass model, the speed, power and torque requirements at the wheel.

Given EM or ICE and gearbox specifications an optimal gear map is obtained covering all the relevant speed versus wheel torque datum as follows.

$$Opt_{Gear}(V; T_{wheel}) = \max_{n_{gear}} \eta_{EM/ICE}(V, T_{wheel}, n_{gear}) \tag{3.2}$$

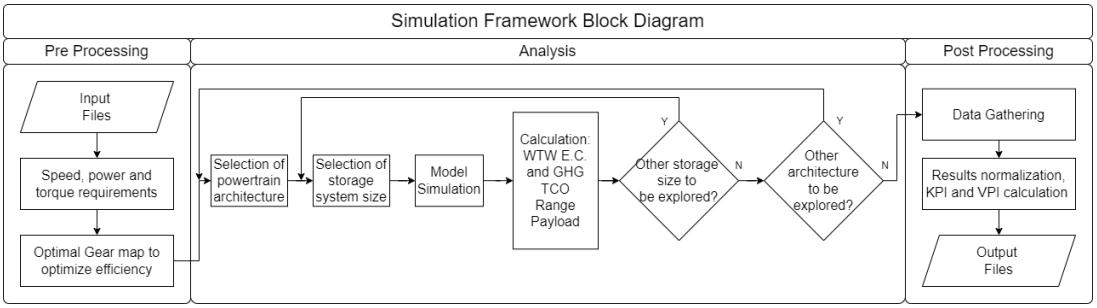

Figure 3.4: Schematic work flow of the simulation framework

Usually, in real vehicle implementation of automatic transmission system, the optimal gear map is coded as a function of throttle and vehicle speed, which allows to explore all the lookup table [33]. In this work the wheel torque instead of the throttle is adopted since the non-causality of the model, which do not consider the throttle command. For ICE in hybrid powertrain configuration the control strategy adopt an optimal operating condition map as function of the request power. The optimal operating point, defined by the engine speed and torque is defined as follows

$$Opt_{OP}(P) = \max_{\omega,T} \eta_{ICE}(\omega, T) \tag{3.3}$$

Subjected to the following constraint

$$|\omega T - P| \leq \varepsilon \tag{3.4}$$

In this way, for each power an optimal point ensuring the maximum ICE efficiency is achieved, and given to the Hybrid Electric Vehicle (HEV) supervisory controller. The FCHEV don't require an optimal map, as for a given power only one operating point exists for a FC system. Then according to goals, different architecture are analyzed and for each a sweep of the energy storage system capacity (BP or H2 tank size) is done. For each run from the model results the main key performance indicator, as discussed in the section 2.2, are calculated and stored. The WTW energy consumption and GHG, and TCO, if not differently reported, have been calculated as the average value on a vehicle trip covering a distance equal to its range. This implies that for HEV and FCHEV vehicle during a share of the trip the vehicle is powered by the battery and for the remaining part from hydrogen tank. This seems a reasonable assumption assuming to adopt a tailored solution for each mobility scenario considered. In the end, a report

file is generated.

3.1.2 Performance evaluation

Energy consumption on driving cycle and range are directly output of the models. In this section the vehicle weight estimation, which is done prior to the simulation and the calculations of the KPIs from model outputs are reported and discussed.

Vehicle Weight

The Unladen Vehicle Weight (UVW) was estimated by the vehicle weight without the powertrain and adding the various mass contribution of the main powertrain component. The weight is estimated according to equation 3.5.

$$W = W_0 + W_{ED} + W_{ICE} + W_{GB} + W_{H2,tank} + W_{FC} + W_{BP} \tag{3.5}$$

where W_o is the baseline weight without propulsion system, W_{ED} is the weight of the electric drive, W_{ICE} the thermal powertrain weight, W_{GB} the gearbox weight, $W_{H2,tank}$ is the weight of the CH2 tank, W_{FC} is the weight of FC system and W_{BP} is the weight of BP. For all the powertrain configurations the regression for the gearbox from [8] have been adopted and it is the following one.

$$W_{GB} = 1.723(i_{g,max} T_{max})^{0.439} \eta_g^{0.219} \tag{3.6}$$

Where $i_{g,max}$ is the maximum gear ratio of the gearbox, T_{max} the maximum torque explicable by the EM or ICE, and n_g is the number of gear ratios of gearbox. All the other weight are calculated by means of a specific weight multiplied by the relative quantity (i.e., size, capacity, power) except for W_{ED} and W_{ICE} for Light Duty Vehicle (LDV) vehicles. For these values obtained by analysing and comparing manufacturers data have been employed.

Total Cost of Ownership

The TCO represent one of the most important indicators considered within this study. In fact, it can drives the adoption of a vehicle solution from industries and commercial activities, as it

is strictly related to their expenditure in the vehicle operating life [9]. TCO has been calculated through the following equation 3.7, derived from the literature [10]. This equation is interesting in comparison to others because it considers all the most relevant contributions of TCO, neglecting only opportunity costs related to charging and refueling.

$$TCO = (PP - RP) + FC + \left(\frac{rP}{1 - (1+r)^{-N}} N - P \right) + IC + MC + T - S + DS + RC \quad (3.7)$$

Where MSRP is the manufacturer suggested retail price, RP the reselling price, FC is the fuel cost in the ownership period, r is the monthly interest rate, N the number of payment rates, P the borrowed amount, IC the insurance cost, MC the maintenance cost, T the taxes, S the subsidies, DS the driver salary, and RC the replacement cost. The calculation is the done assuming a vehicle operating lifetime T_{veh_life} and a lifetime traveled distance d_{veh_life}. The Manufacturer Suggested Retail Price (MSRP) is calculated starting from the vehicle cost without powertrain plus the estimated cost of powertrain and ESS. A simplified method based on yearly depreciation rate has been adopted to assess the residual value of the vehicle after the ownership period. The calculations are done assuming the vehicle operating lifetime T_(veh_life) and the lifetime traveled distance d_(veh_life). For the MSRP calculation, the manufacturing cost is estimated assuming the vehicle cost without the powertrain plus the cost of the powertrain and ESS. Then, the MSRP it is calculated based on the vehicle estimated production cost, assuming to be 1.11 times the vehicle production cost for LCVs [11]. For RP, a simplified method based on yearly depreciation rate (Y_D) has been adopted to assess the residual value of the vehicle after the ownership period. This simplified model assumes that an exponential form of $(1-Y_D)^{(t_{years})}$ can describe in adequate manner the vehicle depreciation in a t_{years} time frame. The insurance cost is estimated based on the following annual premium regression based on vehicle MSRP [12].

$$\text{Annual premium [€]} = 0.0089 \cdot MSRP + 221 \quad (3.8)$$

The maintenance costs are taken from the literature for each powertrain. Greatest uncertainty regards the H2ICEV due to its lack on the market. The taxes have been neglected. This assumption is justified by the nature of the zero-carbon vehicles investigated in this work and the relative policies that favor their diffusion [13]. The subsidies are neglected since they can

substantially vary with the country in which the vehicles are registered. Moreover, the zero-carbon emissions of all the analyzed configurations make reasonable the subsidies equal for all, and due to the comparative nature, can be neglected without affecting the trend of the results. Following similar though also the driver cost has been neglected due to very different salary conditions across the countries with no direct dependence from vehicle powertrain. The mathematical model has been validated, comparing the results with various TCO calculators available online. Thus, the quality of the results is mainly affected by uncertainty and goodness of the parameter values adopted.

Additionally, the replacement costs have been included and calculated according to vehicle lifetime, system durability and usage. For light duty applications actually the fuel cell as already meet durability target potentially allowing to reach the end of life of the vehicle and so it is not considered [14]. For HD applications three commercial available systems report 2e4 (PowerCell Heavy Duty System 100), 2.5e4 (Ballard FCmove™ HD) and 3e4 (Ballard FCveloCity®-HD) hours of system durability. For simplicity's sake, the FC system is considered to be fully replaced after 2.5e4 which is the mean value of the found durability. The same approach is adopted for the battery pack, which is considered replaced after a given number of cycles. In particular 1000 cycles are assumed for LDV and LCV while 1500 is adopted for Heavy Duty Vehicle (HDV), due to the lower DoD adopted. It can be highlighted that an additional contribution to the TCO can be added: the opportunity costs. These are related to the idle time of a vehicle forced to stop its operation to recharge or refill the ESS, can be relevant in some use cases as taxi fleets, freight transport company and in general for commercial activities [15]. In this work these cost are neglected due to the difficulties of make an estimation valid for the vehicle rather than for the application itself. In the following, at least if explicitly defined differently, the specific TCO is presented, normalized by the distance traveled in the vehicle lifetime.

Well-to-Wheel calculations

The WTW efficiency is calculated based on literature assumptions, regarding the electricity transmission and charging losses, and hydrogen production and distribution chain. For the electricity it was assumed that the Direct Current (DC) fast charging efficiency is 87%, according

to the experimental data of a 50kW system [16]. Additionally, a grid transmission loss of 3.5% is assumed according to [17]. This result in global efficiency from the power plant to battery of about 84 %. Regarding hydrogen, a reasonable net efficiency in terms of LHV production process is 70% for the SMR [18] and in a range from 50% to 80% for the electrolysis [19]. A value of 70% has been used in the work, which is representative of both production technologies. Besides the production hydrogen compression and transport losses are considered. For the compression to 700 bar in CH2 systems it is assumed an energy consumption of about 2.8 kWh/kgH2 [20]. Then, a transport consumption of 0.68 kWh/kgH2 it has been considered assuming diesel truck acting on 200km range. Adding these contributions, a total value of about 51 kWh/kgH2 is obtained. A decade ago, Ahluwalia et al. reported 61 kWh/kgH2 [21]. Considering the possible variation due to production efficiency and transport to the refilling station a mean value of 56 kWh/kgH2 has been adopted in this work. Similar thought based on literature data are made for the GHG calculations. Regarding the electricity, assuming EU27 energy mix, the GHG emission factors are 229 and 275 gCO2eq/kWh in 2020 and 2021, respectively [22]. The value of 2020 has been adopted, since the 2021 value has been strongly influenced by the current high gas prices due to the complex international situation. For comparison, in some calculation electricity GHG emission factor of 370 [23] and 540 gCO2eq/kWh [24] for the US and China, respectively. Regarding GHG emissions factor for hydrogen the EU consider low-carbon hydrogen one which have less than 2.4 kgCO2eq/kg [25]. In EU, currently the major share of hydrogen production is based on steam methane re-forming without carbon capture, storage and utilization systems with an GHG emission factor of about 8.9 kgCO2eq/kg [26]. It is assumed for transport the use of truck in gaseous form, which have an impact of 2.5 kgCO2eq/kg [27], while the compression it is assumed as 0.65 kgCO2eq/kg , based on EU energy mix and the previous reported requested energy. The assumption made are slightly optimistic for both electric and hydrogen vehicles, as the actual production of green hydrogen is negligible and for electricity marginal emission factors can be more realistic of today operations. However as the explored solutions are not available yet on the market, these assumption

Charging and Refilling Time

The charging time of the battery is estimated by a dedicated Simulink model implementing the same battery model of the vehicle. A charging profile is given according to the considered maximum recharging power and the time necessary to recharge the battery the DoD considered is taken as output. The imposed charging profile is chosen based on the considered recharge power and the threshold of 150 kW, as reported in Figure 5. The shown profile have been estimated by available technical data.

Regarding hydrogen refueling the following worst case linear regression has been adopted (see equation 8), based on data from OEMs and considering limits and protocols of the SAE J2601 for LDV [28] and HDV [29].

$$t_{refill} = 600 + 25Tank_{kg,H_2}[s] \tag{3.9}$$

Performance indicators

The choice of the optimal powertrain solution for a target vehicle class can be seen as a multi objective optimization problem. Many possible techniques, relative to decision-making theory and operational research, can be adopted to define an optimal solution. In this manuscript, in the results analysis, two different techniques have been employed. The first one, is a qualitative one, and it is named Pugh matrix or decision-matrix method. In this case, a set of options (i.e., in the specific study powertrain layouts) are compared to a baseline case, reporting if according to each metric the option offers equal (= or 0), worse (- or -1) or better (+ or +1) performances. The sum gives a fast evaluation of the better option, but it lacks of quantify the differences in performances, and treats all the KPIs as equally relevant. To partially address those issued, a second method a quantitatively one has been proposed and adopted. Once all the configuration and results are gathered a post-processing phase is carried out evaluating a normalized performance indicators for each KPI. The scaling is done in manner that once scaled each KPI are in a range from -1 to 1, where higher value indicates a better performance. The scaling is made according to the KPI minimum ($KPI_{i,min}$) and maximum values ($KPI_{i,max}$) over all the powertrain architecture for a specific vehicle class. In this manner, the globally worst case has value -1 and the best one +1. The following formula have been adopted.

$$KPI_{i,scaled} = 2\frac{KPI_i - KPI_{i,min}}{KPI_{i,max} - KPI_{i,min}} - 1 \text{ or } 1 - 2\frac{KPI_i - KPI_{i,min}}{KPI_{i,max} - KPI_{i,min}} \tag{3.10}$$

The first equation has been adopted when an higher value of KPI is better, and the latter when it is worse. Then to have only one Vehicle Performance Indicator (VPI) all the selected KPI are summed up according to equation 10.

$$VPI = \Sigma_{i=1}^{n_{KPI}} \alpha_i \cdot KPI_{i,scaled} \tag{3.11}$$

Where α_i is a weighting factor, to tune the desired behaviour of the indicator, preferring to give more importance to certain KPIs. Since each KPIs can be neglected or their relative importance varies according to specific customer/manufactures need, in this work to show the methodology all the considered KPI are assumed to be equally relevant (all the $\alpha_i = 1$).

3.2 Reference data, assumption and boundary conditions

In this section all the most relevant value adopted are reported to improve the independent reproducibility of the results and to make a clear comparison, highlighting all the assumptions made. The data required are numerous and hard to obtain as most are available only by manufacturers or through expensive and complex experimental characterization studies. The vehicle related data, as drag and rolling coefficients, are less important due to the comparative nature of this study. However, for powertrain related parameters particular attention has been paid to depict the most robust and technology neutral picture of the adopted parameters. However, as the technology chosen are all novel and under development relevant variation can be expected also in short time frames. In such a case, the methodology developed can be readopted updating the new parameter values. The analysis carried out are based on the adoption of a reference driving cycle to assess the vehicle performances. For LDV the Worldwide harmonized Light vehicles Test Cycle (WLTC) class 3 driving cycle has been used, which is part of the Worldwide harmonized Light-duty Test Procedures (WLTP) [30]. For Medium Duty Vehicle (MDV) and HDV the Vehicle Energy Consumption calculation TOol (VECTO) driving cycles have been chosen. VECTO is the official simulation platform for the assessment of CO_2 emissions and fuel consumption of the EU [31]. The VECTO driving cycle are distance-based and different based on

heavy-duty application [32], so a conversion to a time versus speed trace has been carried out to use with the developed models assuming a target acceleration versus the grade. For the simulations efficiency map for EM and ICE are needed together with FC polarization curve and battery characteristics curves. The FC i-V polarization curve is reported in panel A of Figure 3.5. The curve has obtained by FC theory adopting Butler–Volmer equation, Area-Specific-Resistance and logarithmic concentration losses and neglecting leakage current [33]. In this manner a continue curve has been obtained in line with high performance FC polarization curve available in the literature. For BP a 21700 (INR-21700-P42A) cell has been chosen as reference. The characteristic curves from manufacturer datasheet together with the model fit adopted in this work is shown in panel B of Figure 3.5. The model assure good accuracy in the working range from SoC 0.1 to 0.9, successfully modeling the losses due to the current drawn. The EM efficiency maps is shown in Figure 3.6. The LD one is representative of a 85 kW and 270 Nm motor [34], while for the HD EM it has been adopted from [35] relative to a 240 kW and 3800 Nm torque capable motor. The adopted H2-ICE efficiency map are reported in 3.7. The LD engine map has been derived from [36] and it is relative to a 2.0 litres 4 cylinder Direct Injection (DI) engine, while the HD one from a 7.8 litres 6 cylinder engine [37]. The most of the parameters adopted regarding the vehicle modeling is reported in Table 3.1. For TCO calculation a series of assumption according to the literature has been made, which are summarized in Table 3.2.

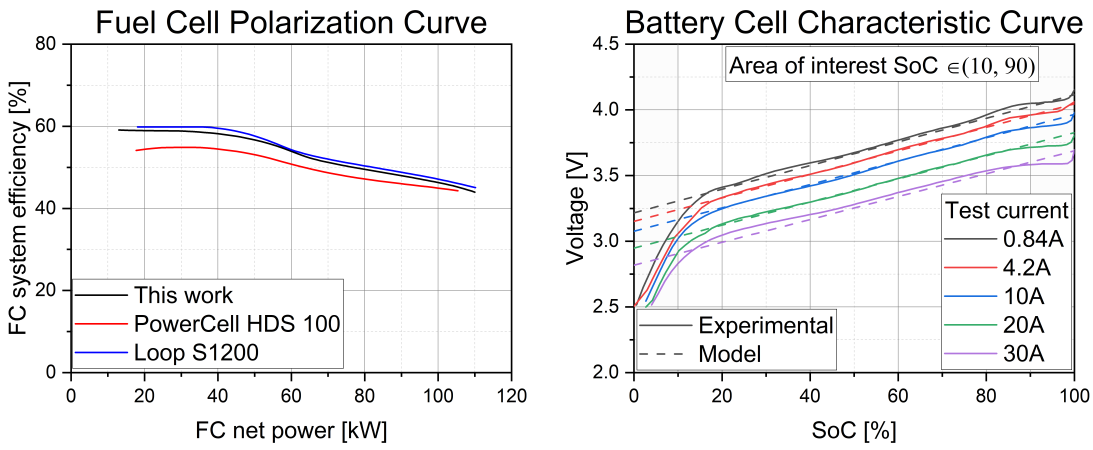

Figure 3.5: Panel A) FC system efficiency curve for an FC size of 110 kW; Panel B) Adopted cell characteristic curves

	LDV	MDV	HDV	Unit
	Vehicle Weight			
W_0	700	4000	12000	[kg]
W_{ED}	320	Linear	Linear	[kg]
W_{ICE}	250	Linear	Linear	[kg]
W_{ICE_HEV}	190	Linear	Linear	[kg]
BP gravimetric energy density	200[38]	200[38]	200[38]	[Wh kg^{-1}]
FC gravimetric energy density	2.6 [39]	2.6	2.6	[kg kW^{-1}]
CH2 gravimetric energy density	14[40]	14	14	[kg kgH_2^{-1}]
BP volumetric energy density	450[41]	450[41]	450[41]	[litre kW^{-1}]
FC volumetric energy density	7[39]	7[39]	7[39]	[litre kW^{-1}]
CH2 volumetric energy density	25[42]	25[42]	25[42]	[litre kgH_2^{-1}]
	Vehicle specifications			
Driving cycle	WLTC c3	VECTO UD	VECTO LH	n/a
Cr	0.011[34]	0.08[43]	0.006[44]	[-]
Cd	0.29[34]	0.54[43]	0.73[44]	[-]
Frontal area A	2.23[34]	10.1[43]	9.75[44]	[m^2]
Wheel diameter d_w	0.63[34]	0.73[43]	0.98[44]	[m]
Rotating mass d_w	5	3	3	
	BP specifications			
Battery Nominal Voltage	360	360	720	[V]
Battery DoD	90	80	75	[%]
Battery Charging Power	100	100	350	[kW]
	FC specifications			
FC size	85	200	370	[kW]
FC number of cell	400	600	1000	[-]
FC (FCHEV) size	14	100	160	[kW]
FC (FCHEV) number of cell	400	600	1000	[-]
	EM specifications			
EM max power	57	180	360	[kW]
EM max torque	180	2850	5700	[Nm]
EM number of gears	1	5	7	[-]
	ICE specifications			
ICE displacement	0.8	6.0	13	[dm^3]
ICE max power	66	216	566	[kW]
ICE max torque	153	1250	2690	[Nm]
ICE number of gears	6	9	14	[-]
ICE (HEV) displacement	0.5	1.8	2.5	[dm^3]
ICE (HEV) max power	41	80	108	[kW]
ICE (HEV) max torque	96	372	512	[Nm]

Table 3.1: Vehicle and component specifications

	LDV	MDV	HDV	Unit
	General costs			
Vehicle lifetime	10[45]	12[46]	12[47]	[years]
Vehicle lifetime distance	1.6e5[45]	3.2e5[46]	1.2e6[47]	[km]
MSRP markup factor	1.4[11]	1.11[11]	1.11[11]	[-]
Loan duration	[48]	3[48]	3[48]	[years]
Loan MSRP percentage	80 [48]	80[48]	80[48]	[%]
Loan yearly interest	7.0[48] 7.0[48]	7.0[48]	7.0[48]	[%]
Insurance	Fitting[12]	Fitting[12]	Fitting[12]	[€/year]
Tax	0[13]	0[13]	0[13]	[€/year]
Subsidies	0[39]	0[39]	0[39]	[€]
EV Yearly depreciation	11.6 [49]	11.0[12]	21.0[50]	[%/year]
ICEV yearly depreciation	10.4 [49]	11.0[12]	21.0[50]	[%/year]
	Maintenance costs			
BEV maintenance cost	0.037[12]	0.0157[12]	0.176[51]	[€/km]
FCEV maintenance cost	0.046 [12]	0.0157[12]	0.200 [51]	[€/km]
HEV maintenance cost	0.056 [12]	0.224[12]	0.188 [51]	[€/km]
ICEV maintenance cost	0.062[12]	0.262[12]	0.200 [51]	[€/km]
	Component costs			
H_2 ICE cost	40[52, 53]	80 as HD	80[54, 55]	[€/kW]
EM + inverter cost	20 half HD	35 as HD	35 [32, 44, 56]	[€/kW]
Battery Pack cost	160[57]	160[57]	160[57]	[€/kWh]
CH_2 tank 700bar cost	750[58–60]	750[58–60]	750[58–60]	[€/kW]
FC system cost	200[56, 61]	450 as HD	450 [58, 59, 62]	[€/kW]
	Replacement			
FC system durability	2.5e4	2.5e4	2.5e4	[hours]
BP cycling capability	1000 [63]	1000[63]	1500[63]	[-]
	Fuel costs			
H_2 refueling cost	10.5[64]	10.5[64]	10.5[64]	[€/kg]
Battery recharging cost	0.3[65]	0.5[65]	0.5[65]	[€/kWh]

Table 3.2: Total cost of ownership model parameters adopted

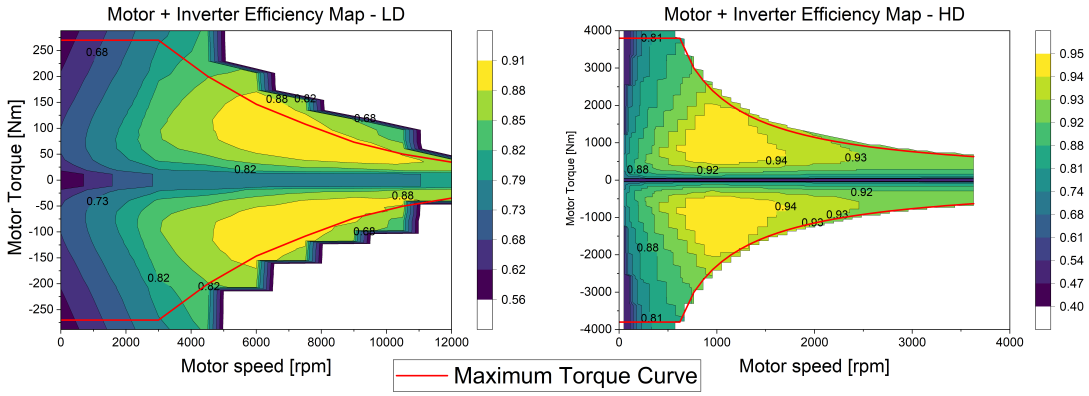

Figure 3.6: Adopted EM efficiency map including inverter losses

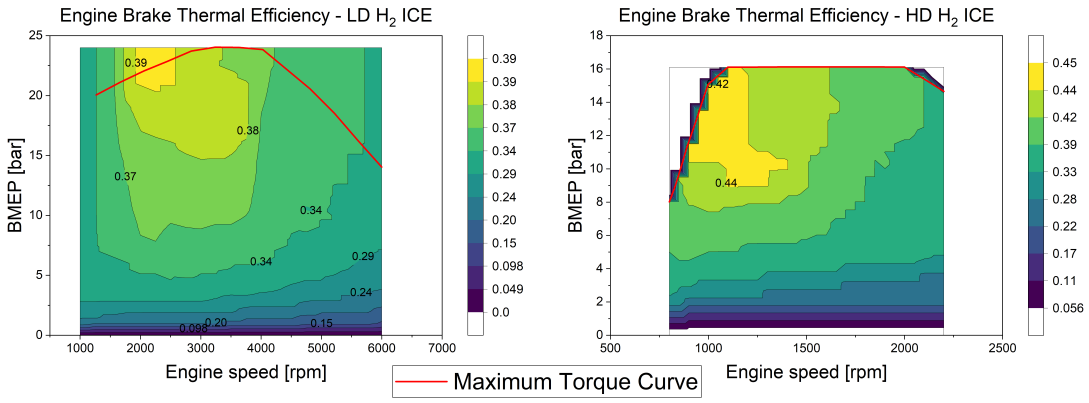

Figure 3.7: Adopted ICE efficiency maps

3.3 Code verification

In this section, the developed numerical procedure and vehicle models, are verified. Since the work scope is not to model a specific target vehicle, but to make reasonable comparison of the various vehicle classes varying their energy storage capacity, the code verification has been made in two different steps: validation of the results of few specific test cases and verification of trend against available data. These are gathered from OEMs datasheet, scientific and technical literature. In Figure 3.8 the comparison of the model results in terms of hydro-gen consumption and energy consumption are reported and compared with experimental data from Argonne National Laboratory. The panel on the left, refers to the first generation of the Toyota Mirai [66], a FCEV. The right panel refers to a BEV, the Volkswagen e-Golf [67]. The results shown that the trend are captured, with an error usually lower than 10%, and generally within ±5%. At the

same ESS capacity it results in a similar error also in range estimation. It should be highlighted, that the auxiliary systems are not considered, as thermal management system, heating systems and electronic loads, which can be the most important contribution to these differences. Moreover, the engine/motor maps and fuel cell characteristics curves, although real are not specific of these two vehicles. These thought makes the measured error good enough for the scope of this work.

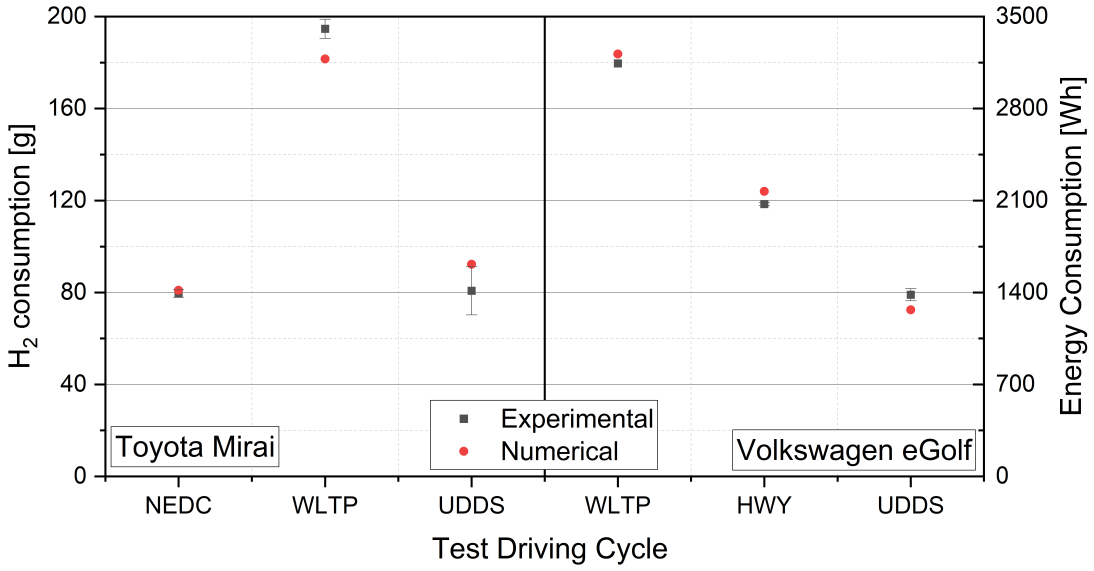

Figure 3.8: Energy consumption validation for LD vehicles

In Figure 10, instead a global comparison among numerous experimental data reported by vehicle manufacturers are compared with the sweep in terms of battery capacity varying the chassis weight. The technical data are then grouped in three class of weight and assigned to one of the numerical curves. It is possible to see that the code can predict quite accurately, the vehicle range capability and energy consumption over a wide range of configurations.

Verified range and vehicle Tank to Wheel (TTW) energy consumption the WTW energy consumption, GHG and TCO estimation are as good as the assumed hypothesis and adopted value taken from specific literature, as discussed before and which are not directly affected by the vehicle model itself. For HDV vehicle it is more difficult found data on vehicle range respect to LDV. However it has been possible to compare the range versus battery size trend of the model with some OEM data as reported in Figure 3.10 showing a discrete match. In terms of energy consumption values of 110 - 125 kWh/100km can be found from OEMs [68], which are in lines

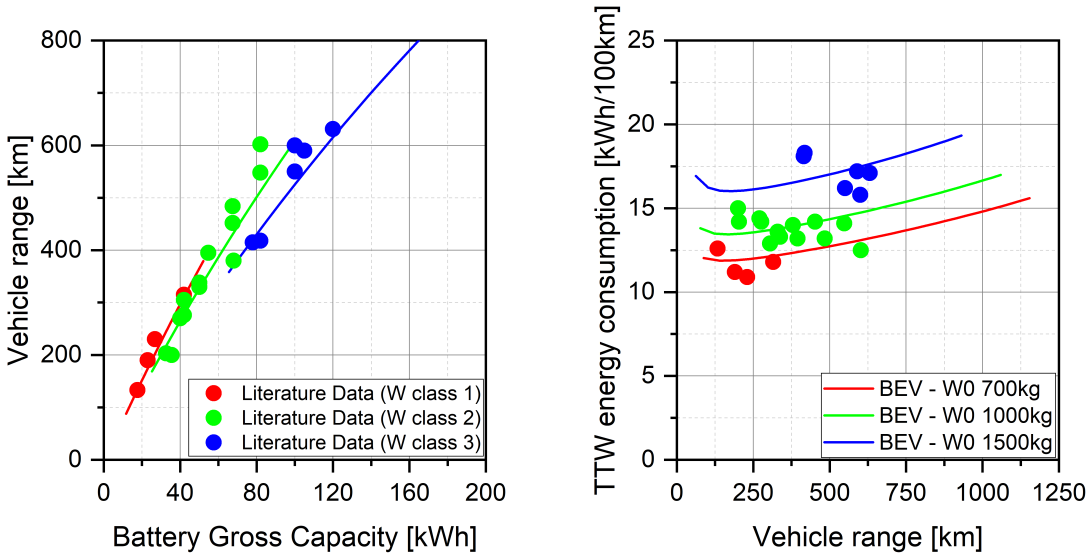

Figure 3.9: Energy consumption and range estimation verification LD BEVs

with the predicted one from the model.

Additionally, it should be highlighted that TCO estimation are itself difficult to compare among different sources, due to different hypothesis, reference context, vehicle usage. A comparison of TCO calculation using the method of this work and online available tools of a H2ICEV is reported in Figure 3.11, reporting both TCO and its breakdown in terms of absolute costs. In particular, for comparison, tools from International Energy Agency (IEA) [69], US Department of Energy United States Department of Energy (US-DOE) [70], and IVECO [71] have been used. The IEA and IVECO tools, allows to modify many parameters of the TCO model, although the choice of the values is made in discrete manner. So, adopting the same value assumed in this work, to check the calculation procedure, the results are equal to the one calculated in this work. The difference for IVECO tools is mainly linked to discretization of the values, and for IEA to the maximum yearly maintenance cost and maximum reselling value. Although these two differences, compensate the relative errors resulting in less than 0.5k€difference on TCO with respect the proposed code. The US-DOE tools, is less prone to user modifications, and doesn't distinguish the various yearly operating costs and doesn't consider the vehicle reselling at the end of the ownership period. This makes its estimation around 20% higher. Although there will be possible shift in the vehicle cost without power-train, the comparative relation among the solutions is correct as the adopted value taken from literature

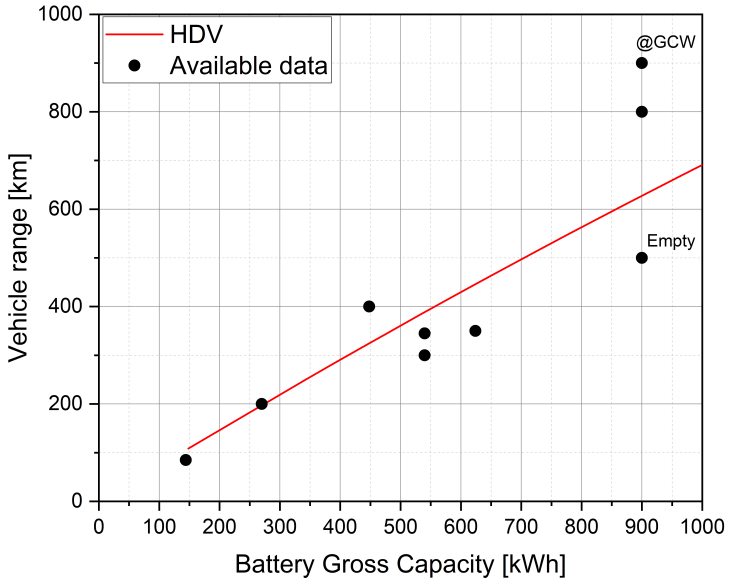

Figure 3.10: Range estimation verification for HD BEVs

are representative of a real case scenario. At this point, the results given by the numerical code developed is considered consistent with reality giving quite good estimations for comparison purposes.

3.4 Results and discussions

A comparative analysis of the various powertrains for the three vehicle classes considered is reported in this section, adopting the methodology discussed in the previous section. The four test vehicle class results (LDV, Light Commercial Vehicle (LCV), MDV, and HDV) are presented concerning their typical use-case scenario and adopted KPIs and characteristics reported in Table 3.1 and 3.2. The analysis has been carried out with a sensitivity on the energy storage capability of the vehicle under analysis. For vehicles with both electrical and hydrogen ESS two analysis has been carried out, fixing one size and let varying the other ESS. In that case, the nomenclature adopted is to write as subscript the ESS kept constant. In that manner, HEV_{BP} means HEV with battery pack size fixed, and HEV_{H_2} indicates the HEV with fixed hydrogen tank size. The adopted values and range of variations are reported for the three considered class of vehicles in Table 3.

After the analysis of the performance of the LDV (section 3.4.1), LCV (section 3.4.2), MDV

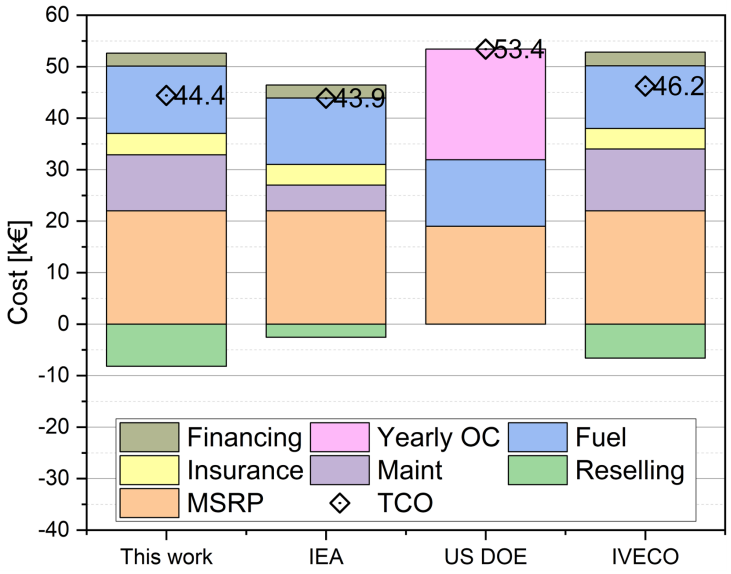

Figure 3.11: TCO verification for an H2ICEV using different tools

Vehicle type	**LDV**		**LCV**		**MDV**		**HDV**	
Vehicle architecture	**BP size [kWh]**	**H_2 tank** [kg]	**BP size [kWh]**	**H_2 tank** [kg]	**BP size [kWh]**	**H_2 tank** [kg]	**BP size [kWh]**	**H_2 tank** [kg]
BEV	5-200	n/a	20-200	n/a	10-400	n/a	100-1500	n/a
FCEV	2	0.2-20	3	1-10	4	0.5-30	30	4-100
H2ICEV	n/a	0.2-20	n/a	1-10	n/a	0.5-30	n/a	4-100
HEV_{H_2}/HEV_{BP}	30	0.2-20	n/a	n/a	4 80	0.5-30	3 250	4-100
$FCHEV_{H_2}/FCHEV_{BP}$	5-200	n/a	n/a	n/a	10-400	5	100-1500	10

Table 3.3: Energy storage range considered in this work for the various vehicle types.

(section 3.4.3) and HDV (section 3.4.4) in the baseline scenario, according to the base data discussed in sections 2.2 and 2.3, different sensitivity analyses have been carried out to assess quantitatively how the changes in boundary conditions affect the vehicle performances. In this work, the proposed sensitivity analyses have regarded the emission factors for electricity and hydrogen, which affects the WTW GHGs (section 3.4.5), the electricity and hydrogen costs (section 3.4.6), which affects the economic convenience of a particular solution. However the methodology proposed can be adopted to analyze further parameters sensitivities such as powertrain efficiency, energy storage system densities, and improvement of aerodynamic performances as examples. In section 3.5, a summary of the main results is given.

3.4.1 Light duty

In this section, the results obtained relative to the LDV are presented. The main results obtained are reported in Figure 3.12. The BEV energy consumption is the best in class over the whole explored ranges and varying from about 16 to 23 kWh/100km. For range higher than 250 km $FCHEV_{BP}$ and $FCHEV_{H2}$ show efficiency similar to BEV (from 15 to 28 kWh/100km). FCEV (23 to 26 kWh/100km), H2ICEV (32 to 36 kWh/100km), HEV_{BP} (17 to 46 kWh/100km) and HEV_{H2} (39 to 24 kWh) offer generally higher energy consumption, but there are some ESS sizes which offers interesting performances (i.e., HEV_{BP} for 200 km range).

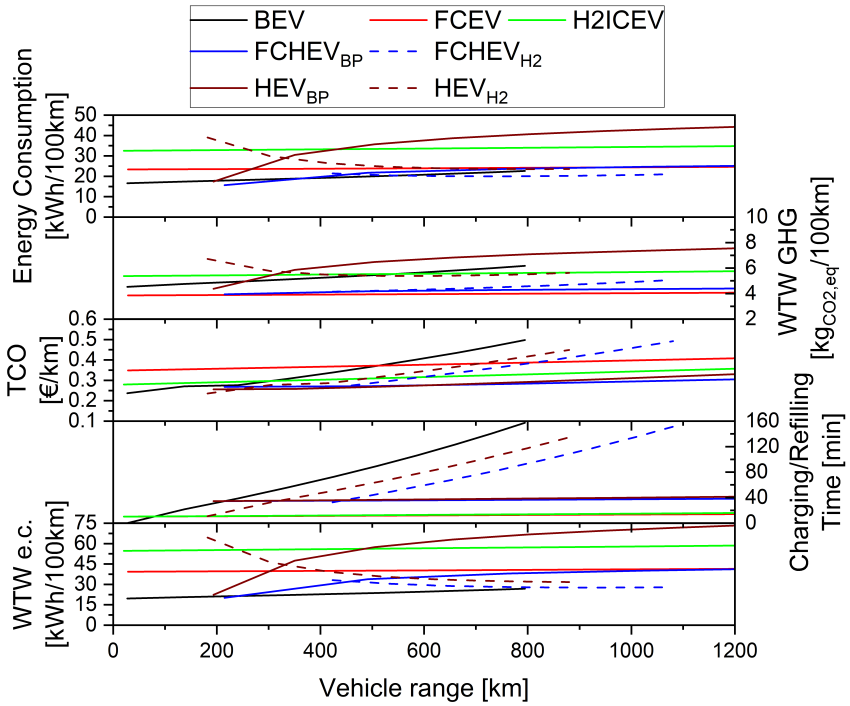

Figure 3.12: KPIs for Light Duty Vehicles

Looking to the WTW GHGs emissions during vehicle operations, the FCEV offers lower emissions (3.8 to 4.3 kgCO2,eq/100km) and very similar to the ones of $FCHEV_{BP}$ and $FCHEV_{H2}$. This results are linked to the assumption made regarding the emission factors (see section 2.2), and a sensitivity analysis on those values are presented in section 3.4. The BEV (4.5 to 6.2 kgCO2,eq/100km) thanks to the higher efficiency is better than H2ICEV (5.4 to 5.9 kgCO2,eq/100km) for range lower than 400 km. HEV_{H2} (6.7 to 5.6 kgCO2,eq/100km) for ranges higher than 500 km also offers values in line with H2ICEV. HEV_{BP} (4.4 to 7.8 kgCO2,eq/100km)

suffer of higher weight and low battery capacity and offer competitive emissions only for low range vehicles (¡300 km). In terms of TCO for range below 200km the BEV offers lower TCO, of about 0.25 €/km, this range can be sufficient for city car applications. For higher ranges the $FCHEV_{BP}$ and HEV_{BP} offer lower TCO varying from about 0.26 €/km at 200km to 0.31€/km at 1000 km. H2ICEV also offer interesting economic performance, due to lower cost powertrain and despite higher fuel consumption, with TCO varying from 0.28 to 0.40 €/km. The FCEV has globally the higher TCO, mainly due to the high FC system cost, which ranges from 0.35 to 0.38 €/km. BEV suffers high battery cost and weight, which makes the TCO increasing sharply, reaching over 0.5 €/km around ranges of 800 km. The charging and refilling time is a clear advantage of hydrogen powertrain, however setting a time limits can be used to understand what range can be achieved within a certain stop of fixed duration. With the assumption of 100kW electric charging and setting a limit of 1 hour, BEV can achieve about 350 km compared to 450 km of HEV_{H2} and 650 km of $FCHEV_{H2}$. The other powertrain solutions doesn't have range limit within 1 hour stop. The WTW energy consumption is strictly related to the already discussed vehicle energy consumption through the assumption of section 2.2. For pure electric or pure hydrogen configuration the WTW energy consumption is 19% and 64% higher than TTW, respectively. For hybrid powertrain according to the ESS size the coefficient varies among those two limits. However, the trend are similar and in a comparative way no added value is giv-en, and so for the other classes only the TTW is presented. A Pugh matrix relative to LDV case is presented in Table 3.4.1, considering as decision KPI the energy consumption, the WTW GHGs emission, the TCO and the charging time. To make possible the comparison among the various powertrains three ranges have been selected of interest for the LDV class (250, 500 and 750km). The BEV is taken as reference. $FCHEV_{BP}$ results for the first two range the layout with more advantages, +2 for both 250 and 500 km range. At 500km it is equaled by $FCHEV_{H2}$. For the 750 km range the $FCHEV_{H2}$ with +4 points is the best solutions. In the scenario assumed, and for the selected ranges, BEV has only advantages in terms of energy consumption, but with penalties on charging time and TCO.

According to the methodology explained in section 2, the VPI curves for LDV are reported in Figure 3.13, to assess quantitatively the vehicle performances. The VPI shown includes the contribution of all the four KPIs considered in the previous Pugh matrix. This methods conferm

Range	Metric	BEV	FCEV	H2ICEV	HEV_{BP}	HEV_{H2}	$FCHEV_{BP}$	$FCHEV_{H2}$
250 km	EC	=	-	-	-	-	+	n/a
	GHG	=	+	-	=	-	+	n/a
	TCO	=	-	-	+	+	+	n/a
	C/R time	=	+	+	+	+	+	n/a
	sum	0-ref	0	-2	1	0	4	n/a
500 km	EC	-	-	-	-	-	-	-
	GHG	=	+	=	-	=	+	+
	TCO	=	=	+	+	+	+	+
	C/R time	=	+	+	+	+	+	+
	sum	0-ref	1	1	0	1	2	2
750 km	EC	-	-	-	-	-	-	+
	GHG	=	+	+	-	+	+	+
	TCO	=	+	+	+	+	+	+
	C/R time	=	+	+	+	+	+	+
	sum	0-ref	2	2	0	2	2	4

Table 3.4: Pugh matrix for the assessment of light duty vehicle varying range.

the Pugh matrix results. Below 200km the BEV has the higher VPI values, but it is overcomed by the FCHEVBP for ranges of 250km and above. From 400 to 600 km the VPIs of $FCHEV_{H2}$ is only slightly lower than $FCHEV_{BP}$. For extremely high range (above 850km) the second best VPI is offered by the FCEV, mainly linked to the best GHG and charging time, relatively low energy consumption, despite very high TCO.

3.4.2 Light Commercial Vehicles

In this section, the main results of the analysis are carried out. In the first section, the results in terms of vehicle energy consumption on TTW basis, Payload, TCO, and WTW GHGs are reported. Then, in the following section, the fuel, electricity, and powertrain cost sensitivity analyses are presented and critically discussed.

Reference scenario analysis

The results obtained are reported, analyzing the three powertrain configurations in the reference scenario. Energy consumption, as a function of the vehicle range capability is shown in Figure 3.14 at both UVW and Maximum Permissible Laden Weight (MPLW) load conditions. The electric propulsion efficiency offers a higher conversion efficiency. The energy consumption of BEV

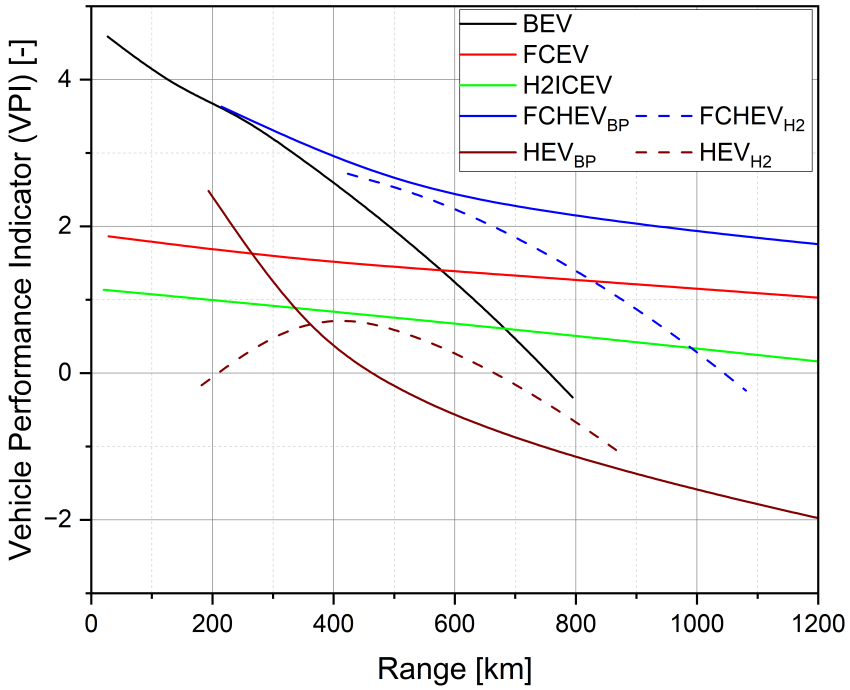

Figure 3.13: VPI for Light Duty Vehicles

ranges between 30-40 kWh/100km. In the case of FCEV it ranges between 50 and 70 kWh/100 km, and in the case of ICEV, within the interval of 65-90 kWh/100 km. The BEV shows a different trend with respect to FCEV and ICEV. This is due to the increment in the energy storage system (ESS) weight to achieve higher ranges. In particular, the additional weight to increase the range for BEV is about one order of magnitude greater than the other powertrain solutions due to the lower energy density of batteries with respect to hydrogen storage systems. This led to a sensible reduction of the payload. Indeed, at about 900 km of range, the UVW and MPLW are coincident, showing the unfeasibility of the solution.

Additional analyses are conducted as a function of the maximum vehicle range capability. In particular, in Figure 3.15 the payload, vehicle range, WTW GHGs, and corresponding TCO1 are reported as a function of the energy stored (battery or tank). Regarding the stored energy, for hydrogen, the reported value is evaluated by the LHV. Regarding the payload, the optimal powertrain solution is the H2ICEV followed by the FCEV. BEV suffers from the battery pack weight, especially for higher vehicle ranges. However, BEV shows comparable payload for ranges below 100 km range. TCO of BEV shows a higher variation due to the battery cost per kWh stored. Additionally, it is characterized by some discontinuities for vehicle ranges below

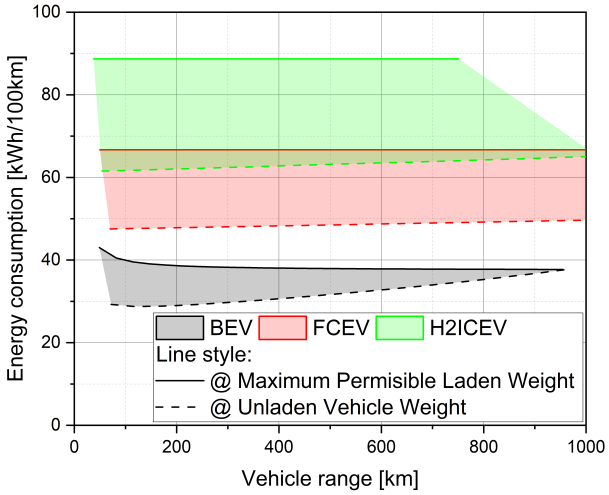

Figure 3.14: Energy consumption varying the maximum vehicle ranges

100 km. These are due to the need of battery replacement, which is no more required increasing the battery size. This is explained by the reduction of the needed charging and discharging cycles in the vehicle operating life as the kilometer driven by the LCV is kept constant. For low quantities of energy stored, below 100 kWh, BEV is the most economically viable solution. For higher ranges, above 100 km, hydrogen-based vehicles overperform BEVs. Looking at the GHG on WTW basis, the H2ICEV suffers from the relatively low conversion efficiency of the ICE. For the considered scenario, as described in the above section, the BEV and FCEV offer comparable impacts in terms of GHGs.

A breakdown of the total vehicle TCO is reported for both UVW (Figure 3.16) and MPLW (Figure 3.17) cases. Vehicle configurations with three range capabilities of 250, 500, and 750 km have been processed. As a general results it is worth nothing that insurance, maintenance, and financing costs are slightly affected by the increased ESS. The MSRP share raise sensibly with BEV range, passing from 42 to 51%. In particular, the ESS rise to 50% of the MSRP share in case of 750 km range. In general, the hydrogen storage has a lower impact on the MSRP. It is worth highlighting as the breakdown of FCEV and H2ICEV does not change much with the range. About half of FCEV TCO is due to the MSRP of the vehicle, which is relatively high due to the FC system cost itself.

The most influential factors for the total TCO are the MSRP, the fuel, and electricity costs. Based on these considerations, a sensitivity analyses on the main factor influencing TCO was

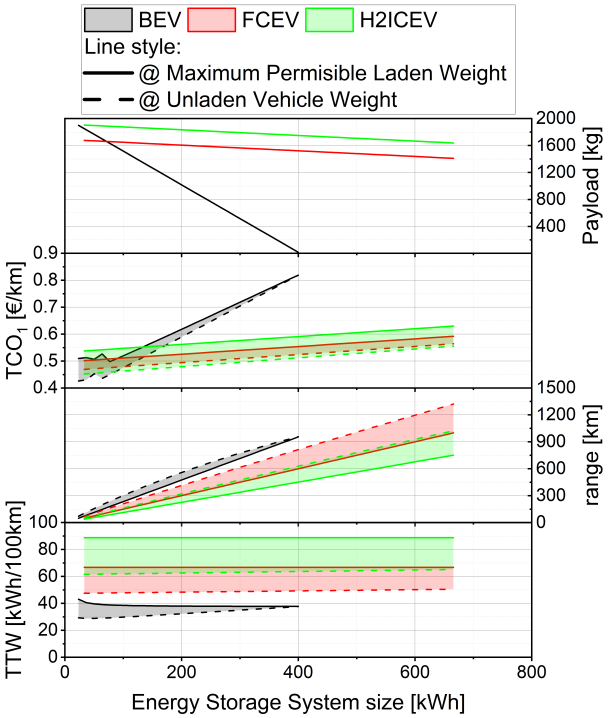

Figure 3.15: KPIs for Light Commercial Vehicles

carried out.

Fuel and electricity cost sensitivity

Due to different reasons such as natural disasters, international crises, and policies, the feedstocks purchase prices can vary sensibly over the years, as history shows for oil [72], or as happened lately for natural gas [73]. Since the fuel and electricity costs represent a relevant share of the TCO (ranges between 20 and 40%), it is important to analyze how their variations influence the most economical powertrain solution. A sensitivity analysis has been carried out, making the parameter sweep as reported in Table 3.4.2.

Parameter	Considered range
Electricity cost [€/kWh]	0.05 - 1.5
Hydrogen cost [€/kg]	0.25 - 30

Table 3.5: Range of variation considered for the fuel and electricity cost sensitivity

The sweep range has been chosen according to the cost reported in technical and scientific

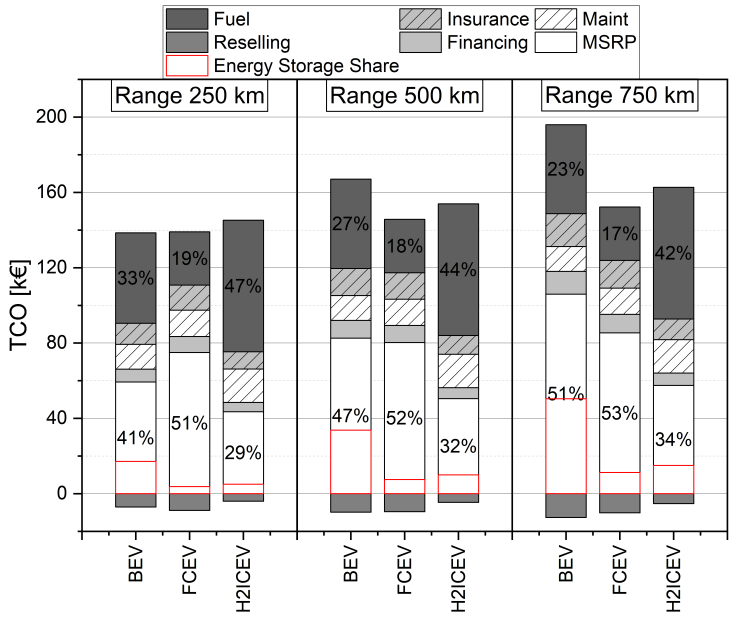

Figure 3.16: TCO breakdown for different vehicles ranges at UVW

literature and service providers' data. The obtained ranges were extended a little and rounded. In particular, regarding the hydrogen cost, the International Council on Clean Transportation (ICCT) has made available a report on the on-site production cost of hydrogen. Considering Italy as a reference scenario with production from solar energy, it is possible to achieve about 8.5 €/kg with a reduction to about 4.8 €/kg by 2030 [64]. The US-DOE reports an actual feasible production cost of 5 $/kg with the goal of reaching 1 $/kg in a decade [74]. Actually, in the case of H2 refueling station, a price of around 10-15 €/kg has recently been registered in Italy. However, peaks up to 25 €/kg have been seen in Europe. The Levelized Cost Of Hydrogen (LCOH) using solar energy is reported to be in the range of 1 to 2.7 €/kg in 2021 [75]. This can be indicative of a scenario in which a delivery company deploys a commercial hub with a private hydrogen refueling station. However, to this cost, additional infrastructure for hydrogen storage, compression, and delivery should be considered, together with the electricity needed and the transport, representing about 50% of the production costs [76]. Regarding electric recharge, in Italy the Enel X Way recharging service offers AC (i.e., slow charging) at 0.58 €/kWh and fast DC and HPC recharging at 0.95 and 0.99 €/kWh. In Figure 3.19, the results of the analysis are reported in terms of TCO for four different vehicle range capabilities.

The domains in which each powertrain offers the lowest TCO are reported. For the sake

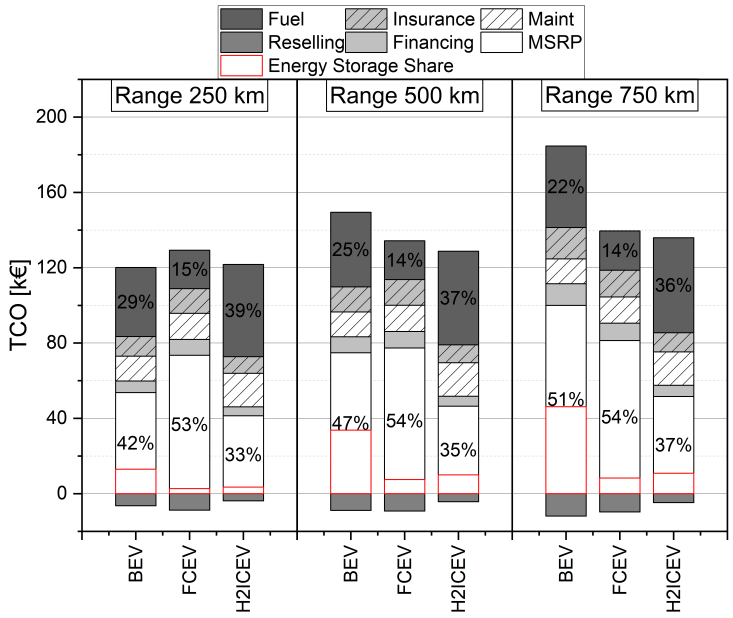

Figure 3.17: TCO breakdown for different vehicles ranges at MPLW

of comparison, a point indicating the reference scenario analyzed in the previous section is added, with bars of variation based on the cost trend in Europe in the last years. The dashed lines, outlining the various region of the graph, are interpolated from the grid points in which the analysis have been carried out. It is possible to see a triple interface point, which drifts towards lower hydrogen and electricity cost for a higher range. In particular, the coordinate of this point moves from 0.95 €/kWh and 12 €/kg at 150 km vehicle range to 0.15€/kWh and 10 €/kg at 750 km. For electricity cost higher than 0.9 €/kWh makes hydrogen solutions highly competitive. The cost of hydrogen drives which hydrogen powered powertrain, FCEV or H2ICEV, offer the lowest TCO. The higher cost of hydrogen makes FCEV most suitable as its improved efficiency allows it to overcome the higher MSRP. For scenarios in which hydrogen is available at a low cost, H2ICEV becomes the best solution from an economic point of view.

Powertrain component cost sensitivity

According to the MSRP breakdown shown in previous sections, the energy storage system, especially the battery pack, and the FC system had a major share in the vehicle cost. Battery cost has become, from 2013 to 2022, about five times cheaper due to large manufacturer investments [77]. Fuel cells, actually, are characterized by a very high cost-to-power ratio. However,

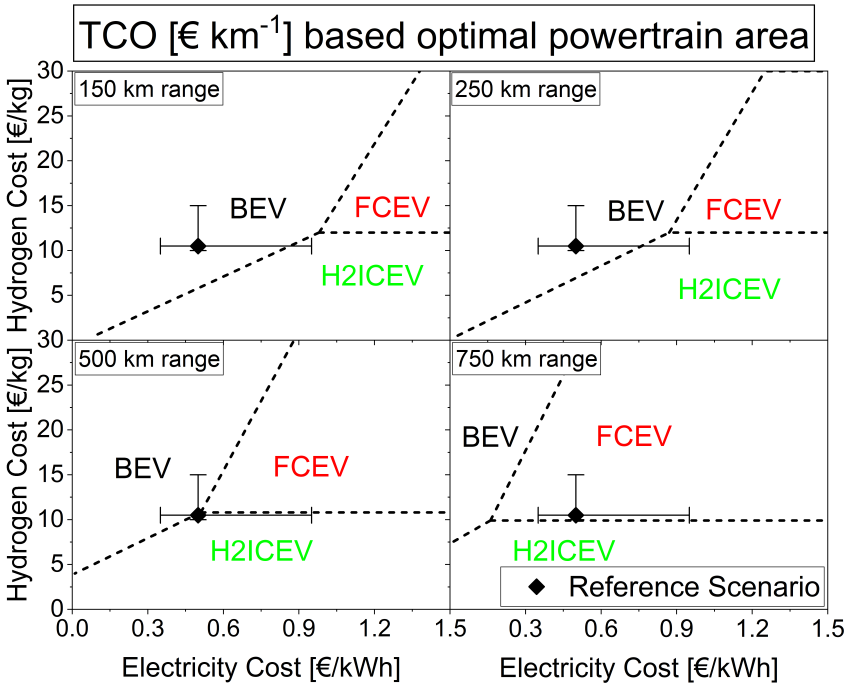

Figure 3.18: TCO sensitivity analysis to the fuel and electricity costs

many studies agree that a substantial reduction can be achieved in the next decade with proper industry investment and large-scale production [50]. These considerations make it interesting to do a sensitivity analysis of the most expensive vehicle components to figure out the optimal powertrain configuration in terms of TCO for different countries and future cost scenarios. The sensitivity analysis has been carried out varying the parameter in the range reported in table 3.4.2.

Parameter	**Considered range**
Battery pack cost [€/kWh]	30 - 600
FC system cost [€/kW]	30 - 600
H2 tank cost [€/kg]	100 - 1500

Table 3.6: Range of variation considered for the fuel and electricity cost sensitivity

The analysis has shown that the specific hydrogen tank cost has only slightly effects on the TCO optimal powertrain. Thus, due to difficulties in graphically representing all the results, only the analysis of the battery pack and FC specific cost is reported. The results in terms of kilometric TCO are reported in Figure 3.19.

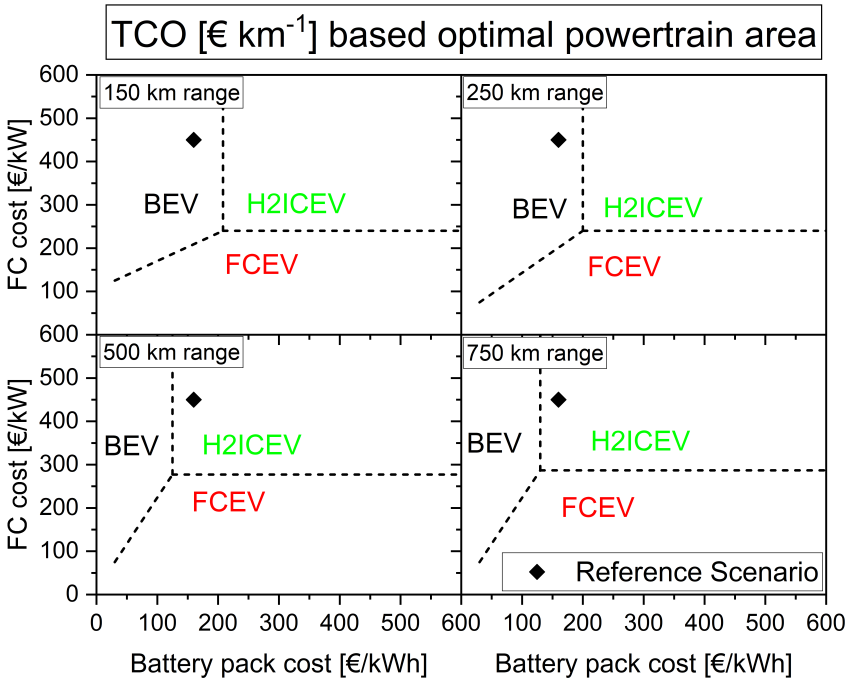

Figure 3.19: TCO sensitivity analysis to the battery and fuel cells costs

The results show that for all the ranges, FC system cost should drop down below 250 €/kW to increase its competitiveness. The vertical line, representing the maximum limit for BEV competitiveness, shifts from 210 €/kWh for vehicles with 150 km range to 130 €/kWh for 750 km case.

3.4.3 Medium duty

In this section, the results obtained relative to the MDV are presented. The main results obtained are reported in Figure 14. The BEV energy consumption is the best in class over the whole explored ranges and varying from about 34 to 42 kWh/100km. For range higher than 300 km $FCHEV_{BP}$ (31 to 51 kWh/100km) and $FCHEV_{H2}$ (48 to 39 kWh/100km) show efficiency similar to BEV (from 15 to 28 kWh/100km). Above 600km also the HEV_{H2} offers low consumption around 42 kWh/100km. FCEV (50 to 52 kWh/100km) offers acceptable consumption only for high range vehicles requirements. The H2ICEV (32 to 36 kWh/100km), at least in the explored condition (i.e., ICE size, driving cycle, etc..) suffer from very low mean efficiency of the working operating points resulting in high consumption of about 130 kWh/100km.

The high energy consumption of H2ICEV layout, with high hydrogen fuel consumption,

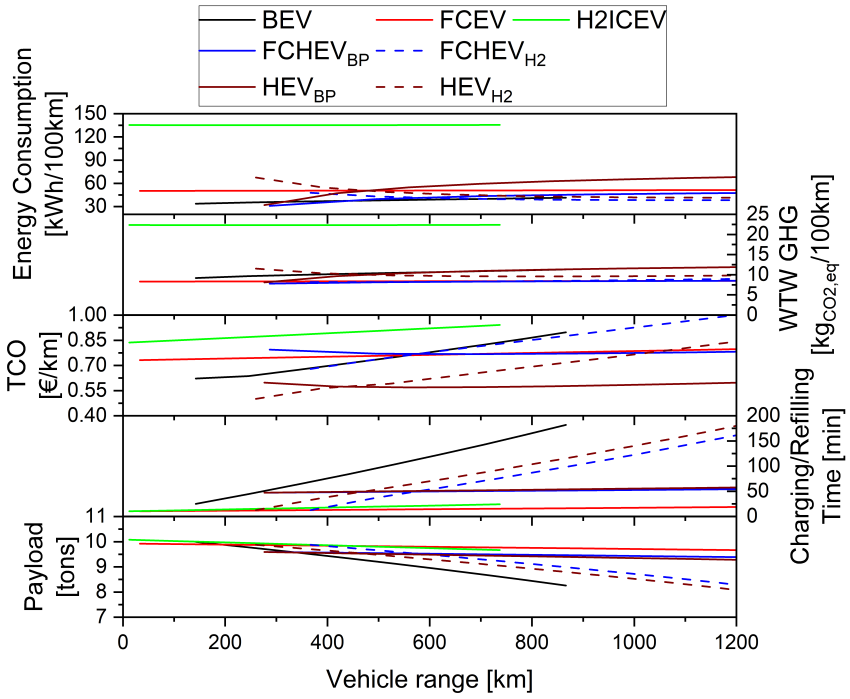

Figure 3.20: KPIs for Medium Duty Vehicles

makes the WTW **GHGs!**s (**GHGs!**s) emissions very high, around 22 kgCO2,eq/100km, and roughly the double of value relative to the other powertrains. As in the LDV case, the lowest emission are related to FCEV, FCHEV$_{BP}$ and FCHEV$_{H2}$ each with values close to 8.5 kgCO2,eq/100km. Regarding thermal hybrid layouts, the HEV$_{H2}$ is characterized by 9.6 kgCO2,eq/100km (+13% respect FCEV) and HEV$_{BP}$ by 10.5 kgCO2,eq/100km (+23% respect FCEV). The BEV layout show a higher variation with the range, showing emissions growing from 9.2 kgCO2,eq/100km (+8% re-spect FCEV) to 11.3 kgCO2,eq/100km (+33% respect FCEV). In terms of TCO, as for LDV, for range below 200km the BEV offers the lowest TCO, of about 0.65 €/km. For higher ranges the HEV$_{BP}$ offer best TCO varying from about 0.57 €/km at 400km to 0.60 €/km at 1200 km. H2ICEV is penalized by the higher fuel consumption found, with TCO varying from 0.84 to 0.94 €/km. Despite the higher chassis cost of MDV, the FC system has however a great impact on the TCO penalizing all the solutions adopting it. The FCEV, among the three FC powered layout, show a more stable behavior with TCO ranging between 0.73 and 0.78 €/km. For the relative sizing adopted, for vehicle with range between 300 and 400km, the HEV$_{H2}$ offer very low TCO, from 0.5 to 0.55 €/km. In a similar way, as discussed for LDV, with the assumption of 100kW electric charging and setting a limit of 90 minutes, which can be representative of an

half working day stop. BEV can achieve about 480 km com-pared to 740 km of HEV_{H2} and 830 km of $FCHEV_{H2}$. The other powertrain solutions doesn't have range limit within the considered 90 minutes stop.

In Table 3.4.3 the Pugh matrix for the MDV case is reported. Also in this case the BEV is taken as reference, and the layout are compared for three ranges (300, 500 and 700km). For all the ranges the hybrid configurations have the best behavior. The HEV_{BP} scores +2 for the 300 and 500 km ranges. But for 500 km it is outclassed by HEV_{H2} scores +3. For the higher range 3 of the 4 hybrid configurations, and in particular, HEV_{H2}, $FCHEV_{BP}$, and $FCHEV_{H2}$, shares the same score of +4.

Range	Metric	BEV	FCEV	H2ICEV	HEV_{BP}	HEV_{H2}	$FCHEV_{BP}$	$FCHEV_{H2}$
300 km	EC	=	-	-	=	-	+	n/a
	GHG	=	+	-	+	-	+	n/a
	TCO	=	-	-	+	+	-	n/a
	Payload	=	+	+	-	+	-	n/a
	C/R time	=	+	+	+	+	+	n/a
	sum	0-ref	1	-1	2	1	1	n/a
500 km	EC	-	-	-	-	-	=	-
	GHG	=	+	-	=	+	+	+
	TCO	=	-	-	+	+	+	=
	Payload	=	+	+	+	+	+	+
	C/R time	=	+	+	+	+	+	+
	sum	0-ref	1	-1	2	3	2	2
700 km	EC	-	-	-	-	-	-	=
	GHG	=	+	-	=	+	+	+
	TCO	=	+	-	+	+	+	+
	Payload	=	+	+	+	+	+	+
	C/R time	=	+	+	+	+	+	+
	sum	0-ref	3	-1	2	4	4	4

Table 3.7: Pugh matrix for the assessment of medium duty vehicle varying range.

To compare globally and quantitatively the MDV powertrain configurations in Figure 3.21 the VPI is reported. For the MDV case the VPI includes energy consumption, WTW GHG, TCO, Payload and charging time. Respect to the LDV case, a more complex picture rises from the VPI trends. BEV offers higher VPI only below 300 km range. Between 300 and 400 km, the HEV_{BP} becomes the best solution, according to the VPI index, for then be surpassed by $FCHEV_{H2}$. For ranges higher than 500km the FCEV has the higher VPI, due mainly to the low GHGs emissions, high payload capability and fast refilling time. The H2ICEV suffers from the low conversion

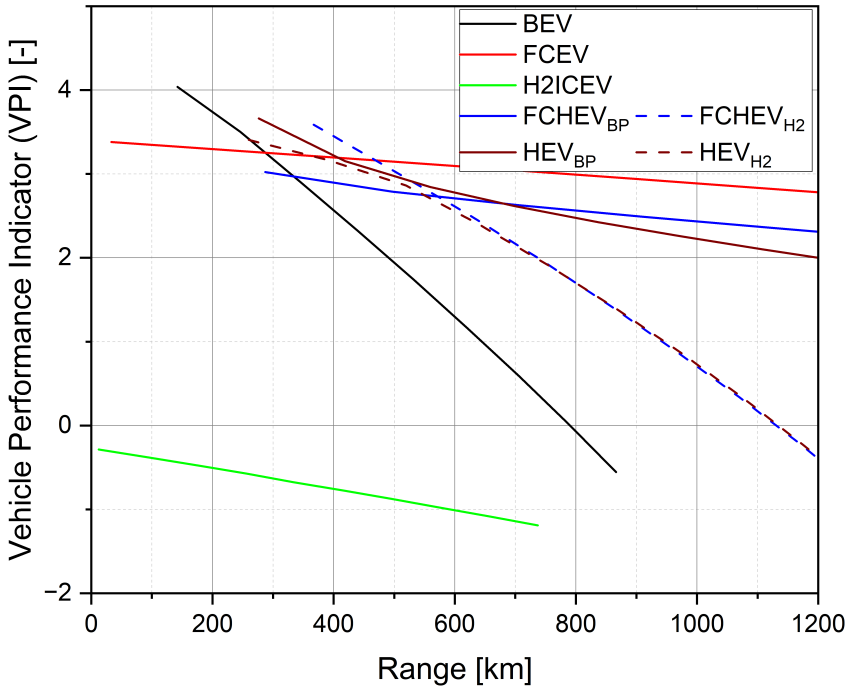

Figure 3.21: VPI for Medium Duty Vehicles

efficiency, which lead also to high GHGs emissions and higher fuel costs, contributing to raise the TCO.

3.4.4 Heavy duty

In this section, the results obtained relative to the HDV are presented. The trend of KPIs with range are shown in Figure 3.22. The BEV offer the lowest energy consumption for ranges below 800 km, varying between 120 and 140 kWh/100km. For higher ranges the FCHEV$_{H2}$ and HEV$_{H2}$ offers quite similar efficiency of about 140 kWh/100km. FCHEV$_{BP}$ show energy consumption competitive with BEV (130 kWh/100km) for 250 km ranges, but for higher range the energy consumption grow up to 190 kWh/100km due to the FC system efficiency. Similar behavior is shown by HEV$_{BP}$ but with globally worse energy consumption. FCEV offers acceptable energy consumption, especially for high range of about 145 kWh/100km. The H2ICEV energy consumption only slightly varies with the range but it is characterized by high energy consumption with a mean value is of about 225 kWh/100km. Regarding the WTW GHGs emissions the FCEV has the lower emission varying from 23.7 to 24.6 kgCO2,eq/100km. Then the two FC hybrid layout, FCHEV$_{BP}$ and FCHEV$_{H2}$, show only small difference between them, varying from

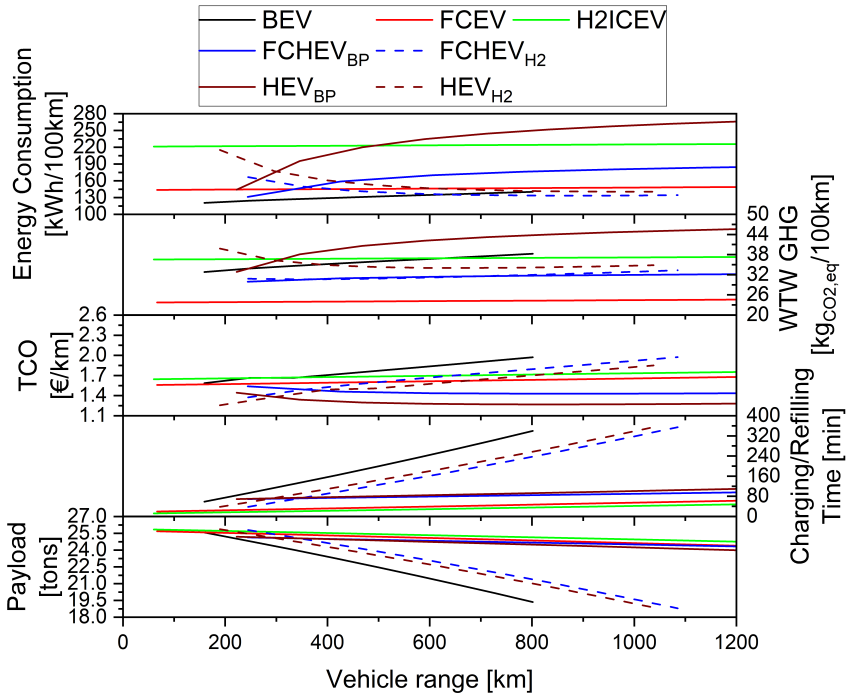

Figure 3.22: KPIs for Heavy Duty Vehicles

29 to 33 kgCO2,eq/100km. BEV (32.8 to 39.5 kgCO2,eq/100km) show a more varying trend, with emission higher than H2ICEV above 600km ranges. HEV$_{BP}$ offers acceptable emission only for low ranges and below 300km, while the HEV$_{H2}$ only for ranges higher than 500km. In terms of TCO the BEV layout suffers of the high cost of the battery and the high capacity required by the HDV application (see Table 3.4. In particular the BEV TCO ranges between 1.58 and 1.97 €/km. However, those values are also influenced by the general high energy demand of HDV, that makes the fuel cost responsible for about 36-38% of the BEV TCO. For this reason, in the following additional analysis on the electricity cost are presented. FCEV (1.56 to 1.68 €/km) and H2ICEV (1.64 to 1.77 €/km) show similar trend and similar values. This is due to the partial compensation of system efficiency and costs between FC and ICE powertrains. For ranges higher than 500km, FCHEV$_{BP}$ and HEV$_{BP}$ has advantageous of TCO of 1.28 and 1.45 €/km, respectively. Looking to the charging and refueling time, also considering 350 kW charging, the highest available standard the recharging time for long range BEV are extremely long. BEV capable of 800km range, with an hypothetical 1500 kWh requires about 6 hours. Hybrid solution with fixed battery size, FCHEV$_{BP}$ and HEV$_{BP}$, require less of 90 minutes, and can be an interesting solution to reduce the stop time. In terms of payload capability H2ICEV and FCEV,

allows maximizing the payload capability with fixed maximum permissible weight of 44 tons. Generally the solutions which rely on hydrogen as main ESS show a reduced payload variation with range. BEV at 800 km loss about 25% of the payload respect to the relative FCEV vehicle or to 250km capable acBEV, with relevant consequences on the economic viability of the solutions.

As previously stated, to better analyze the HDV case, in Figure 3.23 a sensitivity analysis on electricity cost is presented. Besides the baseline case of 0.5 €/kWh, two case with lower cost (0.1 and 0.3 €/kWh) and one with higher cost (1 €/kWh) are considered. The FCEV and H2ICEV lines are not affected by this sensitivity analysis and can be taken as reference. Generally, especially for ranges higher than 400 km, the hybrid solutions offers lower TCO than pure electric BEV. In the 0.1 €/kWh scenario, the BEV has optimal TCO below 600 km and globally offers advantages with respect to pure hydrogen powertrain (FCEV and H2ICEV).

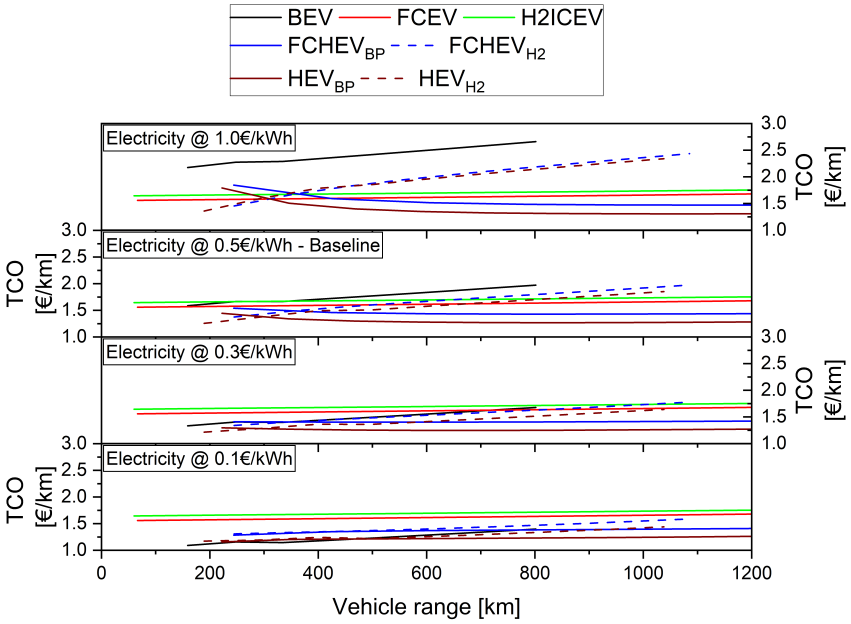

Figure 3.23: TCO sensitivity for Heavy Duty Vehicles

In Table 3.4.4 the Pugh matrix for the HDV case is reported. The BEV is taken as reference, and the layout are compared for three ranges (250, 500 and 750km). The picture depicted by the Pugh matrix for the HDV case is more complex, with no clear advantages of one specific solution, except for the FCHEV$_{H2}$ at 750 km range. For all the ranges the hybrid configurations have the best behavior. The HEVBP scores +2 for the 300 and 500 km ranges. But for 500 km

it is outclassed by HEV_{H2} scores +3. For the higher range 3 of the 4 hybrid configurations, and in particular, HEV_{H2}, $FCHEV_{BP}$, and $FCHEV_{H2}$, shares the same score of +4. Generally, in a qualitative way all the FC powered powertrain show the greatest scores for all the ranges.

Range	Metric	BEV	FCEV	H2ICEV	HEV_{BP}	HEV_{H2}	$FCHEV_{BP}$	$FCHEV_{H2}$
300 km	EC	=	-	-	-	-	-	-
	GHG	=	+	-	=	-	+	+
	TCO	=	+	=	+	+	+	+
	Payload	=	+	+	+	+	+	+
	C/R time	=	+	+	+	+	+	+
	sum	0-ref	3	0	2	1	3	3
500 km	EC	-	-	-	-	-	=	-
	GHG	=	-	-	-	-	-	-+
	TCO	=	+	+	+	+	+	+
	Payload	=	+	+	+	+	+	+
	C/R time	=	+	+	+	+	+	+
	sum	0-ref	3	1	1	3	3	3
700 km	EC	-	-	-	-	-	-	+
	GHG	=	+	-	-	+	+	+
	TCO	=	+	+	+	+	+	+
	Payload	=	+	+	+	+	+	+
	C/R time	=	+	+	+	+	+	+
	sum	0-ref	2	2	1	3	3	4

Table 3.8: Pugh matrix for the assessment of heavy duty vehicle varying range.

The quantitative comparison trough the VPI index for HDV is presented in Figure 3.24. As for the MDV case, also for HDV the VPI includes energy consumption, WTW GHGs, TCO, Payload and charging time. FCEV show the higher VPI over all the ranges. BEV offers good VPI only below 300 km range. After FCEV, the best solution for range higher than 400 km results in $FCHEV_{BP}$. The H2ICEV overcome the BEV at 450km and becomes the third best solution above 700 km, in which reach higher VPI value than hybrid powertrain solutions.

3.4.5 Sensitivity on emission factors

The different path to produce electricity and hydrogen, and their continuous changing towards more sustainable methods, makes hard to define a true real life scenario. In this regards a sensitivity analysis can be effective to understand which powertrain solution offers lowest GHGs emissions for various emission factors for both hydrogen and grid electricity. The grid emission

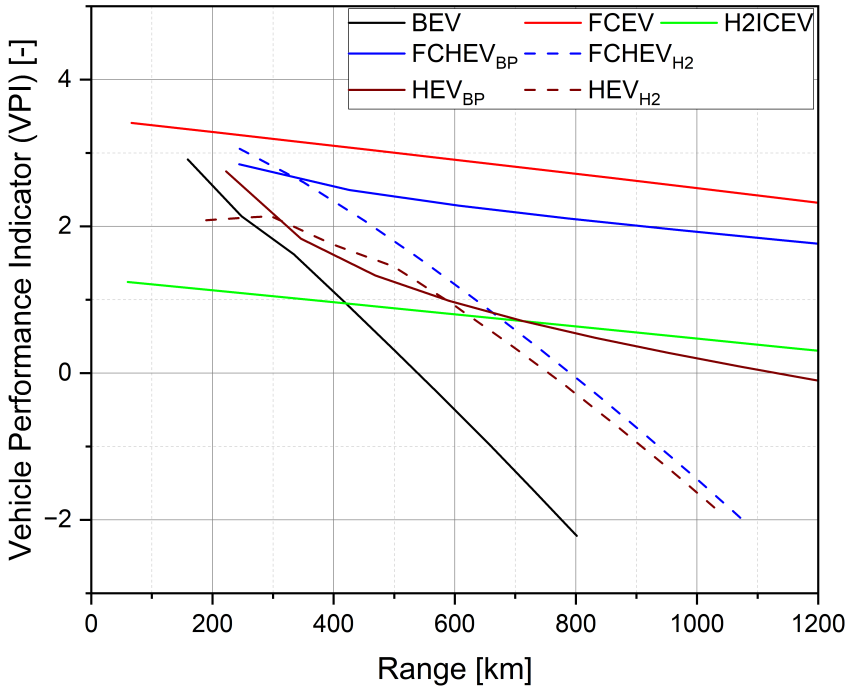

Figure 3.24: VPI for Heavy Duty Vehicles

factors has been varied between 0.01 and 1 kgCO2,eq/kWh and the hydrogen emission factors between 0.01 and 40 kgCO2,eq/kWh. The sensitivity analysis results are presented in Figure 3.25, where for each vehicle type and range considered, the emission factors plane is divided in two or more areas for which one powertrain solutions offers lower GHGs emissions. It should be noted for some selected range, and for the explored ESS size, some powertrain layout fails to achieve target range.

To better understand the value, different emission scenario have been considered as reported in Table 3.4.5, and reported graphically in Figure 3.25, with drop lines, to make possible fast comparison and intersection among different grid and hydrogen emission factors.

Scenario	Electricity EF $[kg_{CO_2,eq}/kWh]$	Note	Hydrogen EF $[kg_{CO_2,eq}/kg]$	Note
ES1	0.067	France 2021 Mix	1.25	Wind Electrolysis + C.
ES2	0.230	EU26 2020 Mix	5.5	Green H_2 + T. + C.
ES3	0.540	China 2020 Mix	12.05	SMR + T. + C.
ES4	0.950	Estonia 2021 Mix	31.05	Grid Electrolysis + T. + C.

Table 3.9: Different emission scenario assumed for the emission factors sensitivity analysis. SMR Steam Methane Reforming; T. Transport; C. Compression;

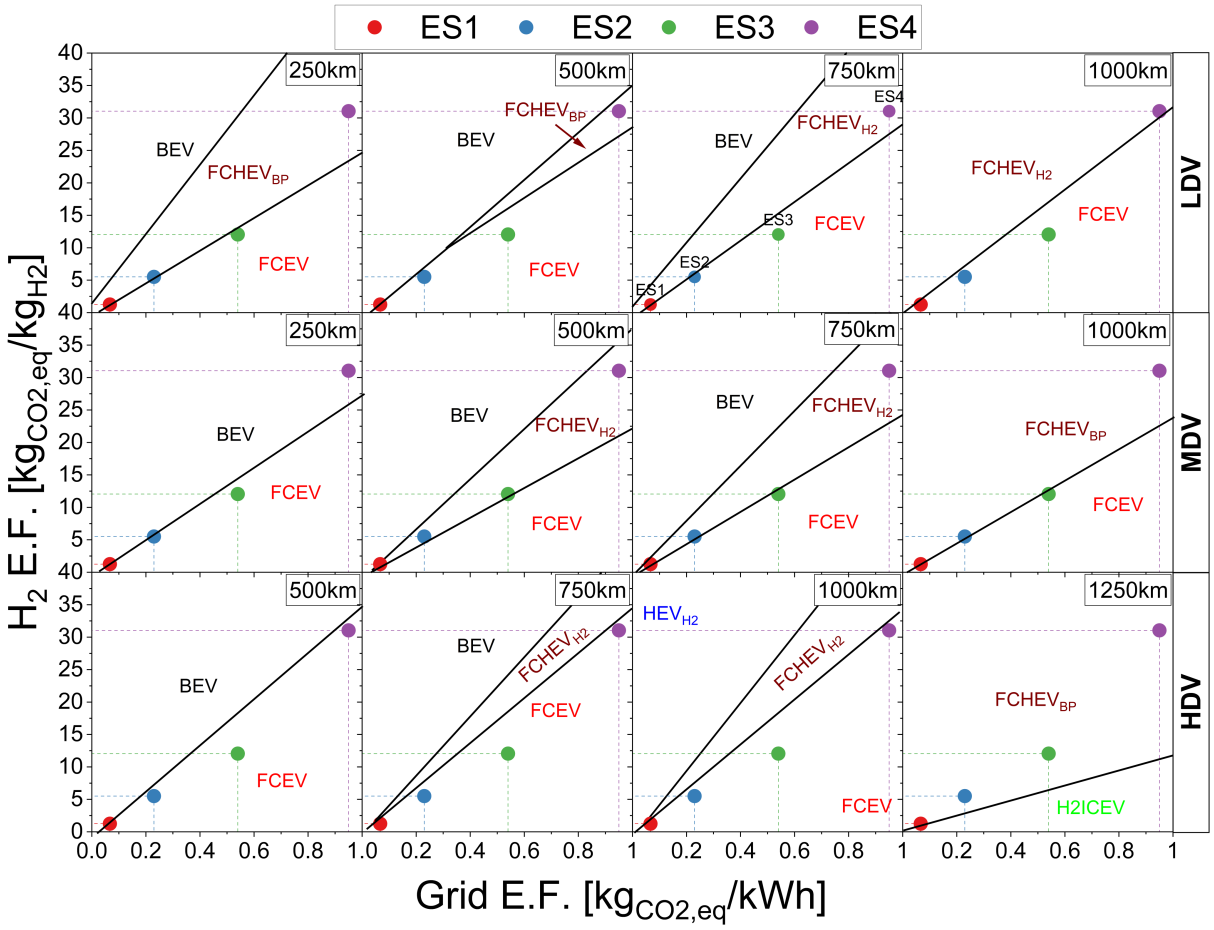

Figure 3.25: WTW GHGs sensitivity to electricity and hydrogen emission factors for light, medium and heavy duty vehicles.

Analysing LDV and looking to the first three emission scenario, FCEV are in all cases the powertrain layout offering lower GHGs emissions. For the scenario ES4 the hybrid FC layouts overcome pure FCEV. For the 1000km case for all the emission factor range considered the FCEV and FCHEV$_{H2}$ are the less impacting powertrain solutions. BEV to be the most sustainable solution need to have low grid emission factors, as ES1 and ES2, but hydrogen production should also have high environmental impact as in the ES3 and ES4. The depicted picture for MDV is quite similar to the LDV case. Generally FCEV dominates in area the bottom right corner, characterized by low hydrogen and high grid emission factors. For the three lower ranges, BEV dominates the all upper left area, for then be replaced by FCHEV$_{BP}$ in the 1000km case. For 500 and 750 km cases, exist an intermediate area, in which the lowest GHGs emissions are given by FCHEV$_{H2}$. For HDV vehicles FCEV, guarantee lowers GHGs emissions below 1000km ranges

in the bottom right corner. Oppositely, in the upper left corner, the BEV ensure lower GHGs emissions for 500 and 750 km cases. In the 1000km case also the thermal hybrid layout HEV_{H2} offers low TCO. For the 1250 range almost in all emission factor plane, the $FCHEVB_{BP}$ offers lower GHG emissions, except in very high grid and very low hydrogen emission factors area in which it is overcomed by the H2ICEV. Globally for range below 750km, it is possible to define a limit lines, valid for all the classes, for which BEV results in lower emissions. The region delimited by this line is the one represented by the inequality $EF_{H2} > 65 \cdot EF_{grid}$. This allows to have a fast rule-of-thumb rules to define BEV optimal area.

3.4.6 Sensitivity on electricity and fuel costs

Fuel costs are of main concern when the TCO is considered, and in the last years high fuel fluctuations have been recorded in many world region, due to complex economic, political and international situations. Moreover, the recharge costs varies sensibly, among service providers and on the nominal charging power. Slow charging from a private wallbox with a photovoltaic system can be considered to be free excluding plant depreciation costs, however fast charging in public street in Europe can easily be higher than 1 €/kWh. In similar way, also hydrogen, suffering a not consolidated production, and distribution, at writing time in Europe can oscillate between 10 and 25 €/kg, according online hydrogen refuelling station monitoring services. To account of those unavoidable oscillations, and make possible future scenarios analysis, in Figure 3.26.

To make easier the comparison, a square with the discussed boundaries of electricity and hydrogen costs have been added to the graph. As for the section 3.4 for some selected range, and for the explored ESS size, some powertrain layout fails to achieve target range. Looking at LDV in the most likely cost area, for the 250km case the two thermal hybrid powertrains offer the lowest TCO, for higher range the FC hybrid becomes cheaper. BEV to have the lowest TCO should have low range capabilities, and so small and cheaper batteries, and should be recharged at very low cost (¡0.3 €/kWh) affordable only with subscription or home charging. On the other side if hydrogen can be purchased with very low cost, as 5 €/kg or less, the H2ICEV solutions can be an interesting solution For short range MDV, if low charging price can be achieved (¡0.5 €/kWh) the BEV has the lowest TCO. For higher recharging prices the FCEV can be cheaper. For

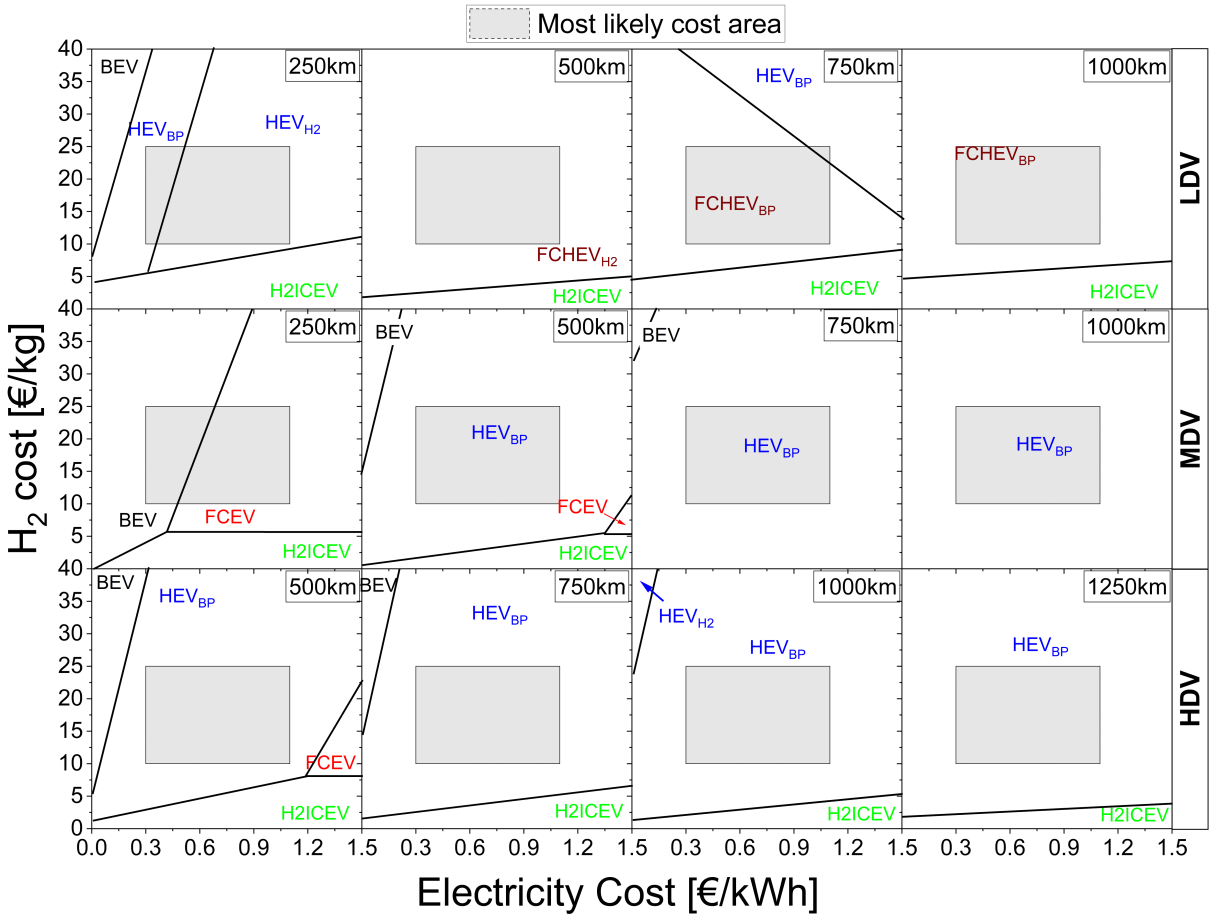

Figure 3.26: Sentivity of TCO to the electricity and hydrogen costs for light, medium and heavy duty vehicles

250 and 500km range if low cost hydrogen is available (¡6 €/kg) the H2ICEV can be a valuable alternative. For higher ranges (750 and 1000 km), the HEV_{BP} offers almost the lowest TCO for all the explored fuel costs. The HDV scenario is dominated by HEV_{BP} powertrain which offers the lowest TCO in the shaded area for all the explored ranges (500, 750, 1000 and 1250km). As for LDV if hydrogen can be purchased at very low price burning it in ICE can be affordable. Looking at BEV, once again, to be competitive requires very low recharging power. However for HDV, due to the need of 350kW recharging or also higher power, it seems to be unlikely that this low price can be achieved in a diffused way. For the case of 500 km range, exist an area, characterized by high electricity cost (¿1.2 €/kWh) and hydrogen cost in the range from 7 to 22 €/kg for which a FC powertrain can be a good solution from TCO point of view.

3.5 Main results

On the basis of the results gathered and presented in this chapter a brief summary is presented. A customized methodology has been developed and created for the comparison of various powertrain layouts relying on a set of parametric vehicle models. A framework capable of evaluating the performances in a holistic way and built on a physics based model represent a novelty in the specific field. The developed numerical tool have been verified against various data gathered by the scientific and technical literature. Additional verification, not reported for sake of confidentiality, have involved available experimental data. Therefore, the following main point can be drawn.

- The BEV layout offers usually lowest energy consumption, at the expense of higher cost and weight (of battery pack), limiting their advantages to low range vehicles.
- FCEV are strongly penalized by high TCO, especially for low range vehicles. This is due to the high FC system costs. Expected cost lowering, in next years, can lead to a relevant FC role especially in LDV applications.
- Hydrogen storage, from weight perspective can help to achieve higher payload capability with respect to BEV. However, vessel size, volume requirements and safety can make more demanding their integration.
- The hybrid solutions, especially the FCHEV, offers for various high range vehicles and classes, optimal performance from TCO, energy efficiency and WTW GHGs emissions point of views. They also offers advantages in recharging time with respect to BEV.
- The sensitivity analysis on emissions factor have highlighted the possibility of define a rough limit for which hydrogen powertrain offers lower GHGs emission than BEV. This is true when $EF_{H2} < 65 \cdot EF_{grid}$.
- The sensitivity analysis on electricity and hydrogen cost has shown that hydrogen to be convenient in ICE the cost should be lower than 6 €/kg. On the other hand, for BEV, LDV and HDV, they require low electricity recharging cost (0.3 €/kWh or lower), while the hybrid powertrain layout HEV and FCHEV offers the lowest TCO for the most likely cost scenarios.

Bibliography

[1] Lino Guzzella, Antonio Sciarretta, et al. *Vehicle propulsion systems*. Vol. 1. Springer, 2007.

[2] A. E. Pg Abas et al. "Techno-Economic Analysis and Environmental Impact of Electric Vehicle". In: *IEEE Access* 7 (2019). Conference Name: IEEE Access, pp. 98565–98578. ISSN: 2169-3536. DOI: 10.1109/ACCESS.2019.2929530.

[3] Cyprien Ternel, Anne Bouter, and Joris Melgar. "Life cycle assessment of mid-range passenger cars powered by liquid and gaseous biofuels: Comparison with greenhouse gas emissions of electric vehicles and forecast to 2030". en. In: *Transportation Research Part D: Transport and Environment* 97 (Aug. 2021), p. 102897. ISSN: 1361-9209. DOI: 10.1016/j.trd.2021.102897.

[4] José I. Huertas, Antonio E. Mogro, and Juan P. Jiménez. "Configuration of Electric Vehicles for Specific Applications from a Holistic Perspective". en. In: *World Electric Vehicle Journal* 13.2 (Feb. 2022). Number: 2 Publisher: Multidisciplinary Digital Publishing Institute, p. 29. ISSN: 2032-6653. DOI: 10.3390/wevj13020029.

[5] L Guzzella and A Amstutz. "The QSS toolbox manual". In: *Institut für Mess-und Regeltechnik, Eidgenössische Technische Hochschule Zürich. Zürich* (2005).

[6] Michele Pipicelli et al. "Comparative Assessment of Zero CO2 Powertrain for Light Commercial Vehicles". en. In: Aug. 2023, pp. 2023–24–0150. DOI: 10.4271/2023-24-0150.

[7] Giovanni Giardiello et al. "Comparative Analysis on Fuel Consumption Between Two Online Strategies for P2 Hybrid Electric Vehicles: Adaptive-RuleBased (A-RB) vs Adaptive-

Equivalent Consumption Minimization Strategy (A-ECMS)". In: *WCX SAE World Congress Experience* (Mar. 2022). ISSN: 0148-7191. DOI: 10.4271/2022-01-0740.

[8] Harald Naunheimer et al. "Overview of the Traffic – Vehicle – Transmission System". en. In: *Automotive Transmissions: Fundamentals, Selection, Design and Application*. Ed. by Harald Naunheimer et al. Berlin, Heidelberg: Springer, 2011, pp. 28–72. ISBN: 978-3-642-16214-5. DOI: 10.1007/978-3-642-16214-5_2.

[9] Erik Figenbaum. "Retrospective Total cost of ownership analysis of battery electric vehicles in Norway". en. In: *Transportation Research Part D: Transport and Environment* 105 (Apr. 2022), p. 103246. ISSN: 1361-9209. DOI: 10.1016/j.trd.2022.103246.

[10] Jens Hagman et al. "Total cost of ownership and its potential implications for battery electric vehicle diffusion". en. In: *Research in Transportation Business & Management*. Innovations in Technologies for Sustainable Transport 18 (Mar. 2016), pp. 11–17. ISSN: 2210-5395. DOI: 10.1016/j.rtbm.2016.01.003.

[11] Ricardo Energy & Environment. *Assessing the impacts of selected options for regulating CO2 emissions from new passenger cars and vans after 2020*.

[12] Andrew Burnham et al. *Comprehensive total cost of ownership quantification for vehicles with different size classes and powertrains*. Tech. rep. Argonne National Lab.(ANL), Argonne, IL (United States), 2021.

[13] Denis Dineen, Lisa Ryan, and Brian Ó Gallachóir. "Vehicle tax policies and new passenger car CO2 performance in EU member states". In: *Climate Policy* 18.4 (Apr. 2018). Publisher: Taylor & Francis _eprint: https://doi.org/10.1080/14693062.2017.1294044, pp. 396–412. ISSN: 1469-3062. DOI: 10.1080/14693062.2017.1294044.

[14] Tsuyoshi Takahashi et al. "Accelerated Durability Testing of Fuel Cell Stacks for Commercial Automotive Applications: A Case Study". en. In: *Journal of The Electrochemical Society* 169.4 (Apr. 2022). Publisher: IOP Publishing, p. 044523. ISSN: 1945-7111. DOI: 10.1149/1945-7111/ac662d.

[15] I-Yun Lisa Hsieh et al. "Recharging systems and business operations to improve the economics of electrified taxi fleets". en. In: *Sustainable Cities and Society* 57 (June 2020), p. 102119. ISSN: 2210-6707. DOI: 10.1016/j.scs.2020.102119.

[16] Antonino Genovese, Fernando Ortenzi, and Carlo Villante. “On the energy efficiency of quick DC vehicle battery charging”. en. In: *World Electric Vehicle Journal* 7.4 (Dec. 2015). Number: 4 Publisher: Multidisciplinary Digital Publishing Institute, pp. 570–576. ISSN: 2032-6653. DOI: 10.3390/wevj7040570.

[17] Yuancheng Zhao et al. “An Optimal Domestic Electric Vehicle Charging Strategy for Reducing Network Transmission Loss While Taking Seasonal Factors into Consideration”. en. In: *Applied Sciences* 8.2 (Feb. 2018). Number: 2 Publisher: Multidisciplinary Digital Publishing Institute, p. 191. ISSN: 2076-3417. DOI: 10.3390/app8020191.

[18] Yongliang Yan et al. “Techno-economic analysis of low-carbon hydrogen production by sorption enhanced steam methane reforming (SE-SMR) processes”. en. In: *Energy Conversion and Management* 226 (Dec. 2020), p. 113530. ISSN: 0196-8904. DOI: 10.1016/j.enconman.2020.113530.

[19] S. Shiva Kumar and Hankwon Lim. “An overview of water electrolysis technologies for green hydrogen production”. en. In: *Energy Reports* 8 (Nov. 2022), pp. 13793–13813. ISSN: 2352-4847. DOI: 10.1016/j.egyr.2022.10.127.

[20] Yorick Ligen, Heron Vrubel, and Hubert H. Girault. “Mobility from Renewable Electricity: Infrastructure Comparison for Battery and Hydrogen Fuel Cell Vehicles”. en. In: *World Electric Vehicle Journal* 9.1 (June 2018). Number: 1 Publisher: Multidisciplinary Digital Publishing Institute, p. 3. ISSN: 2032-6653. DOI: 10.3390/wevj9010003.

[21] R. K. Ahluwalia, T. Q. Hua, and J. -K. Peng. “Fuel cycle efficiencies of different automotive on-board hydrogen storage options”. en. In: *International Journal of Hydrogen Energy*. International Symposium on Solar-Hydrogen-Fuel Cells 2005 32.15 (Oct. 2007), pp. 3592–3602. ISSN: 0360-3199. DOI: 10.1016/j.ijhydene.2007.03.021.

[22] *Greenhouse gas emission intensity of electricity generation in Europe*. en.

[23] OAR US EPA. *Summary Data*. en. Data and Tools. Aug. 2020.

[24] Climate Transparency. *Climate Transparency Report*. 2021.

[25] *Global energy-related CO2 emissions by sector – Charts – Data & Statistics*. en-GB.

[26] G. Kakoulaki et al. “Green hydrogen in Europe – A regional assessment: Substituting existing production with electrolysis powered by renewables”. en. In: *Energy Conversion and Management* 228 (Jan. 2021), p. 113649. ISSN: 0196-8904. DOI: 10.1016/j.enconman.2020.113649.

[27] Christina Wulf et al. “Life Cycle Assessment of hydrogen transport and distribution options”. en. In: *Journal of Cleaner Production* 199 (Oct. 2018), pp. 431–443. ISSN: 0959-6526. DOI: 10.1016/j.jclepro.2018.07.180.

[28] Fuel Cell Standards Committee. *Fueling Protocols for Light Duty Gaseous Hydrogen Surface Vehicles*. May 2020. DOI: https://doi.org/10.4271/J2601_202005.

[29] Fuel Cell Standards Committee. *Fueling Protocol for Gaseous Hydrogen Powered Heavy Duty Vehicles*. Sept. 2014. DOI: https://doi.org/10.4271/J2601/2_201409.

[30] G. O. Duarte, G. A. Gonçalves, and T. L. Farias. “Analysis of fuel consumption and pollutant emissions of regulated and alternative driving cycles based on real-world measurements”. en. In: *Transportation Research Part D: Transport and Environment* 44 (May 2016), pp. 43–54. ISSN: 1361-9209. DOI: 10.1016/j.trd.2016.02.009.

[31] Nikiforos Zacharof et al. “Estimating the CO $_2$ Emissions Reduction Potential of Various Technologies in European Trucks Using VECTO Simulator”. In: Sept. 2017, pp. 2017–24–0018. DOI: 10.4271/2017-24-0018.

[32] Tommi Jokela et al. “Combined Sizing and EMS Optimization of Fuel-Cell Hybrid Powertrains for Commercial Vehicles”. In: *WCX SAE World Congress Experience*. ISSN: 0148-7191. SAE International, Apr. 2019. DOI: https://doi.org/10.4271/2019-01-0387.

[33] Ryan O’hayre et al. *Fuel cell fundamentals*. John Wiley & Sons, 2016.

[34] Michele Pipicelli et al. “Assessment of Battery–Supercapacitor Topologies of an Electric Vehicle under Real Driving Conditions”. en. In: *Vehicles* 5.2 (June 2023). Number: 2 Publisher: Multidisciplinary Digital Publishing Institute, pp. 424–445. ISSN: 2624-8921. DOI: 10.3390/vehicles5020024.

[35] Nived Abhay et al. “Efficiency Map based Modelling of Electric Drive for Heavy Duty Electric Vehicles and Sensitivity Analysis”. In: *2021 IEEE Transportation Electrification Conference & Expo (ITEC)*. ISSN: 2377-5483. June 2021, pp. 875–880. DOI: 10.1109/ITEC51675.2021.9490191.

[36] Dimitri Seboldt et al. “Hydrogen Engines for Future Passenger Cars and Light Commercial Vehicles”. en. In: *MTZ worldwide* 82.2 (Feb. 2021), pp. 42–47. ISSN: 2192-9114. DOI: 10.1007/s38313-020-0603-1.

[37] Daniel Koch, Thomas Ebert, and Alvaro Sousa. “Engine Adaptation from Diesel to H2 HP-EGR Lean Combustion Concept”. en. In: *MTZ worldwide* 81.5 (May 2020), pp. 30–37. ISSN: 2192-9114. DOI: 10.1007/s38313-020-0223-9.

[38] Chen Yang. “Running battery electric vehicles with extended range: Coupling cost and energy analysis”. en. In: *Applied Energy* 306 (Jan. 2022), p. 118116. ISSN: 0306-2619. DOI: 10.1016/j.apenergy.2021.118116.

[39] *Heavy Duty Modules - Fuel Cell Power Products — Ballard Power*.

[40] Yasuhiro Nonobe. “Development of the fuel cell vehicle mirai”. en. In: *IEEJ Transactions on Electrical and Electronic Engineering* 12.1 (2017), pp. 5–9. ISSN: 1931-4981. DOI: 10.1002/tee.22328.

[41] Nitin Muralidharan et al. “Next-Generation Cobalt-Free Cathodes – A Prospective Solution to the Battery Industry’s Cobalt Problem”. en. In: *Advanced Energy Materials* 12.9 (2022). _eprint: https://onlinelibrary.wiley.com/doi/pdf/10.1002/aenm.202103050, p. 2103050. ISSN: 1614-6840. DOI: 10.1002/aenm.202103050.

[42] Qing Sheng Wei et al. “Experimental investigation of supercapacitor based regenerative energy storage for a fuel cell vehicle equipped with an alternator”. en. In: *International Journal of Hydrogen Energy* 47.3 (Jan. 2022), pp. 1954–1964. ISSN: 0360-3199. DOI: 10.1016/j.ijhydene.2021.10.102.

[43] Adam Ragatz and Matthew Thornton. *Aerodynamic drag reduction technologies testing of heavy-duty vocational vehicles and a dry van trailer*. Tech. rep. National Renewable Energy Lab.(NREL), Golden, CO (United States), 2016.

[44] Frans J. R. Verbruggen, Emilia Silvas, and Theo Hofman. “Electric Powertrain Topology Analysis and Design for Heavy-Duty Trucks”. en. In: *Energies* 13.10 (Jan. 2020). Number: 10 Publisher: Multidisciplinary Digital Publishing Institute, p. 2434. ISSN: 1996-1073. DOI: 10.3390/en13102434.

[45] Peter Weldon, Patrick Morrissey, and Margaret O’Mahony. “Long-term cost of ownership comparative analysis between electric vehicles and internal combustion engine vehicles”. en. In: *Sustainable Cities and Society* 39 (May 2018), pp. 578–591. ISSN: 2210-6707. DOI: 10.1016/j.scs.2018.02.024.

[46] Taylor Zhou et al. “Life cycle GHG emissions and lifetime costs of medium-duty diesel and battery electric trucks in Toronto, Canada”. en. In: *Transportation Research Part D: Transport and Environment* 55 (Aug. 2017), pp. 91–98. ISSN: 1361-9209. DOI: 10.1016/j.trd.2017.06.019.

[47] David A. Cullen et al. “New roads and challenges for fuel cells in heavy-duty transportation”. en. In: *Nature Energy* 6.5 (May 2021). Number: 5 Publisher: Nature Publishing Group, pp. 462–474. ISSN: 2058-7546. DOI: 10.1038/s41560-021-00775-z.

[48] Mariangela Scorrano, Romeo Danielis, and Marco Giansoldati. “Dissecting the total cost of ownership of fully electric cars in Italy: The impact of annual distance travelled, home charging and urban driving”. en. In: *Research in Transportation Economics* 80 (May 2020), p. 100799. ISSN: 0739-8859. DOI: 10.1016/j.retrec.2019.100799.

[49] Lukas Schloter. “Empirical analysis of the depreciation of electric vehicles compared to gasoline vehicles”. en. In: *Transport Policy* 126 (Sept. 2022), pp. 268–279. ISSN: 0967-070X. DOI: 10.1016/j.tranpol.2022.07.021.

[50] Hussein Basma, Yuanrong Zhou, and Felipe Rodríguez. “FUEL-CELL HYDROGEN LONG-HAUL TRUCKS IN EUROPE: A TOTAL COST OF OWNERSHIP ANALYSIS”. In: (2022).

[51] Yun Wang et al. “PEM Fuel cell and electrolysis cell technologies and hydrogen infrastructure development – a review”. en. In: *Energy & Environmental Science* 15.6 (June 2022). Publisher: The Royal Society of Chemistry, pp. 2288–2328. ISSN: 1754-5706. DOI: 10.1039/D2EE00790H.

[52] David Hart. “Hydrogen, End Uses and Economics”. en. In: *Encyclopedia of Energy*. Ed. by Cutler J. Cleveland. New York: Elsevier, Jan. 2004, pp. 231–239. ISBN: 978-0-12-176480-7. DOI: 10.1016/B0-12-176480-X/00352-1.

[53] Zehao Sun et al. “Hydrogen engine operation strategies: Recent progress, industrialization challenges, and perspectives”. en. In: *International Journal of Hydrogen Energy* (Oct. 2022). ISSN: 0360-3199. DOI: 10.1016/j.ijhydene.2022.09.256.

[54] Cameron Rout et al. *A Comparative Total Cost of Ownership Analysis of Heavy Duty On-Road and Off-Road Vehicles Powered by Hydrogen, Electricity, and Diesel*. en. SSRN Scholarly Paper. Rochester, NY, Apr. 2022. DOI: 10.2139/ssrn.4087236.

[55] R Vijayagopal, D Nieto Prada, and A Rousseau. *Fuel Economy and Cost Estimates for Medium and Heavy Duty Trucks*. Tech. rep. Argonne National Lab.(ANL), Argonne, IL (United States), 2019.

[56] Chad Hunter et al. *Spatial and temporal analysis of the total cost of ownership for class 8 tractors and class 4 parcel delivery trucks*. Tech. rep. National Renewable Energy Lab.(NREL), Golden, CO (United States), 2021.

[57] Nic Lutsey and Michael Nicholas. “Update on electric vehicle costs in the United States through 2030”. In: *Int. Counc. Clean Transp* 12 (2019).

[58] Giacomo Di Vece et al. “Development of a Total Cost of Ownership Model to Compare BEVs, FCEVs and Diesel Powertrains on Bus Applications”. In: June 2022, pp. 2022–37–0030. DOI: 10.4271/2022-37-0030.

[59] Ben Sharpe and Hussein Basma. “A meta-study of purchase costs for zero-emission trucks”. In: *Working Paper* 2022-09 (2022).

[60] *SRIA Key Performance Indicators (KPIs)*. en.

[61] Elliot Padgett and Gregory Kleen. *Early Market Transportation Fuel Cell Cost*. 2020.

[62] R. K. Ahluwalia et al. “Performance and cost of fuel cells for off-road heavy-duty vehicles”. en. In: *International Journal of Hydrogen Energy* 47.20 (Mar. 2022), pp. 10990–11006. ISSN: 0360-3199. DOI: 10.1016/j.ijhydene.2022.01.144.

[63] Olaf Teichert et al. “Techno-economic cell selection for battery-electric long-haul trucks”. en. In: *eTransportation* 16 (Apr. 2023), p. 100225. ISSN: 2590-1168. DOI: 10.1016/j.etran.2022.100225.

[64] Yuanrong Zhou, Stephanie Searle, and C Baldino. *Cost of Renewable Hydrogen Produced Onsite at Hydrogen Refueling Station in Europe*. 2022.

[65] Lukas Lanz et al. “Comparing the levelized cost of electric vehicle charging options in Europe”. en. In: *Nature Communications* 13.1 (Sept. 2022). Number: 1 Publisher: Nature Publishing Group, p. 5277. ISSN: 2041-1723. DOI: 10.1038/s41467-022-32835-7.

[66] *D3 2016 Toyota Mirai — Argonne National Laboratory*. en.

[67] *D3 2015 Volkswagen e-Golf — Argonne National Laboratory*. en.

[68] *Volvo’s heavy-duty electric truck is put to the test: excels in both range and energy efficiency*. en.

[69] *Electric Vehicles: Total Cost of Ownership Tool – Data Tools*. en-GB.

[70] *Alternative Fuels Data Center: Vehicle Cost Calculator*.

[71] *TCO - IVECO New Zealand*.

[72] Jun Wen, Xin-Xin Zhao, and Chun-Ping Chang. “The impact of extreme events on energy price risk”. en. In: *Energy Economics* 99 (July 2021), p. 105308. ISSN: 0140-9883. DOI: 10.1016/j.eneco.2021.105308.

[73] Oliver Ruhnau et al. “Natural gas savings in Germany during the 2022 energy crisis”. en. In: *Nature Energy* (May 2023). Publisher: Nature Publishing Group, pp. 1–8. ISSN: 2058-7546. DOI: 10.1038/s41560-023-01260-5.

[74] *Hydrogen Shot*. en.

[75] Eero Vartiainen et al. “True Cost of Solar Hydrogen”. In: *Solar RRL* 6.5 (2022). _eprint: https://onlinelibrary.wiley.com/doi/pdf/10.1002/solr.202100487, p. 2100487. DOI: https://doi.org/10.1002/solr.202100487.

[76] G. Correa et al. “Evaluation of levelized cost of hydrogen produced by wind electrolysis: Argentine and Italian production scenarios”. en. In: *Journal of Energy Storage* 52 (Aug. 2022), p. 105014. ISSN: 2352-152X. DOI: 10.1016/j.est.2022.105014.

[77] *Lithium-ion Battery Pack Prices Rise for First Time to an Average of $151/kWh*. en-US. Section: Press Release. Dec. 2022.

Chapter 4

Driving automation systems and vehicle energy efficiency

DAS are spreading to enhance driver comfort and safety. Major part of new cars incorporates at least one Advanced Driving Assistance System (ADAS) as the adaptive or eco cruise control, lane keeping and path tracking. In fact, most of the new cars belong to L1, L2 or L3 automation level according to Society of Automotive Engineers (SAE) J3016 standard. ADAS, DAS are usually prerogative of the Information Comunication Technology (ICT) field. This chapter aims to analyze the autonomous vehicle system architecture to answer to the following research questions.

I. "How a driving automation system can improve the vehicle energy efficiency?"

II. "What is the impact of a driving automation system on vehicle energy efficiency?"

To this aim, an intensive study of the technical and scientific literature has been carried out, and a statistical methodology for the assessment of CAV vehicle efficiency is proposed. The extensive literature survey has been required by the need of build up a dataset for the statistical assessment. The research methods adopted for the literature review and the CAV energy assessment are reported in Section 4.1. An overview of the CAV architecture is pictured in Section 4.2, highlighting the key points and the working principles. Section 4.3 reports the adopted sensors. A discussion on the treatment and processing of sensor data is reported in Section 4.4, including discussions on processing units and data application to CAVs with the

aim of improving energy efficiency. Then, in Section 4.5, an energy analysis is carried out based on a Monte Carlo simulation that quantitatively addresses DAS impact on vehicle energy consumption. Then, a case-study aimed to confirm the statistical analysis results are reported in section 4.6.

4.1 Methodology

In this section, the methodologies adopted are presented. First, the methodology adopted for the literature review is discussed. Then, the statistical methods used to assess the influence of CAV hardware on energy consumption are described. Regarding the literature survey, an extensive scientific and technical literature study has been carried out using a keyword-based search method on Elsevier Scopus, Google Scholar, IEEE Explorer, and Web of Science databases. “CAV”, “AV”,”Self driving”, “Autonomous vehicles”,“Connected and autonomous vehicle”, “sensors”, “Lidar”, “4D radar”, “automotive”, “communication protocols”, “energy efficiency”, “ADAS”, and “energy efficiency” are the main keywords adopted, with some variations and combinations. Additional manuscripts on specific topics have been selected by searching through the citations of the found articles. A further selection of the most relevant and scientifically sound manuscripts was made. About 130 manuscripts were selected from about 350.

The literature survey had make possible to gather many data and create a dataset. This should be analysed with proper techniques to obtain the greatest information content possible from the data. It is interesting in to use a data-driven approach to answer to th following research question: “Which variant of the same vehicle, differing only by the presence or not of a driving automation system, has the lowest energy consumption?” The simplest choice of analyze the dataset is to adopt descriptive statistics, but it was found useful to use a more sophisticated method as the Monte Carlo one. The Monte Carlo calculation, which is particularly suited for statistical exploration, uses random number generators to recreate the inherent uncertainty of the input parameters and study their influence on the model outputs [18]. A scheme of the workflow followed is shown in Figure 2. First, the database has been generated by gathering data from BEV energy consumption, possible efficiency improvement with DAS, number and

type of sensors, and sensor power consumption.

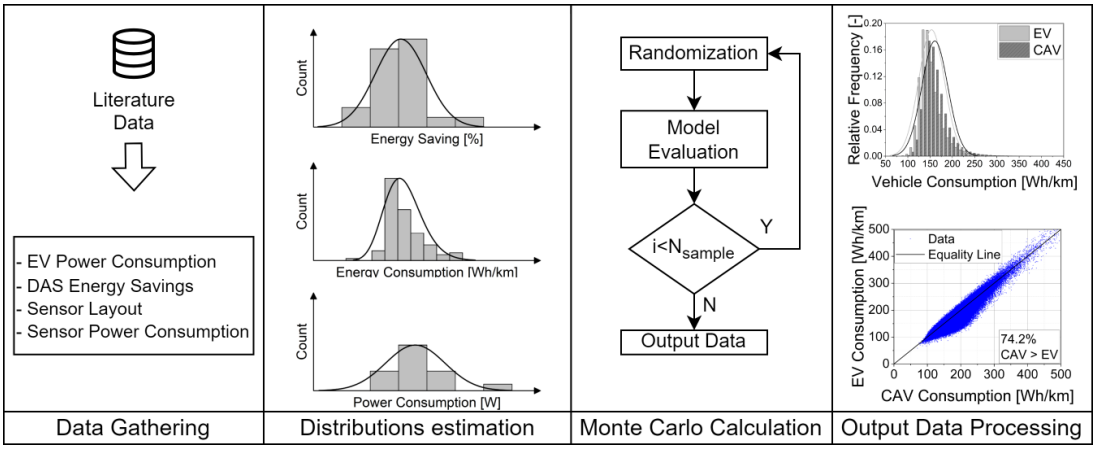

Figure 4.1: Workflow of the statistical assessment of CAV energy consumption

Second, from the data gathered the distributions were chosen based on the population characteristics (i.e., discrete values and strong asymmetry), and the fitting on data has been made in MATLAB R2022b. The fittings have been generated based on maximum likelihood estimation techniques, except for normal distributions for which the unbiased variance estimator has been used. The energy consumption can be approximated with a Burr distribution, $EC_{EV}(\alpha_{EC,EV}, c_{EC,EV}, k_{EC,EV})$, with $\alpha_{EC,EV}$, $c_{EC,EV}$, and $k_{EC,EV}$ as scale, first and second shape parameters respectively. The vehicle data collected from vehicle manufacturers, about 200 specifications, belong to different classes of light-duty vehicles. The consumption data relate to WLTC commonly adopted for homologation purposes. The power consumption of the CAV technology requires a preliminary modeling of the number of sensors and computing units, made through Poisson distributions $n_i(\lambda_i)$, and the corresponding power consumption, made through Normal distributions $P_i(\mu_i; \sigma_i)$. Thus, the total hardware electrical consumption $P_{CAV,HW}$ is evaluated according to equation 4.1.

$$P_{CAV,HW} = \Sigma_i n_i(\lambda_i) \cdot P_i(\mu_i; \sigma_i) \tag{4.1}$$
$$with\ i \in (lidar, radar, ultrasonic, camera, computing)$$

Additionally, the vehicle energy saving, due to the adoption of driving automation systems, can be represented by the normal distribution $\Delta EC_{CAV}(\mu_{\Delta EC,CAV}; \sigma_{\Delta EC,CAV})$. Third, the previous distributions have been used for fed the random number generators for the Monte Carlo

simulations. The analyzed model output is the energy consumption of the vehicle including the DAS system power requirements. In detail, random samples generated by the given distributions have been fed to the deterministic energy model (equation 4.2).

$$\frac{100 - \Delta EC_{CAV}(\mu_{\Delta EC,CAV}; \sigma_{\Delta EC,CAV})}{100} \cdot EC_{EV}(\alpha_{EC,EV}, c_{EC,EV}, k_{EC,EV}) + P\_(CAV, HW) \cdot \frac{\tau_{DC}}{d_D C} \tag{4.2}$$

τ_{DC} and d_{DC} are the duration (in hours) and the distance (in km) of the test driving cycle, respectively. The first term relates to the statistical estimation of the vehicle energy efficiency with the DAS system, while the second term represents the CAV hardware consumption.

4.2 CAV architectures

In this section, the CAV system is discussed. It is is a complex system surrounded by a mutable environment. The definition of the primary tasks of the CAV and formalize its functions is a valuable starting points for understanding the layout. Essentially, it accomplish the mission of moving from point “A” to ”B”, defining a trajectory to be followed and generating the correct commands to the powertrain, steering, and braking systems. Meanwhile, it interacts with the environment, perceiving the vehicle surroundings to guarantee a safe, comfortable, and law-respecting operation. One possible abstraction of a CAV can be described by the Observe Orient Decide and Act (OODA) loop [1]. This is one of the predominant design paradigms for CAVs, which is graphically reported in Figure 4.2 [2]. According to this loop, the following loop-steps can be defined:

i. Observe: the data are gathered from the sensors and, eventually, the ones received by infrastructures and other vehicles through V2x connectivity;

ii. Orient: the data are used to reconstruct the surrounding environment and localize the vehicle;

iii. Decide: a decision-making algorithm defines the best trajectory to follow to fulfil the mission goal, respecting the constraints;

iv. Act: the command for the actuators to follow the desired trajectory is generated and injected into the physical layer (i.e., electronic control units and actuators).

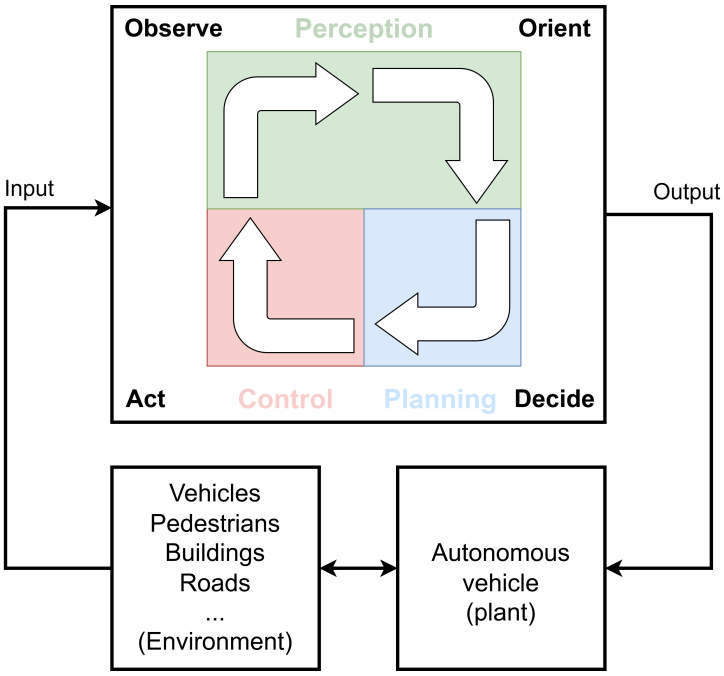

Figure 4.2: CAV architecture according to OODA loop

The OODA loop is not the unique abstraction method to describe CAVs. Another common abstraction is splitting the CAV architecture into four layers: the sensor, perception, planning, and control [3]. The two schematic architectures differ more in taxonomy than functionality. From these CAV abstractions, the main hardware components are outlined. The observe phase requires sensors to make the CAV system able to perceive and understand its state and the surrounding environment. Numerous and various sensors are adopted to cope with this aim. An overview of common sensors with their high-level classification is reported in Table 4.2.

Proprioceptive sensors, such as odometry, are not exclusive of CAV, although they are needed for autonomous driving. They can be found in numerous non-autonomous vehicle applications, as they often ensure the functionality of powertrain, braking, and vehicle safety systems. The GNSS, the Inertial Measurement Unit (IMU), and wheel encoders are the most relevant for CAV applications. Other proprioceptive sensors, such as temperature, pressure, and position sensors, guarantee the operation of all the auxiliary vehicular systems. The exteroceptive sensors are a prerogative of SAE J3016 L1 and subsequent level vehicles, as they are able to sense the envi-

	Active	Passive
Exteroceptive	LIDAR	CAMERA
	RADAR	
	Ultrasonic	
Proprioceptive		GNSS
		Wheel encoders
		IMU

Table 4.1: Main CAV sensors

ronment. They are mainly **LiDAR!** (**LiDAR!**), cameras, ultrasonic, and RAdio Detection And Ranging (RADAR). The sensor does respond to the requirement of object detection, environment recognition, and ego-vehicle localization [4]. The term Simultaneous Localization And Mapping (SLAM) is adopted when the last two are achieved in synergy. Usually, the CAV design foresees numerous sensors to ensure a 360 degree angle view around the vehicle. Proper data processing techniques and sensor fusion algorithms are required as an intermediate step between sensor acquisition and perception algorithm. Data for decision tasks can be provided by the V2x communication or from databases as high-definition maps. The V2x data can include sensor data from infrastructures, pedestrians, and other vehicles, and possibly also information on their future trajectories. These data can be used for localization, control optimization, cooperative perception, intention-awareness, and improved operation safety [5]. Then, all the acquired information is elaborated according to the vehicle mission by the decision process. This includes global and local planning and behavioural planning to ensure safe and regulation-compliant operations [6]. The output of the decision task is usually a trajectory to follow and provided to the control/act layer. The latter generates the actuator signals for path tracking, adopting usual control techniques such as Proportional Integral Derivative (PID) control, Linear Quadratic Regulator (LQR) Control, and Model Predictive Control (MPC) [7].

4.2.1 Sample configurations

The CAVs typically require a set of different and redundant sensors to match their peculiar characteristics and ensure reliable and safe operations. Increasing the automation level, L4 and L5

autonomous systems, LIght Detection And Rangings (LIDARs) are required to sense the vehicle surroundings and get reliable data [8]. In some specific applications, as in the case of Mobileye True Redundancy™ the design choice is to have two independent sensor systems, one based on camera and the other on LiDAR and RADAR, both able to ensure autonomous operation. In general, although single independent perception systems can help to keep the platform costs within acceptable limits, redundancy should be ensured by adopting different sensors covering the same surrounding areas [9]. A schematic layout of a possible sensor configuration is reported in Figure 4.3. For example, the University of Technology of Belfort-Montbliard autonomous car is equipped with a GNSS, an IMU, a RADAR, 2 360° LIDAR, 1 solid-state LIDAR and 2D LIDAR, 2 fisheye lateral camera and 2 stereo camera one in front and one rear looking [10]. The NAVYA Autonom® Shuttle Evo have 2 360° and 8 2D LIDARs, 2 cameras, GNSS, IMU and V2x connectivity. The Mobileye DRIVE™ proposed architecture features 11 cameras, 6 RADAR (4 short and 2 medium range) and a 9 Lidar (6 short and 3 long range).

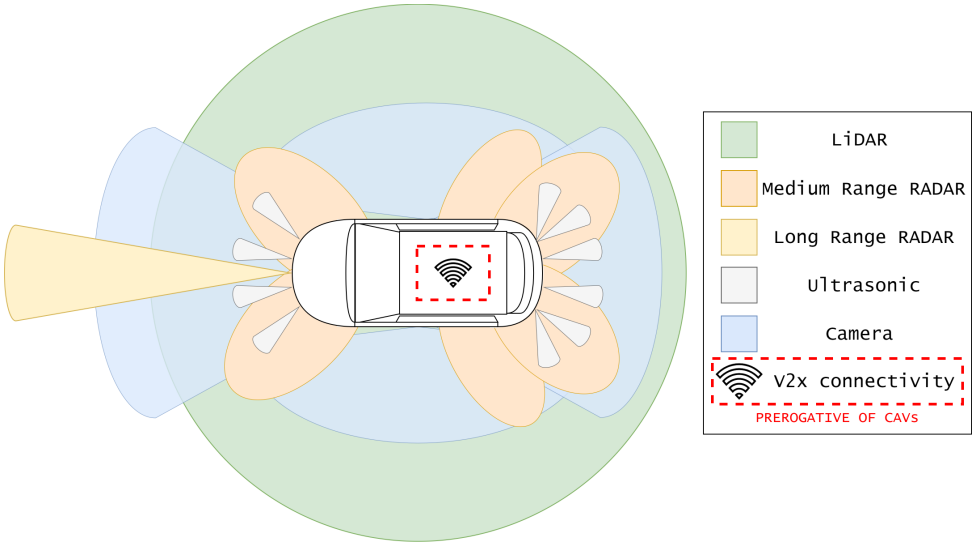

Figure 4.3: AV and CAV sensors architecture

Mobileye Supervision assures ADAS futures, such as automated parking capability and hands-free highway driving, and uses 7 long-range and 4 short-range cameras to perceive the surrounding environment. The NVIDIA DRIVE Hyperion™ autonomous driving vehicle platform has 12 external and 3 internal cameras, 9 radars, one LiDAR and 12 ultrasound sensors. The more complex Mobileye Drive™, which can be classified as L4 or L5 autonomous system according

to SAE J3016, have 13 cameras, 3 long-range LIDARs, 6 short-range LIDARs and 6 RADARs. This solution use two independent redundant systems for the perception, namely camera with radars and LIDARs, to achieve high level of safety. Both solutions are based on two and six Mobileye EyeQ5 High System-on-Chip (SoC), respectively, capable of DL of 16 Trillion of Operations Per Second (TOPS) each. The redundancy can also be applied to the processing units, as in the case of Tesla "third hardware version (HW3)", with a duplex configuration of two processing units able to operate the vehicle independently. Due to re-liability constraints to ensure safe operation, the hardware for automotive applications is subject to rigorous testing and design constraints. The Automotive Electronics Council (AEC) provides the requirements for integrated circuits (AEC-Q100) and passive compo-nents (AEC-Q200) to be defined as automotive-grade components. Those standards pose stringent operative temperature conditions, usually between -40 °C and +125°C. Additionally, automotive electrical and electronic parts should comply with the ISO16750 defining severe test conditions. Moreover, all critical vehicle systems to guarantee functional safety should comply with ISO2626, which defines four levels of Automotive Safety Integrity Level (ASIL) from A to D, with D being the highest safety level [11].

4.3 Sensors

In this section, the sensors needed for the autonomous navigation of the vehicle are analyzed more deeply, discussing their working principle, major constraints, and margin of improvement. The main sensors of CAVs, as described in section 3, are camera, LIDAR, RADAR and ultrasonic. The need to adopt different kinds of sensors arises from their peculiar characteristics (sensitivity, reliability, etc.). Sensors and their processing algorithms for automotive applications are tested in adverse weather conditions to assess their reliability and operational limits. The test relies on:

- On-road vehicle, true world, real scenario testing
- Sensor testing, true world condition reproduction
- Sensor testing, tailored simulation test bench, laboratory

The first tests are the most significant to test CAVs but require a huge effort in both time and

cost. Only a few datasets are available with true sensor data recorded by vehicles in different weather conditions in on-road testing for processing algorithms offline development and testing. One example dataset is the RADIATE, which includes RADAR, LIDAR, camera and odometry data under normal, rainy, snowy and foggy conditions [12]. Regarding the sensors and their development, testing at the laboratory scale is usually preferred. Ad-hoc test rooms are adopted to ensure high reproducibility of the results. Meteorological visibility, fog, rain and snow particle size distribution, and rain intensity are measured and reproduced according to the desired test conditions. Rasshofer et al. have successfully developed an electro-optical laser radar target simulator system to reproduce LIDAR response in a snowing environment [13]. Also, a virtual environment can be adopted to test sensors. For example, Espineira et al. developed a 3D virtual environment with a noise model depending on rain distribution to generate synthetic Lidar data in adverse conditions [14]. Usually, a combination of geometrical environment reconstruction, sensor physics and stochastic methods for accounting noise end environmental conditions is adopted to virtual test a sensor [15]. A similar approach can be adopted for Hardware in the Loop (HiL) testing of visual systems. The camera system under test is pointed toward an image rendered by a 3D graphic engine, and the vision algorithm is tested in different driving conditions and scenarios [16]. Each sensor interacts differently with the weather conditions. Cameras suffer light conditions and adverse weather. A camera pedestrian recognition algorithm has been shown to reduce the detection rate from 90% to 70% passing from daylight to night conditions at the same detection accuracy [17]. Fog is another typical problem for a camera system. However, different post-processing techniques are being developed to mitigate this problem. These can be pre-processing techniques before the elaboration of the single image [18] or can be directly integrated into object detection algorithms [19]. The **LiDaR!** (**LiDaR!**) are sensitive to weather conditions, especially fog. From the test in a fog camera with 2 different LiDAR with 905nm wavelength and a target with 90% reflectivity the maximum viewing distance is around half of the meteorological one [20]. Also, in extreme conditions (33mm/h rainfall), the rain does not significantly influence LiDAR detection, while fog creates measurement and detection errors [21]. Radar usually is less affected by adverse weather conditions concerning LIDAR. In particular, under various conditions, detection precision testing has registered only a 5% loss for radar systems and up to 25% for LiDAR [22]. Particular attention

should be given to water film deposition on the radome, which can strongly attenuate the radar signal, while negligible effects are given by ice formation [23]. Generally, adverse weather conditions affect the sensor by reducing its effective range, limiting the safe operation of CAVs [24]. The sensitivity to external conditions of each sensor allows the adoption of sensor fusion algorithms to overcome their limitations partially. The weather less influences radar but it is insufficient for CAV operations. Cameras are required for signal, traffic, and visual recognition but are the most sensitive to light, snow, and rain conditions. LIDAR is someway influenced by weather, especially fog, but not as strong as for camera, and is not sufficient for CAV operation alone. In general, adopting a variety of sensors, with sensor fusion techniques, seems the most promising architecture to achieve reliability and accuracy [25]. Section 4.4 "Data Processing" briefly discusses the sensor fusion algorithms. Besides perception, achieving high-accuracy localization of the CAV is of primary concern for vehicle functionality, and the GNSS is the main solution to achieve the aim. Due to its relevance, it is added in the following discussion. In the following, the sensors are described in terms of working principle, main characteristics and specification, pro and cons, and applications.

Camera

Cameras, or imaging sensors, can detect the light emitted by the environment on a photosensitive surface sensor. These sensors are mainly based on Charge-Coupled Device (CCD) and Complementary Metal Oxide Semiconductor (CMOS) technologies [26]. At the beginning of the digital image era, the CCD was preferred due to its superior image quality. Currently, CMOS imaging sensors are commonly adopted since they offer lower cost, high image quality, and framerates [27]. The interest in the depth camera (also sometimes called 3D flash LIDAR) is growing. They incorporate a light-emitting source and measure the distance from the object through the **Tof!** (**Tof!**) principle [28]. In a single module, a vision **RGB!** (**RGB!**) and depth camera often coexist, offering high-resolution colour and depth information, which is helpful in SLAM and object detection and tracking [29]. Table 5 reports a comparison of some commercial camera systems. Typically, resolutions of about 2 Megapixels with a framerate of at least 30 fps are adopted. Power consumption is usually below 10 W, which tends to increase for systems, including processing unit. Automotive ethernet and SerDes links as Gigabit Multimedia

Serial Link (GMSL) or FPD-Link are commonly adopted as communication protocols due to high bandwidth requirements. Vision systems can detect, track, and predict the behaviour of other vehicles, although they face some issues arising from unpredictable working conditions and different environments [30]. Additionally, the vision system can recognize traffic signs and information on displays, which is impossible with other types of exteroceptive sensors [31]. For those reasons, CAV configurations should include cameras. For automotive applications, different manufacturers include camera and image processing units capable of real-time processing, object detection and SLAM. The cameras are characterized mainly by their resolution, framerate and Field of View (FoV). In Figure 4.4, resolution, FoV and minimum pixel levels are related to the minimum distance required to detect an object correctly. Object detection requires approximately between 100 and 600 pixels [32]. Thus, squares of 10, 20 and 30 pixels sides have been considered. Changing the focal length (i.e., optical lens) improves the maximum detection distance but reduces the FoV. Increasing the resolution can effectively improve the detection distance for all focal lengths, but more data are transferred and elaborated with a higher computational power request, and this has to be considered in a CAV design.

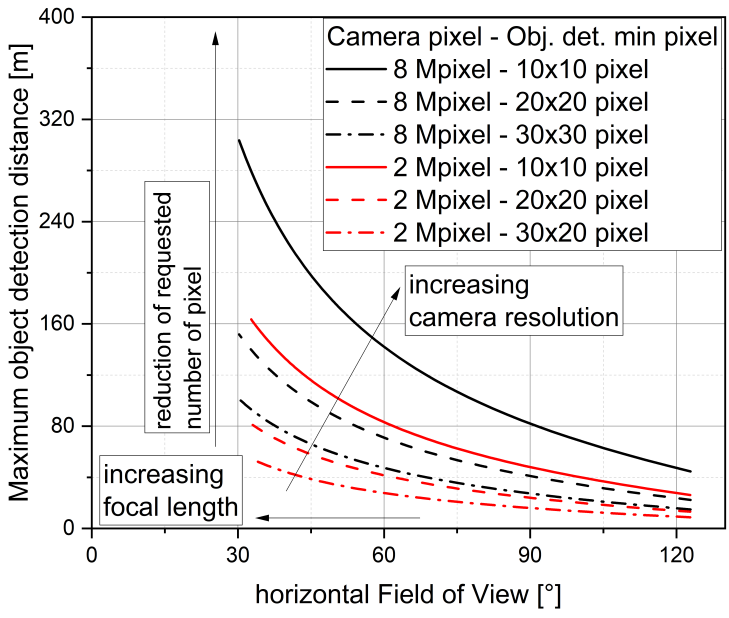

Figure 4.4: Camera characteristics sensitivity for object detection

Figure 5. Sensitivity of the camera specifics for object detection.

Common vision system architecture adopts a fisheye or wide angle lens to monitor the

nearfield vehicle surroundings at 360 degrees with a reduced number of cameras [33], and a telephoto lens with narrow FoV, to catch distant objects, at the vehicle front [34].

4.3.1 Lidar

The LiDAR is an integrated system able to scan the FoV, through laser beams, to evaluate object distance and, in some cases, relative speed. As output, it generates a list of points, named Point Cloud Data (PCD), and identified by their coordinate relative to the system reference frame and, in some cases, intensity or point speed [35]. The LIDAR system is composed of one or more single detectors. Each generates a laser beam, and a control unit computes the distance from the reflected signal. A beam steering or scanning system is used to sense the environment to explore larger areas, changing the directionality of the beams. These systems can be mechanical or solid-state, whereas the latter is preferred in the automotive field for its higher reliability due to the lack of moving parts [36]. However, solid-state models are limited in the horizontal FoV, which usually requires the adoption of more than one LIDAR to sense the vehicle surroundings [37]. The processing unit is responsible for the system management and processing of the data for the output generation. In some cases, as in the case of IBEO Lux or Microvision MAVIN™, the em-bedded processing unit is capable of object detection, classification and tracking, while usually these tasks are computed to the CAV processing units. A typical LIDAR schematic is shown in Figure 4.5.

LiDAR can be classified based on measurement methods: Time of Flight (ToF) and Frequency Modulated Continuous Wave (FMCW) [36]. Direct ToF systems use a high power laser pulse to sense the environment and use the speed of light to estimate the distance. FMCW uses the signal frequency variation due to the Doppler effect to measure both distance and relative speed [38]. In Table 6 a comparison of the main technical specification of a group of available LIDAR systems is presented. The maximum range of the LIDAR is usually ex-pressed as the maximum distance at which, with a 90% of probability, a Lambertian target with 10% of reflectance is detected [39]. The automotive Lidars have a range capability of at least 100m and can reach up to 250m. 3D Lidars usually offer measurement frequencies of 10 to 25 Hz, with 2D ones potentially offering higher rates up to 100 Hz. Power consumption is usually between 10 and 20 W. However, there are more pow-er-demanding devices, which typically include an advanced

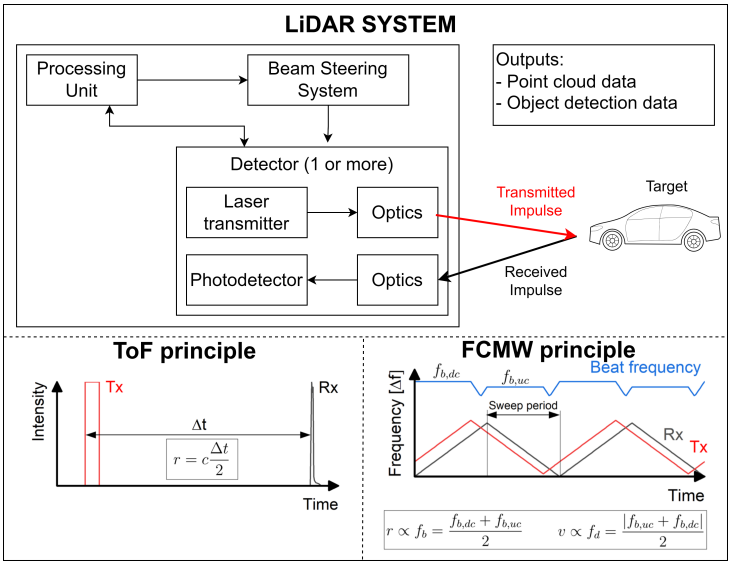

Figure 4.5: Schematic of a LiDAR

computing unit inside, reaching up to 50 W. Generally, the vFOV is around 20° or 30°, while a solid-state system can offer up to 100-120° of hFOV. It is worth pointing out that these systems suffer from mutual interferences when more than one LiDAR is used, such as in the case of high penetration of CAVs [40]. The interferences, which are of greatest concern in ToF **LiDAR!**, can reduce the Signal to Noise Ratio (SNR) ratio, leading to a reduced operative range and, in some cases, introduce ghost ob-ject detection [41]. Different methods are analyzed in the literature to overcome these problems, such as Optical Code Division Multiple Access (OCDMA) modulation [42] and true-random signal [43]. Another problem is the multiple return of signals (or echoes), which occurs when the beam pass through semi-transparent surfaces [44], have an high dynamic range [45] or in adverse weather conditions [46]. Many available system can ac-quire more than one returns, giving in output all the return or one selected by an internal algorithm. The single detector is usually made by a laser source operating in the Near InfraRed (NIR) spectrum from 850 to 950 nm or Short-Wave InfraRed (SWIR) at 1550nm. The 905nm wavelength detectors are widely adopted due to the well-established CMOS based technology, low cost and market availability [47], while the 1550nm technology requires more exotic and expensive materials such as Indium phosphide. Due to its unconstrained operation in a public environment, the safety of laser sources for the eyes is of primary concern [8]. The laser sources should be Class 1 according to IEC 60825-2. Since the beam effect on the eye depends on wavelength,

the power limit changes with the laser wave-length. IEC 60825-2 allows higher power for SWIR systems, which can be helpful in achieving a longer range due to its lower absorption by the cornea, lens and humours. Different beam steering are applied to LIDAR systems with different characteristics. Typical applications use a rotating mirror which assure a 360 degree of horizontal FoV but with lower Mean Time Between Failures (MTBF) due to mechanical rotating part. Due to automotive sector requirements, in the recent years, solid state system with Micro Electro-Mechanical Systems (MEMS) mirror are gaining big attention. Although there are micro motion of the mems mirrors the MBTF is higher and compatible with automotive applications. In some applications a flash LiDAR configuration was used, in which a diffusive laser light and a bidimensional photodiodes are used, which are sometimes referred also as ToF camera [48]. However, due to eye safety, the emitted power is limited and consequently, the range is unsuitable for vehicle purposes. A recent development is the Optical Phased Array (OPA) in which the beam is steered appropriately modulating multiple sources [49]. OPA technology has shown promising acMBTF (1e6 hours about 12 years), due to the absence of mechanical and MEMS mirrors, and is in line with the automotive requirements. Many forecasts show that OPA LIDAR will gain market share in the next years. The MTBFs of other LIDARs are not publicly available, so a quantitative comparison is not possible.

4.3.2 Radar

RADAR is an active sensor system that uses the ToF principle to measure distances. The radar for automotive applications can be classified according to their operating frequency or maximum range. Typical radar frequencies are 24 GHz and 77 GHz (more attractive for the industry) [50]. Research toward higher frequencies, and above 100 Ghz, is a pursuit to increase bandwidth, range accuracy, antenna and packaging downsizing but with a significant drawback in higher atmospheric attenuation losses reducing range capability [51]. These systems are often referred to as “mmWave” radar due to their wavelength. Short Range Radar (SRR), Medium Range Radar (MRR), and Long Range Radar (LRR) can be distinguished. A typical automotive radar layout is reported in Figure 7. A comparison of the main characteristics of automotive RADAR systems is reported in Table 7. It can be noted that the maximum range is less than 300 m, with an inverse relationship with the horizonta FoV. They adopt ethernet or Controller Area

Network (CAN) as communication protocols and typically require low power, less than 20 W.

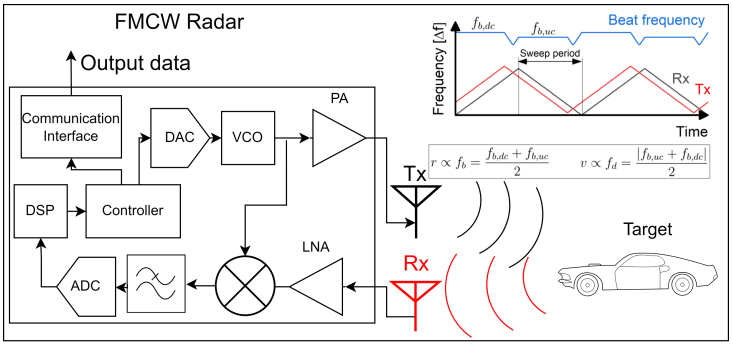

Figure 4.6: Schematic of a FMCW Radar layout

Automotive radars commonly adopt the Monolithic Microwave Integrated Circuit (MMIC) to lower the cost [52]. MMIC technology enables the developing of highly inte-grated systems, reducing their volume and power requirements [53]. Modern automotive radar integrates the MMIC, transmitters, receivers, microcontroller and other signal processing units in one integrated unit [54]. Generally, automotive radars are FMCW and able to provide information relative to the range, Doppler (speed) and azimuth [55]. An in-crease in the chirp frequency (i.e., the frequency of the function used to modulate the carrier) is investigated to improve range measurement resolution [56]. Regarding antenna layout, most systems adopt a Multi Input Multi Output (MIMO) technology, allowing to synthesize virtual arrays with larger apertures with only a limited number of physical antennae, offering higher angular resolution and smaller packaging size [57]. MIMO radar allows to measure also the Direction Of Arrival (DOA) of the radar return [58]. Numerical methods are adopted to optimize the antenna pattern in a MIMO system, improve DOA estimation, and avoid signal ambiguity [59]. Recent developments are directed at developing a novel generation of MIMO radar in which elevation is measured (4D radar) [60]. The interest in 4D imaging radar relies on the capability to generate dense cloud points as output, allowing object recognition similar to LiDAR [61]. Multicarrier modulation radar can improve radar detection capabilities, add additional data communication, and mitigate interferences among radar system [62].

4.3.3 Ultrasonic

The ultrasonic distance sensor, or Sound detection and Ranging (SONAR), exploit the ToF principle by adopting sound waves in the ultrasonic band. This kind of sensor is usually adopted to sense the area around and close to the vehicle and mostly during parking and low-speed manoeuvring as the cost is low, the operating range is limited [63], the angular discrimination and sensibility to environmental conditions are small [64]. The measurement frequency is limited. As an example, a typical system layout is reported in Figure 8. The monostatic configuration, characterized by a unique element to transmit and receive the sound waves, is preferred to the bistatic, in which independent elements are used, due to low mounting space requirement and reduced costs [65]. A comparison of ultrasonic sensors is reported in Table 8. The minimum range is in the order of centimetres, while the maximum is usually below 5 meters. The frequency rate is usually less than 20 Hz, with a low power consumption of less than 5 watts. The automotive ultrasonic sensor integrates an Application Specific Integrated Circuit (ASIC) for generating and receiving sound pulses, reliability checks, distance calculation and digital communication with the vehicle electronics [66].

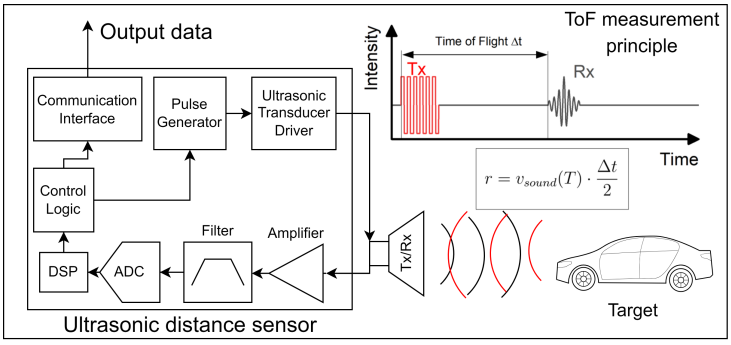

Figure 4.7: Schematic of ultrasonic distance sensor

The speed of sound value adopted in the ToF equation can induce a measurement uncertainty. A model-based range estimation employing external air temperature is usu-ally adopted to reduce the error related to the speed of sound uncertainty [67]. The operating frequency choice is based on the minimum and maximum distance to be measured and the spatial resolution [68]. An increase in frequency results in greater attenuation due to the air limiting the maximum distance. The ringing-decay time is the time required from the start of the pulse gen-

eration to stop the piezoelectric membrane that, is usually of about 700 µs, before which it is impossible to receive the echo [69]. For monostatic configuration, the adoption of a higher frequency signal can reduce the ringing-decay time, improving the minimum measurable distance [70]. Ultrasonic sensor arrays have been proven capable of tracking static and dynamic objects at still and low vehicle speeds, adopting Kalman family filtering techniques [71]. It is possible to measure the relative speed using the doppler effect as made with LiDAR and RADAR [72]. The ultrasonic sensor can be subject to denial-of-service (jamming), spoofing and acoustic cancellation at-tacks, which can be counteracted by techniques such as frequency hopping, background noise analysis and intelligent signal processing [73]. Also, without knowledge of the sensors, it is possible to succeed with a spoofing attack, resulting in the detection of a fake object [74]. Those problems limit the usage of ultrasonic measurements to only part of CAV operations.

4.3.4 GNSS

The GNSS are systems capable trough radio signals to determine the coordinates of a receiver starting from a constellation of artificial satellites. Different GNSS systems are globally available, as the United States of America Global Positioning System (GPS), European Galileo system, Russian GLONASS and Chinese Beidou. The vehicle onboard GNSS is required as it perform consistent and precise measurements of the CAV position and time [75]. Modern receivers can receive signals from different constellations to im-prove accuracy, reliability, and coverage. In the following, the discussion focuses on the GPS only, since it is the most used worldwide. The signals of each satellite allow to calculate the distance from the receiver to the satellite, which is affected by the time clock error of the receiver. In fact, as the evaluated distance includes this error source, the term pseudorange is adopted. To make a fix (i.e., solve GPS equation to find position) at least four pseudoranges (i.e., four satellite in view) are required due to the four unknown variables, three spatial coordinates and one time error. Standard GNSS often offers position accuracy in the order of meters. Different techniques can be employed to further increase the accuracy of the position measurements by adopting differential GPS, multiple frequencies receiver, and wide area augmentation systems among all. Generally, those methods eliminate most of the positioning uncertainty due to common-mode errors. Recently, the GPS

constellation has introduced two additional civilian transmission bands (L2C and L5, other than standard L1) to achieve this goal, adopting multi-frequency receivers [76]. A major problem is maintaining accurate position data in GPS-denied conditions (as. Tunnels, forests, etc). A typical method is sensor fusion, integrating data from other sources. Typically an IMU is used to provide high-frequency acceleration and angular speed data that could be integrated to find the velocity, position and attitude of the vehicle [77]. Kalman filters are usually adopted to combine GPS and IMU data to improve the state estimation accuracy while avoiding error drift [78]. In the case of CAV additional sensors can be adopted for the sensor fusion. For example, LIDAR can effectively reduce position error in GPS-denied conditions by tracking target objects detected by the point cloud [79]. GPS receivers can output data with frequency from 1 Hz to 20Hz depending on the complexity and cost of the used devices. The position accuracy of standard receiver is of the order of magnitude of a few meters in nominal conditions. Advanced receivers, exploiting multi-frequency capabilities or augmentation systems can achieve accuracy in the order of centimetres with GPS or Galileo constellations. Low-cost and reliable receivers with accuracy in the order of decimetres is of primary concern for CAV applications [80]. Usually, the GNSS receiver power consumption is limited to a few watts, and as it is typically unique in an AV layout, its power consumption can be neglected.

4.4 Data management and processing

In this section, the sensor data generation, processing and management are discussed. Indeed, the nature and the quantity of the available data arise new challenges regarding their transmission, processing and storage technologies. This section aims to summarize the main aspects and the most relevant problems from a global perspective without entering the details of the algorithms for brevity, as it is outside the scope of the manuscript. Firstly, a quantitative analysis of the amount of data generated by a CAV has been carried out, reporting some considerations on the communication protocol and the storage requirements. Secondly, the main techniques adopted to exploit the data information content for autonomous driving are discussed, reporting typical workflow and assessing requirements in terms of computational power. Finally, a brief discussion is presented on how the elaborated data can be exploited to improve vehicle energy

Sensor	Raw data rate [Mb/s]	Note
3D Lidar	≈ 1700	14M points/s, 16 bytes/point
2D Lidar	≈ 20	165k point/s, 16 bytes/point
Ultrasonic	$\approx 3x10-4$	20 Hz, 2 bytes/point
Radar	$\approx 3x10-2$	32 points/cycle, 20 Hz, 48bit/point
4D Radar	≈ 0.3	256 points/cycle, 20 Hz, 64bit/point
Camera	≈ 3750	2.6 MP, 45 fps, 32-bit, raw
Camera	≈ 960	2.0 MP, 30 fps, 16-bit, raw

Table 4.2: Example sensors data rate

efficiency.

4.4.1 Data generation and management

Sensor data, especially LIDAR and camera data, requires a high amount of memory, high bandwidth, and computing power, raising problems for their storage. For processing data, artificial intelligence techniques, as machine learning, deep learning, and reinforcement learning algorithms, are adopted [81]. These techniques require extensive datasets, which should be properly stored, for the training and achieving adequate performance and reliability. In this context, data format standardisation and compression are of fundamental importance [82]. For example, for LIDAR data, a standard file format is the LASer (LAS), which includes headers, time and other metadata in binary form [83]. Some compression algorithms, such as the LASzip, have been developed to offer high data compression (by factor 10) while ensuring direct access to compressed data without prior global decompression [84]. Database classified by criteria as space location, vehicle class, etc., on a distributed cluster architecture is an effective solution for storing a huge amount of LiDAR data [85]. Hardware accelerators become essential as the compression should be made ideally in real-time. In this context, Field Programmable Gate Array (FPGA) hardware compression has been demonstrated to be up to 250 times faster than software implementation [86]. Table 4.4.1 reports the data rate values for sensors and the base assumption adopted for the calculations. Ultrasonic, RADAR and 2D LIDAR sensor rates are significantly lower than cameras and 3D LIDARs.

The different sensor data rate suggest adopting different file formats and onboard communication protocols to optimize performance and reduce the total architectural costs. For CAVs, two main classes of communication protocols can be distinguished: network and point-to-point protocols. Due to the inclusion of new HMI interfaces, ADAS System and other advanced vehicular system, different communication protocols have been established in recent years. In this context, and toward de-facto automotive standard CAN, various communication protocols as Flexray, LIN, Automotive ethernet have been developed. A comparison among various automotive protocols is reported in 4.4.1. Adopting high bandwidth sensors such as cameras and LIDARs requires high bandwidth protocols, for which automotive ethernet and SerDes can be suitable solutions. These two standards offer different pros and cons and it is unclear which of them will be the future de-facto standard [87]. LIDAR usually adopts ethernet while Camera Serializer-Deserializer (SerDes) communications cascade to a processing unit and then to the vehicular networks through ethernet.

4.4.2 Data processing

Each data source needs to be elaborated by proper techniques that take into account the peculiarities of each sensor. The detailed data workflow is generally hard to reconstruct, as few details are available and they differs among the different platforms as it is strictly related to the specific hardware adopted. For the sake of clarity, a possible flow is hereafter discussed. The distance of surrounding objects relative to the CAV is essential for its safe operation. It can be measured by adopting RADAR, LIDAR, Depth camera and ultrasonic sensors or estimated by standard vision camera through the cooperation of two or more cameras (stereo-vision) exploiting trigonometry [88]. Recently, interest in monocular depth estimation has grown due to the development of artificial intelligence techniques, which represent an enabling technology, providing great improvement with respect to previous algorithm families [89]. Thus, the same information, but with different accuracy and reliability, can be estimated in many different ways. A general example workflow of CAV with the main processing step for each sensor type is presented in Figure 4.8.

All the data are pre-processed before further elaboration steps. The preprocessing involves filtering, as lowpass filter, noise rejection [90] and data transformation, as coordinate frame

Protocol	**Wires**	**Bandwidth**	**Max lenght**	**Safety critical**	**Application examples**
Automotive ethernet	2	up to 10 Gbps	10-15	No	Lidar, Radar
CAN	2/4	up to 1 Mbps	40m	yes	Wide applications
CAN-FD	2	up to 5 Mbps	25m	yes	Electronic Control Units
LIN	3	20 kbps	40m	no	Body, Sensor, Mirrors
FlexRay	2/4	10 Mbps	22m	yes	x-by-wire, ADAS
PSI5	2	189 kbps	40m	no	Airbags, Ultrasonic
GMSL	2	up to 12 Gbps	15m	yes	Camera
FPD-Link	2	4.16 Gbps	15m	yes	Camera
MOST	2	up to 150 Mbps	-	no	Multimedia, infotainment
SENT	3	333 kbps	5m	yes	Powertrain

Table 4.3: Main specifications of various automotive communication protocols

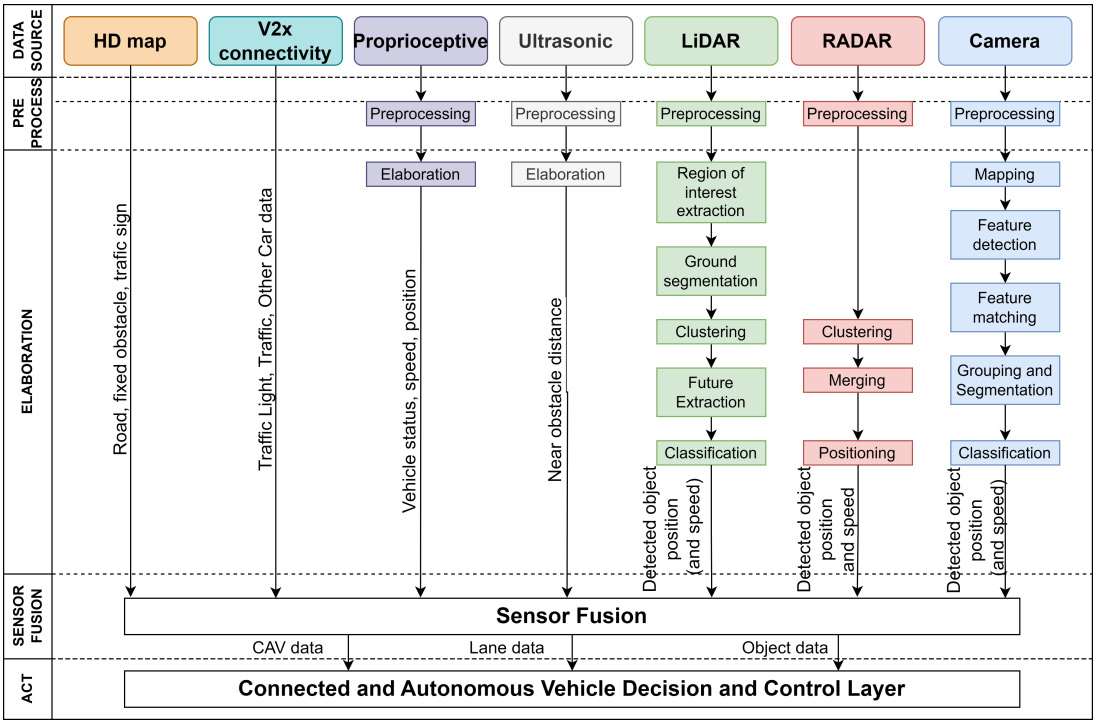

Figure 4.8: Example of CAV data processing pipeline

roto-translation [91] or image colour space conversion [92]. Then, according to the considered sensor, a specific elaboration follows. V2x connectivity, proprioceptive and ultrasonic sensors, and HD map require simple data elaboration compared to LIDAR, RADAR, and camera applications. For LIDAR, the cloud points are filtered based on regions of interest. Then, the ground plane is estimated to remove the relative points. The remaining points are then clustered (i.e., machine learning grouping based on similarity [93]). Then, future extraction is carried out for each cluster, which is propaedeutic for the successive object classification [94]. In a similar way, radar data are clustered in groups and then merged. The position and relative speed are obtained by assuming the target shape [95]. 4D RADAR, in particular, has an elaboration pipeline quite similar to the LIDAR ones. Different step sequences can be made to extract future, group data, and classify the objects by camera data after proper preprocessing, such as conversion in HSL space conversion and boundary boxes creation [96]. Many proposed techniques for all sensors rely on convolutional neural networks, deep neural networks, autoencoders and classifiers as support vector machines [97]. The obtained data from all the considered sources should be joined through proper sensor fusion techniques. Those strongly influence the effectiveness

of the sensor layout. Recently, interest in multimodal data fusion algorithms is growing due to the need to perceive the environment through different sensors, such as vision, radar and lidar systems [98]. In general, more reliable and accurate data can be obtained through sensor fusion. Wang et al., through a multi-modal multi-scale fusion algorithm for LIDAR and 4D RADAR achieved about 5 – 10% higher accuracy with respect to only the LiDAR [99]. Similar improvements have been found in object detection by adopting a multimodal VoxelNet to fuse vision and Lidar data [22]. Multimodal sensor fusion can effectively improve the detection performance under various adverse weather conditions as fog, rain and snow [100]. Neural networks are also rising to cope with the sensor fusion problem, in which the processed data of each sensor are given in input to another neural network for the data fusion [101]. However, CAVs also offer the possibility of cooperative sensor fusion, exploiting data from different vehicles with a proper processing pipeline as described in [102]. The specific hardware platform defines the way in which the processing pipeline is executed. Both centralized and distributed computing on different processing unit can be adopted. Often, some processing is made at the sensor level. A dedicated processing unit integrated in the sensor or as its companion sometimes offers the object detection and tracking as well. Indeed multi-camera system exists with multicamera linked through **GMLS!** (**GMLS!**) to an elaboration unit which send the elaborated data, including object detection data including position and speed, to the CAV central unit for sensor fusion.

Similarly to the processing algorithms, the Processing Units (PUs) used vary and depend on specific system, architecture, and design choices. The main processing unit can be classified as Central Processing Units (CPU), Graphical Processing Unit (GPU), Digital Signal Processor (DSP), ASIC and FPGA solutions [103]. The choice among special purpose and general purpose PU is guided by a tradeoff between the development complexity of the hardware and computational efficiency. But it is worth pointing out that the different choice is linked also to the particular development step at which the hardware architecture development is. ASICs offer higher performance and energy efficiency but the high development costs can be sustainable only for production series unit. FPGA show slightly less performance, but its flexibility makes it feasible for hardware development and testing, and applications with an expected low number of products [104]. High general-purpose units such as CPU and GPU can be useful in develop-

ment, but recently there have also been employed on prototype CAVs. Usually, for autonomous vehicles, cooperation of different processing units is employed at different levels. DSP and ASICs are often integrated in the sensors, while CPU, GPU, and sometimes FPGA are employed in the central processing units, responsible for sensor fusion and decision-making. A comparison of the deep learning capabilities of some automotive hardware platforms are reported in Figure 4.9.

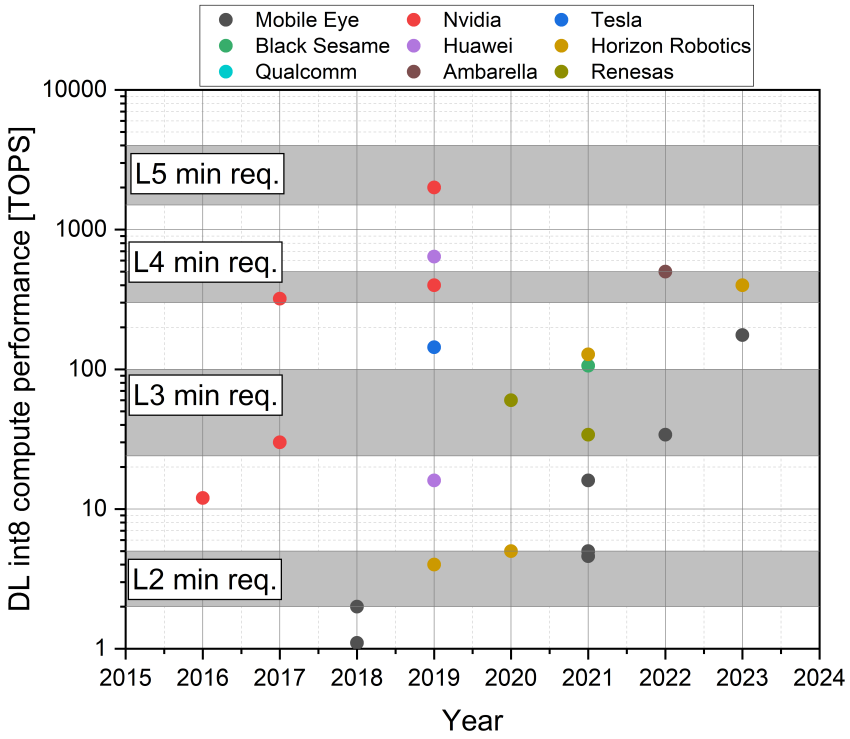

Figure 4.9: Comparison of different hardware platform performances in DL computation as int8 TOPS

Some gray bands are reported highlighting minimum requirements for various automation levels according to technical literature. A need for more powerful PU can be highlighted in the graph. At the actual state of the art to reach L5 targets, more PU should be employed or High Performance Computing (HPC). However, the latter solution suffers from low energy efficiency.

4.4.3 Data exploitation for energy management and efficiency improvements

The processed data can be used to optimize the vehicle energy efficiency. Sensor data and connectivity can help to give complete information to the ego-vehicle regarding road slope, future speed limits and preceding vehicle future speed [105]. In this way it is possible to optimize the vehicle speed profile, avoiding unnecessary braking and accelerating phases, and choosing optimal powertrain operating points. Generally, knowing the external conditions makes it possible to solve an optimization problem to reduce the vehicle energy consumption while maintaining safe and comfortable operations [106]. V2x and sensor data can be also used to optimize the vehicle behaviour in signalized intersections to optimize speed profile and maximize the braking energy recovery [107]. Generally a proper developed controller can achieve better driving style than average human driver therefore obtaining lower energy consumption [108]. However, while the strategy to anticipate the following car behaviour is, on one hand, effective in reduce energy consumption, on the other hand, it could lead to an increase of travel time [109]. There are many works in the literature developing several control strategies, with various techniques. Most of them from the control point of view can be classified as MPC, differing in the formulation of the optimal control problem. The algorithms have been tested in various scenario and on different vehicles. Data regarding the possible improvement due to the optimal control strategy exploiting DAS system and V2x connectivity have been gathered from the literature (data sources: [106, 108–114]). With this dataset, the distribution of the expected DAS energy saving, $\Delta EC_{CAV}(\mu_{\Delta EC,CAV}; \sigma_{\Delta EC,CAV})$ has been estimated. The results shown that the data can be fitted with a Normal with mean $\mu_{\Delta EC,CAV} = 4.8$ and standard deviation $\sigma_{\Delta EC,CAV} = 3.9$. This distribution has been employed for the Monte Carlo simulation (see next section).

4.5 CAV energy efficiency

In this section, exploiting the data gathered and discussed in the previous sections, a statistical analysis is presented to assess the net energy efficiency of CAVs. The distribution obtained by the literature data analysis, according to the methodology described in section 4.1, are reported in Table 4.5. In particular, all the values generating the distributions adopted for the Monte

Carlo simulation are reported in order to provide details for the reproducibility of the results.

Among the sensors, the LIDAR is the more demanding from the energy point of view, and processing unit has the greatest power consumption. Moreover, the processing unit due to a number of different hardware solutions (i.e., ASIC, FPGA, CPU), as discussed in section 4.4, are characterized by the highest standard deviation. Once the power consumption distribution is estimated, combining them with the number of sensors and computing units given by Poisson distributions, the overall CAV hardware power consumption $P_{CAV,HW}$ can be statistically evaluated. The resulting distribution is presented in Figure 4.10. The obtained data can be approximated with a Lognormal distribution with $\mu = 6.52$ and $\sigma = 0.46$.

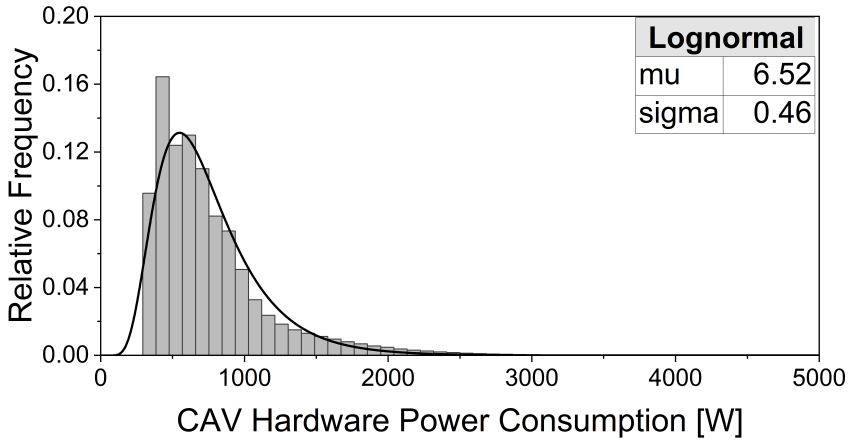

Figure 4.10: CAV Hardware power requirements

With those distributions, the Monte Carlo method has been employed to assess the net energy consumption of the CAVs, considering 1e6 sample (Figure 4.11). Panel A reports the energy consumption distribution of EVs and relative CAV versions. The CAVs shows about 5% (7.4 Wh/km) higher energy consumption with a slightly higher standard deviation. Panel B reports a scatter plot of the consumption of each EV and its CAV version. Points below the bisector line indicate that the CAV version has higher energy consumption than the EV because the energy saving does not compensate the higher consumption. About 76% of the samples fall in this area, and as the most likely scenario. In case of high-er baseline energy consumption scenario (200 Wh/km), the CAV hardware consumption become less influential, reducing the spreading of the point around the bisector line.

A further analysis has been conducted to analyse the influence of the DAS energy saving and

Type	Name	Parameter	Value
Normal	P_{camera}	μ_{camera}	4.25
		σ_{camera}	1.03
	P_{lidar}	μ_{lidar}	16.00
		σ_{lidar}	10.36
	P_{radar}	μ_{radar}	8.98
		σ_{radar}	7.28
	$P_{ultrasonic}$	$\mu_{ultrasonic}$	1.95
		$\sigma_{ultrasonic}$	1.70
	P_{lidar}	μ_{lidar}	16.00
		σ_{lidar}	10.36
	ΔEC_{EV}	$\mu_{\Delta EC_{EV}}$	15.82
		$\sigma_{\Delta EC_{EV}}$	3.94
Poisson	n_{camera}	λ_{camera}	6
	n_{lidar}	λ_{lidar}	4
	n_{radar}	λ_{radar}	6
	$n_{ultrasonic}$	$\lambda_{ultrasonic}$	1.1
	$n_{computing}$	$\lambda_{computing}$	7
Burr	EC_{EV}	$\alpha_{EC_{EV}}$	135.05
		$c_{EC_{EV}}$	18.22
		$k_{EC_{EV}}$	0.39

Table 4.4: Distribution parameters found by the literature data acquired and adopted for the Monte Carlo simulation

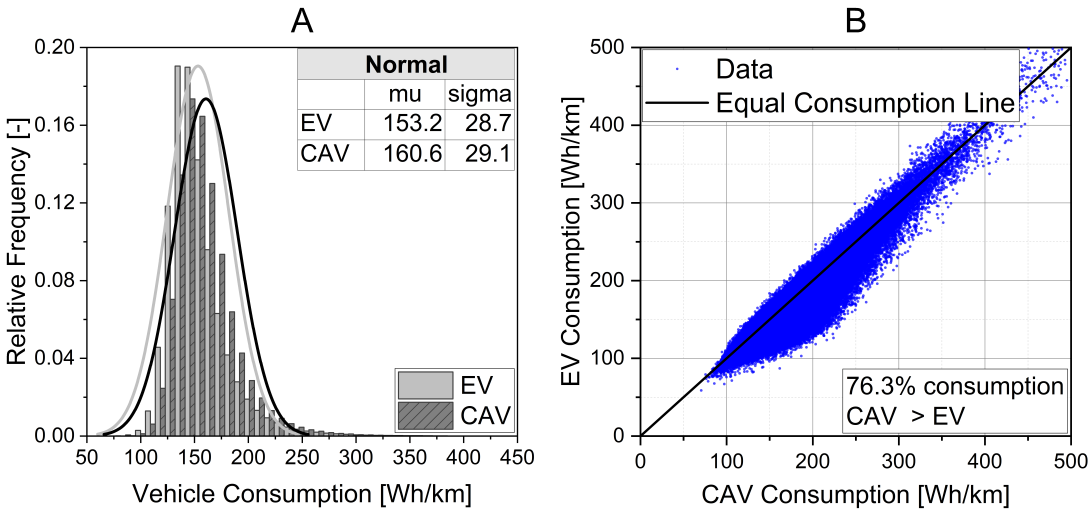

Figure 4.11: A) Distribution of energy consumption for EV and CAV. B) Comparison of the consumption of EV and CAV

CAV hardware power consumption. The Monte Carlo simulation samples have been grouped into two clusters based on the EV energy consumption. The two considered clusters are representative of compact cars (segment C – EV energy consumption $EC_{EV} \in (130, 150)$) and luxury or sport-utility vehicles (segment F – EV energy consumption $EC_{EV} \in 180, 200)$). The differences between CAV and EV energy consumption for the two vehicle classes are reported in Figure 4.12. The not clear boundaries arise from the statistical nature of the Monte Carlo simulation data. For compact cars, the difference ranges between -20% and 70%, while for luxury cars between -10 to 40%. Both centroids demonstrate 6% higher consumption of CAVs. EV energy consumption results as one of the main drivers of the impact of CAV efficiency. The graphs also allow, for a fixed vehicle, to define the maximum power of the CAV hardware to avoid worsening of the energy efficiency. As sake of example, for a compact car with 10% of energy saving, thanks to DAS control strategies, poses a breakeven point around 1000 W (EV and CAV same energy consumption).

Although the CAV power consumption analysis focuses on light-duty vehicles, the data can be used to make some thoughts on medium-duty and heavy-duty vehicles. For heavy-duty, an increase of about 10-30% of the CAV hardware can be expected due to a possible higher number of sensors required to cover a wider surrounding area. Higher energy-saving with respect to light-duty vehicles are expected, especially for long-haul heavy-duty trucks. This arises from

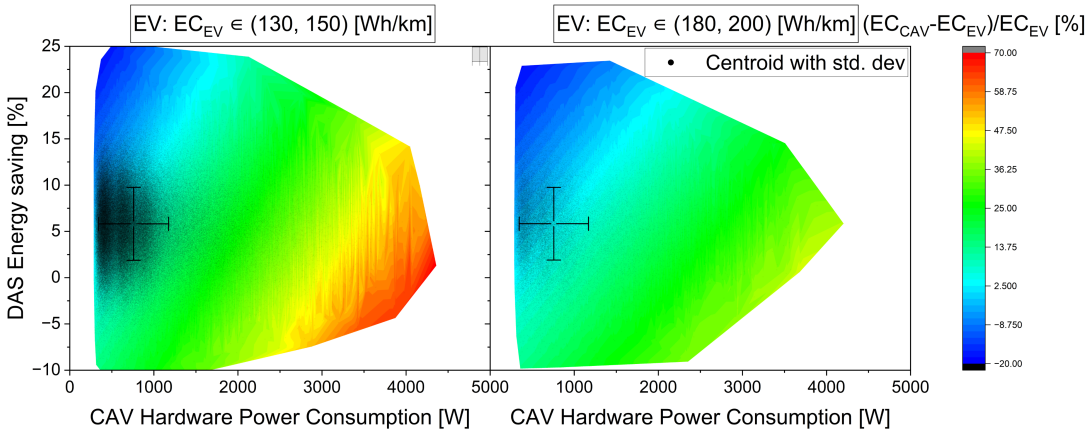

Figure 4.12: Influence of the DAS energy saving and CAV hardware power consumption on CAV and EV energy consumption for two light-duty vehicle classes

the typical mission profile (i.e., long range, near constant speed), which can effectively benefit from exploiting aerodynamic drag reduction for truck platoons, which requires short intravehicular distances possible to maintain, in a safe manner, only with DAS systems. Optimization studies show that 9% fuel consumption reduction can be achieved by combining intravehicular distance and lateral position in a truck platoon [115]. The higher CAV hardware energy consumption (700-1700 Wh/km) [116] is less critical. Figure 4.13 shows the Monte Carlo simulation results with the mean and standard deviation of various clusters characterized by different EV energy consumption. The simulation data have been extrapolated through curve fitting to extend, notwithstanding the high R2 obtained, the results for higher energy-demanding vehicle applications. Two EV consumption thresholds identify three different regions. The first represents light-duty vehicles, the second light-commercial and medium-duty vehicles and the third heavy-duty vehicles.

Light-duty vehicles are likely to worsen the net vehicle energy consumption by adopting autonomous driving technology. The introduction of a fully autonomous system will likely be advantageous from an energy perspective regarding the heavy-duty energy consumption regions, with an approximated energy reductions (obtained by extrapolation) of up to 8 %. These results are likely improved for the medium-duty sector, and the expected variation is in the order of ±3% compared to the reference EV.

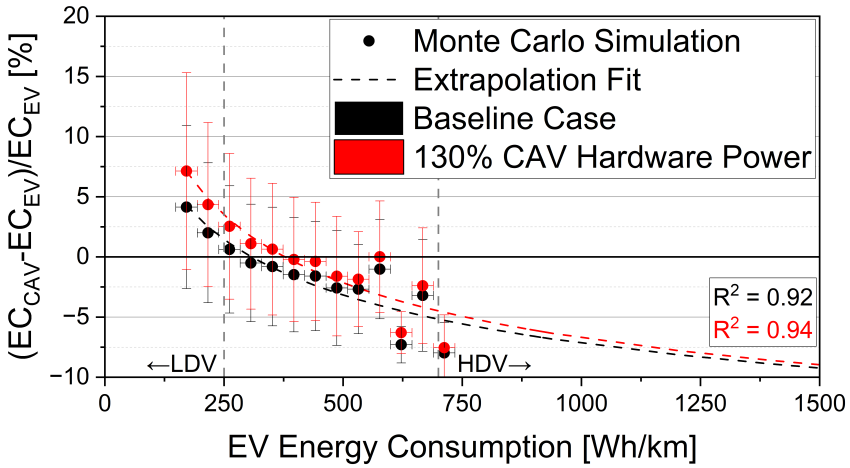

Figure 4.13: CAV energy consumption differences for various vehicle classes

4.6 Battery Electric Vehicle case study

This section reports preliminary steps toward the assessment of a driving automation system trough numerical and experimental activities analyzing an existing real case study. The aim is to assess the potential impact of the autonomous driving strategy on vehicle energy consumption through the analysis of this case study. Figure 4.14 shows the main steps of this project. The activities, partially developed in this PhD program are still ongoing, and regards the creation of a detailed model of the vehicle, validated trough a proper experimental test campaign. After the model validation, a scenario simulation with the development of proper control strategy will be aimed to the assessment of powertrain efficiency improvement with the adoption of DAS. In the end, the final step is to include in the model the hardware power consumption, validated also on experimental data, to assess the global vehicle efficiency.

The vehicle architecture is reported in Figure 4.15. On the left is reported the powetrain architecture, while on the right side the autonomous driving system sensor layout is reported. The autonomous architecture relies on lidar, camera and ultrasonic sensors. Two lidar have a 360° sense area achieved through a mechanical rotating beam steering system, and are used to scan the vehicle-near field, focusing on the sideways. Another lidar, but of the solid-state time are used to accurately scan the front of the vehicle. Camera are used to get traffic sign, and to improve the reliability of the autonomous system. They scan both the front-side and the rear area. The ultrasonic are used to sense the very near field, for obstacle detection and parking

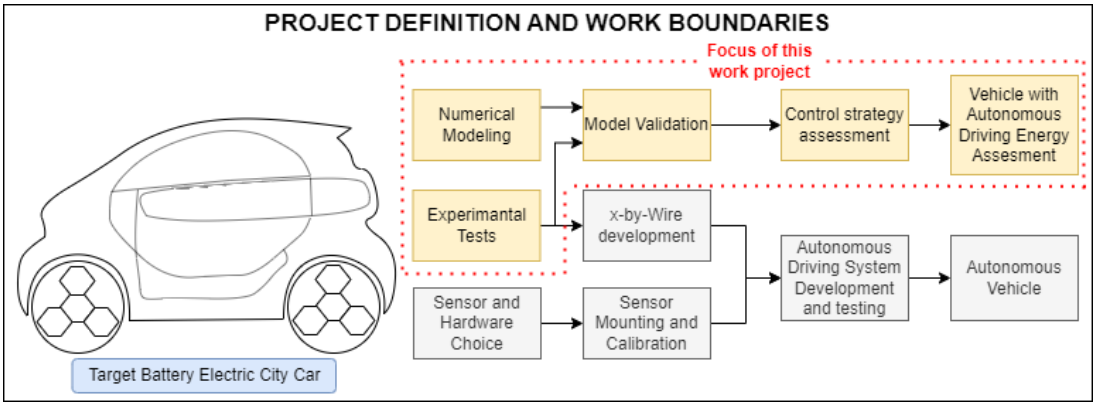

Figure 4.14: Project outlines and investigation steps

maneuver.

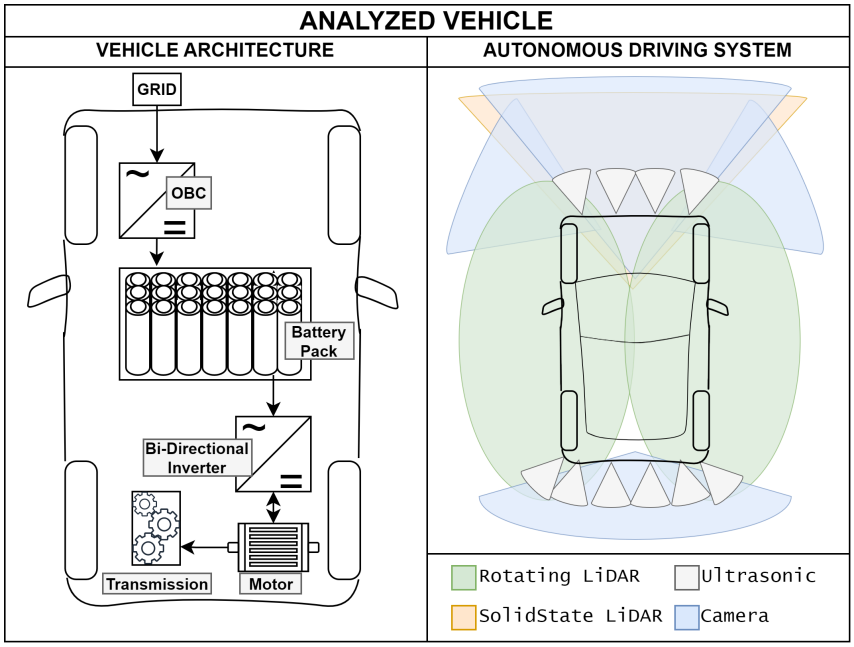

Figure 4.15: Case study BEV layout; left: powertrain layout; right: sensors layout

A summary of the main characteristics are reported in Table 4.6. The energy source is a battery pack made with LFP cells with an operating voltage of 72V and a energy capacity of about 10.3 kWh. An on-board charger rated of about 2.2 kW used for charging the vehicle from home grid, while an internal DC-DC converter gives 12V bus for control units and some auxiliaries. The electric drive is composed by a single gear transmission with mechanical differential. The motor is PMSM with a rated power of 7.5 kW and peak power of 11 kW.

Property	Value	Unit
Curb weight	≈ 650	kg
Motor rated power	7.5	kW
Motor nominal power	11	kW
Battery type	$LiFePO_4$	-
Battery nominal voltage	72	V
Battery capacity	10.3	kWh

Table 4.5: Summary of hardware and power consumptions

The first step in this assessment has regarded the creation of the vehicle model. Figure 4.16 reports the workflow defined to be followed. The vehicle model has been created based on a commercial software suite, starting from OEM datasheet and measurement made on the vehicle. However, those data are a good starting point but not sufficient for the model tuning and validation. For this reason a proper experimental campaign has been designed and currently undergoing to gather data useful to improve the model accurac

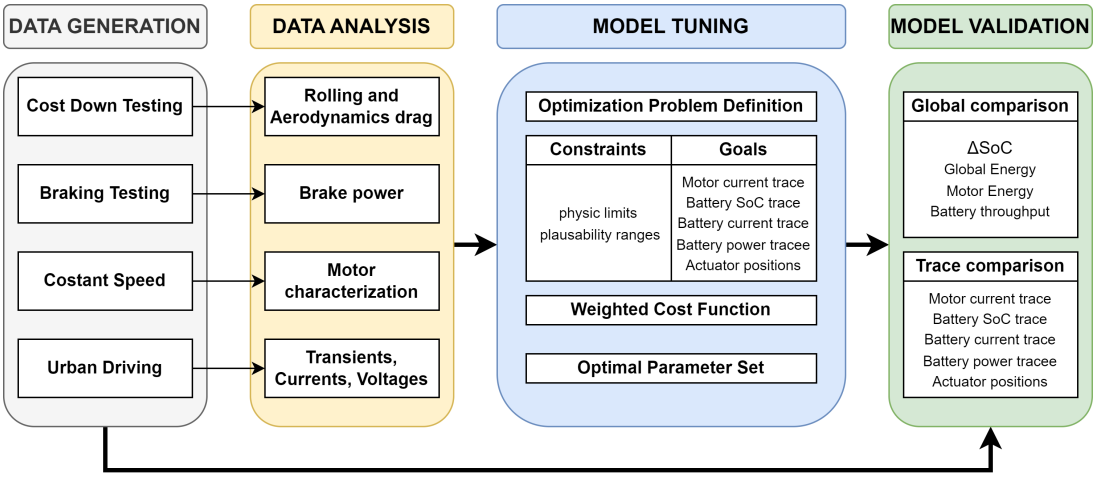

Figure 4.16: Workflow for numerical model tuning

To cope this goal the vehicle has been equipped with a Vector CANcase to get access, reading and storing, to all the data flowing through the vehicle CAN network. Those data regards vehicle speeds, voltage and currents of battery, converters and motor, various temperatures, inserted gear and many other information. The acquisition rate of the various messages is depending by its criticality and varies from 1 to 100 Hz, with most signals of interest at 50 Hz.

The definition of a proper test sequence allows to get the vehicle behavior in transient and quasi-stationary conditions. Many test have been recorded to correctly characterize the vehicle including, coast-down, steady speed, braking and urban driving tests. Figure 4.17 reports as example some acquired driving cycle, acquired to characterize the unknown vehicle parameters.

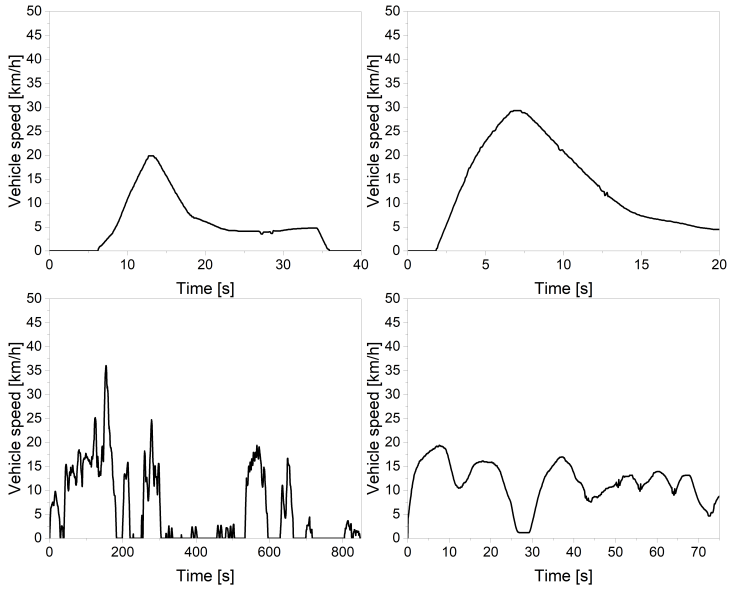

Figure 4.17: Examples of experimentally acquired driving cycles

The model has been tuned with the data available which will be further updated in the future. Besides the model creation, the data regarding the autonomous platform in developing have been gathered. The data are relative to the chosen sensor and hardware platform, technical datasheet of the manufacturers and experimental power measurement on a laboratory. Table 4.6 define all the hardware used for the autonomous system with their consumption. It can be noticed that about two thirds of the electrical power requirements is for the computing platform.

From measurements a statistical distribution of the total hardware power consumption have been estimated and represented in figure 4.18. The distribution is represented by a Normal with mean $\mu = 596$ W and standard deviation $\sigma = 27.6$ W. It is interesting to compare the found distribution of this specific case study with the one estimated in the previous section by literature data. The comparison in shown in figure 4.19. The peak of the case study are well aligned with the peak of the literature distributions. The comparatively low spreed is a consequence of the well defined hardware. This can be taken also as a suggestion that the previous results are well estimated.

Group	Component	Number	Consumption [W]	Description
Computing	CPU	1	100-225	Intel i7-10700k
	GPU	1	180-220	Nvidia RTX 3070
	SBC	1	50	Jetson AGX
	Other	1	100	PSU, RAM, Inverter, Storage, Motherboard
Control	ECU	3	5-10	Custom ECUs
Sensor	Camera	4	15	FHD GMSL2
	Lidar	1	28	Solid state
		2	12	Rotating
	IMU	1	2	
	Ultrasonic	10	0.2	

Table 4.6: Summary of hardware and power consumptions

The experimental activities are still going on to further improve the model validation. Next steps will be aimed at developing test scenario and control strategy exploiting DAS data. Then a numerical test matrix will be defined and simulated to address the raised research questions in the next future.

4.7 Main results

A comprehensive analysis and discussion of CAV architectures regarding layout, sensors, and processing has been conducted. The data gathered have been used to assess the net energy consumption of CAV considering both DAS energy saving and hardware power consumption. The main manuscript outcomes are summarised in the following.

- CAV architecture likely requires multiple sensors to achieve fully autonomous operation. A proper combination of different sensors can simplify vehicle operations and improve safety and reliability under different operating conditions.
- Data management is a crucial point. Sensor data storage and processing should be carefully addressed as they strongly influence vehicle performance. In particular, data elaboration and sensor fusion are key pillars to be further developed to achieve fully operational

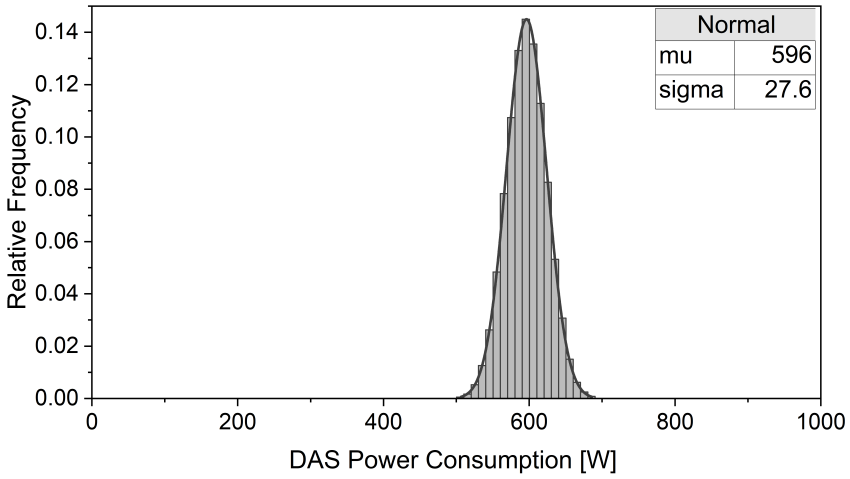

Figure 4.18: Hardware power distribution estimation

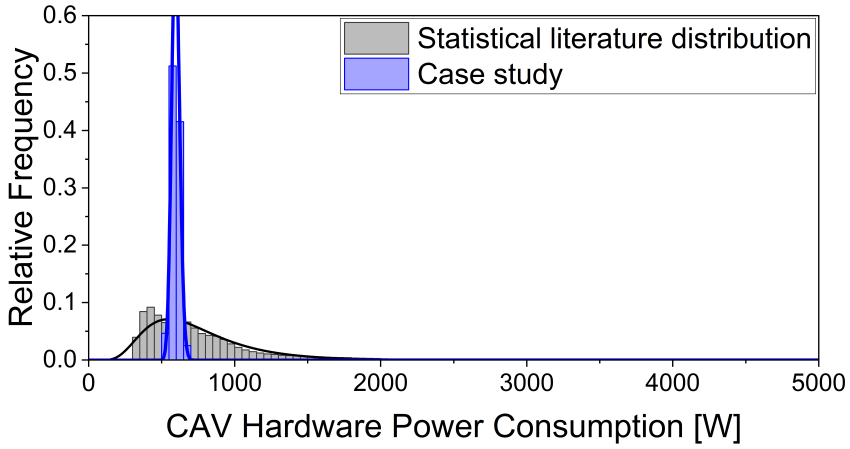

Figure 4.19: Hardware power distribution comparison between this case study and the estimated by literature (see Figure 4.10)

CAVs. The improvement of the algorithms should be adequately supported by the production of more powerful and energy-efficient processing units.

- The energy analysis has shown that in an analogy of Maxwell's demon paradigm, attention should be addressed to the environmental impact of the CAVs. Many studies consider the information considered for free, while in reality they have a not negligible cost from both economic and energetic point of view. In fact, if on one hand, it is possible to leverage data to improve vehicle energy efficiency, on the other hand, producing and elaborating data is energy consuming. Considering both contributions, the hypothetical

advantages are not obvious.

- The Monte Carlo analysis has shown that based on actual data, in about 75% of simulated scenarios, light-duty CAVs consume more energy than EVs. On average, 6% higher energy consumption can be expected by CAVs. Regarding other vehicle classes, the simulation data extrapolation suggests that no or negligible effect could be expected for medium-duty vehicles. Heavy-duty vehicles will probably take advantage of autonomous driving systems due to their higher energy demand, resulting in a lower impact of the DAS system.

- A preliminary assessment aimed at converting a small battery electric city car to an AV have allowed to partially validate the estimated CAV platform consumption distribution estimated in the statistical study.

Bibliography

[1] Mohammadreza Torkjazi and Ali K. Raz. "A Taxonomy for System of Autonomous Systems". In: *2022 17th Annual System of Systems Engineering Conference (SOSE)*. June 2022, pp. 198–203. DOI: 10.1109/SOSE55472.2022.9812673.

[2] Piergiuseppe Mallozzi et al. "Autonomous Vehicles: State of the Art, Future Trends, and Challenges". en. In: *Automotive Systems and Software Engineering: State of the Art and Future Trends*. Ed. by Yanja Dajsuren and Mark van den Brand. Cham: Springer International Publishing, 2019, pp. 347–367. ISBN: 978-3-030-12157-0. DOI: 10.1007/978-3-030-12157-0_16.

[3] Shoaib Azam et al. "System, Design and Experimental Validation of Autonomous Vehicle in an Unconstrained Environment". en. In: *Sensors* 20.21 (Jan. 2020). Number: 21 Publisher: Multidisciplinary Digital Publishing Institute, p. 5999. ISSN: 1424-8220. DOI: 10.3390/s20215999.

[4] David González et al. "A Review of Motion Planning Techniques for Automated Vehicles". In: *IEEE Transactions on Intelligent Transportation Systems* 17.4 (Apr. 2016). Conference Name: IEEE Transactions on Intelligent Transportation Systems, pp. 1135–1145. ISSN: 1558-0016. DOI: 10.1109/TITS.2015.2498841.

[5] Sanghoon Lee et al. "Design of V2X-based vehicular contents centric networks for autonomous driving". In: *IEEE Transactions on Intelligent Transportation Systems* 23.8 (2021). Publisher: IEEE, pp. 13526–13537.

[6] Pablo Marin-Plaza et al. "Global and Local Path Planning Study in a ROS-Based Research Platform for Autonomous Vehicles". en. In: *Journal of Advanced Transportation*

2018 (Feb. 2018). Publisher: Hindawi, e6392697. ISSN: 0197-6729. DOI: 10.1155/2018/6392697.

[7] Xiaohua Song et al. “A Review of the Motion Planning and Control Methods for Automated Vehicles”. en. In: *Sensors* 23.13 (Jan. 2023). Number: 13 Publisher: Multidisciplinary Digital Publishing Institute, p. 6140. ISSN: 1424-8220. DOI: 10.3390/s23136140.

[8] Mial E Warren. “Automotive LIDAR Technology”. In: *2019 Symposium on VLSI Circuits*. ISSN: 2158-5636. June 2019, pp. C254–C255. DOI: 10.23919/VLSIC.2019.8777993.

[9] Andreas Reschka. “Safety Concept for Autonomous Vehicles”. en. In: *Autonomous Driving: Technical, Legal and Social Aspects*. Ed. by Markus Maurer et al. Berlin, Heidelberg: Springer, 2016, pp. 473–496. ISBN: 978-3-662-48847-8. DOI: 10.1007/978-3-662-48847-8_23.

[10] Zhi Yan et al. “EU Long-term Dataset with Multiple Sensors for Autonomous Driving”. In: *2020 IEEE/RSJ International Conference on Intelligent Robots and Systems (IROS)*. ISSN: 2153-0866. Oct. 2020, pp. 10697–10704. DOI: 10.1109/IROS45743.2020.9341406.

[11] Luc van Dijk and Günter Sporer. “Functional safety for automotive ethernet networks”. In: *Journal of Traffic and Transportation Engineering* 6.4 (2018), pp. 176–182.

[12] Marcel Sheeny et al. “RADIATE: A Radar Dataset for Automotive Perception in Bad Weather”. In: *2021 IEEE International Conference on Robotics and Automation (ICRA)*. ISSN: 2577-087X. May 2021, pp. 1–7. DOI: 10.1109/ICRA48506.2021.9562089.

[13] R. H. Rasshofer, M. Spies, and H. Spies. “Influences of weather phenomena on automotive laser radar systems”. English. In: *Advances in Radio Science* 9.B.2 (July 2011). Conference Name: Kleinheubacher Berichte 2010 - Publisher: Copernicus GmbH, pp. 49–60. ISSN: 1684-9965. DOI: 10.5194/ars-9-49-2011.

[14] Juan P. Espineira et al. “Realistic LiDAR With Noise Model for Real-Time Testing of Automated Vehicles in a Virtual Environment”. In: *IEEE Sensors Journal* 21.8 (Apr.

2021). Conference Name: IEEE Sensors Journal, pp. 9919–9926. ISSN: 1558-1748. DOI: 10.1109/JSEN.2021.3059310.

[15] Jian Zhao et al. “Method and Applications of Lidar Modeling for Virtual Testing of Intelligent Vehicles”. In: *IEEE Transactions on Intelligent Transportation Systems* 22.5 (May 2021). Conference Name: IEEE Transactions on Intelligent Transportation Systems, pp. 2990–3000. ISSN: 1558-0016. DOI: 10.1109/TITS.2020.2978438.

[16] Fabio Reway, Werner Huber, and Eduardo Parente Ribeiro. “Test Methodology for Vision-Based ADAS Algorithms with an Automotive Camera-in-the-Loop”. In: *2018 IEEE International Conference on Vehicular Electronics and Safety (ICVES)*. Sept. 2018, pp. 1–7. DOI: 10.1109/ICVES.2018.8519598.

[17] Imen Jegham and Anouar Ben Khalifa. “Pedestrian detection in poor weather conditions using moving camera”. In: *2017 IEEE/ACS 14th International Conference on Computer Systems and Applications (AICCSA)*. ISSN: 2161-5330. Oct. 2017, pp. 358–362. DOI: 10.1109/AICCSA.2017.35.

[18] Md. Imtiyaz Anwar and Arun Khosla. “Vision enhancement through single image fog removal”. In: *Engineering Science and Technology, an International Journal* 20.3 (June 2017), pp. 1075–1083. ISSN: 2215-0986. DOI: 10.1016/j.jestch.2016.11.015.

[19] Xianglin Meng et al. “YOLOv5s-Fog: An Improved Model Based on YOLOv5s for Object Detection in Foggy Weather Scenarios”. en. In: *Sensors* 23.11 (Jan. 2023). Number: 11 Publisher: Multidisciplinary Digital Publishing Institute, p. 5321. ISSN: 1424-8220. DOI: 10.3390/s23115321.

[20] Mario Bijelic, Tobias Gruber, and Werner Ritter. “A Benchmark for Lidar Sensors in Fog: Is Detection Breaking Down?” In: *2018 IEEE Intelligent Vehicles Symposium (IV)*. ISSN: 1931-0587. June 2018, pp. 760–767. DOI: 10.1109/IVS.2018.8500543.

[21] M. Kutila et al. “Automotive LiDAR performance verification in fog and rain”. In: *2018 21st International Conference on Intelligent Transportation Systems (ITSC)*. ISSN: 2153-0017. Nov. 2018, pp. 1695–1701. DOI: 10.1109/ITSC.2018.8569624.

[22] Vishwanath A. Sindagi, Yin Zhou, and Oncel Tuzel. “MVX-Net: Multimodal VoxelNet for 3D Object Detection”. In: *2019 International Conference on Robotics and Automation (ICRA)*. ISSN: 2577-087X. May 2019, pp. 7276–7282. DOI: 10.1109/ICRA.2019.8794195.

[23] Alebel Arage et al. “Effects of water and ice layer on automotive radar”. In: *Proc. of the German Microwave Conf.* Citeseer, 2006.

[24] Jorge Vargas et al. “An Overview of Autonomous Vehicles Sensors and Their Vulnerability to Weather Conditions”. en. In: *Sensors* 21.16 (Jan. 2021). Number: 16 Publisher: Multidisciplinary Digital Publishing Institute, p. 5397. ISSN: 1424-8220. DOI: 10.3390/s21165397.

[25] Thomas Herpel et al. “Trade-off between coverage and robustness of automotive environment sensor systems”. In: *2008 International Conference on Intelligent Sensors, Sensor Networks and Information Processing*. Dec. 2008, pp. 551–556. DOI: 10.1109/ISSNIP.2008.4762047.

[26] Zongwei Liu et al. “An Overview of the Latest Progress and Core Challenge of Autonomous Vehicle Technologies”. en. In: *MATEC Web of Conferences* 308 (2020). Publisher: EDP Sciences, p. 06002. ISSN: 2261-236X. DOI: 10.1051/matecconf/202030806002.

[27] Trong Hop Do and Myungsik Yoo. “Visible light communication based vehicle positioning using LED street light and rolling shutter CMOS sensors”. In: *Optics Communications* 407 (Jan. 2018), pp. 112–126. ISSN: 0030-4018. DOI: 10.1016/j.optcom.2017.09.022.

[28] Radu Horaud et al. “An overview of depth cameras and range scanners based on time-of-flight technologies”. en. In: *Machine Vision and Applications* 27.7 (Oct. 2016), pp. 1005–1020. ISSN: 1432-1769. DOI: 10.1007/s00138-016-0784-4.

[29] Felix Endres et al. “3-D Mapping With an RGB-D Camera”. In: *IEEE Transactions on Robotics* 30.1 (Feb. 2014). Conference Name: IEEE Transactions on Robotics, pp. 177–187. ISSN: 1941-0468. DOI: 10.1109/TRO.2013.2279412.

[30] Sayanan Sivaraman and Mohan Manubhai Trivedi. “Looking at Vehicles on the Road: A Survey of Vision-Based Vehicle Detection, Tracking, and Behavior Analysis”. In: *IEEE Transactions on Intelligent Transportation Systems* 14.4 (Dec. 2013). Conference Name: IEEE Transactions on Intelligent Transportation Systems, pp. 1773–1795. ISSN: 1558-0016. DOI: 10.1109/TITS.2013.2266661.

[31] J. Stallkamp et al. “Man vs. computer: Benchmarking machine learning algorithms for traffic sign recognition”. In: *Neural Networks*. Selected Papers from IJCNN 2011 32 (Aug. 2012), pp. 323–332. ISSN: 0893-6080. DOI: 10.1016/j.neunet.2012.02.016.

[32] Juraj Ciberlin et al. “Object detection and object tracking in front of the vehicle using front view camera”. In: *2019 Zooming Innovation in Consumer Technologies Conference (ZINC)*. May 2019, pp. 27–32. DOI: 10.1109/ZINC.2019.8769367.

[33] Marius Drulea et al. “Omnidirectional stereo vision using fisheye lenses”. In: *2014 IEEE 10th International Conference on Intelligent Computer Communication and Processing (ICCP)*. Sept. 2014, pp. 251–258. DOI: 10.1109/ICCP.2014.6937005.

[34] Horatiu Florea et al. “Enhanced Perception for Autonomous Driving Using Semantic and Geometric Data Fusion”. en. In: *Sensors* 22.13 (Jan. 2022). Number: 13 Publisher: Multidisciplinary Digital Publishing Institute, p. 5061. ISSN: 1424-8220. DOI: 10.3390/s22135061.

[35] Henry Alexander Ignatious, Hesham-El- Sayed, and Manzoor Khan. “An overview of sensors in Autonomous Vehicles”. In: *Procedia Computer Science*. 12th International Conference on Emerging Ubiquitous Systems and Pervasive Networks / 11th International Conference on Current and Future Trends of Information and Communication Technologies in Healthcare 198 (Jan. 2022), pp. 736–741. ISSN: 1877-0509. DOI: 10.1016/j.procs.2021.12.315.

[36] You Li and Javier Ibanez-Guzman. “Lidar for Autonomous Driving: The Principles, Challenges, and Trends for Automotive Lidar and Perception Systems”. In: *IEEE Signal Processing Magazine* 37.4 (July 2020). Conference Name: IEEE Signal Processing Magazine, pp. 50–61. ISSN: 1558-0792. DOI: 10.1109/MSP.2020.2973615.

[37] Thinal Raj et al. “A Survey on LiDAR Scanning Mechanisms”. en. In: *Electronics* 9.5 (May 2020). Number: 5 Publisher: Multidisciplinary Digital Publishing Institute, p. 741. ISSN: 2079-9292. DOI: 10.3390/electronics9050741.

[38] Fumin Zhang, Lingping Yi, and Xinghua Qu. “Simultaneous measurements of velocity and distance via a dual-path FMCW lidar system”. en. In: *Optics Communications* 474 (Nov. 2020), p. 126066. ISSN: 0030-4018. DOI: 10.1016/j.optcom.2020.126066.

[39] Stefan Muckenhuber, Hannes Holzer, and Zrinka Bockaj. “Automotive Lidar Modelling Approach Based on Material Properties and Lidar Capabilities”. en. In: *Sensors* 20.11 (Jan. 2020). Number: 11 Publisher: Multidisciplinary Digital Publishing Institute, p. 3309. ISSN: 1424-8220. DOI: 10.3390/s20113309.

[40] Gunzung Kim, Jeongsook Eom, and Yongwan Park. “Investigation on the occurrence of mutual interference between pulsed terrestrial LIDAR scanners”. In: *2015 IEEE Intelligent Vehicles Symposium (IV)*. ISSN: 1931-0587. June 2015, pp. 437–442. DOI: 10.1109/IVS.2015.7225724.

[41] Il-Pyeong Hwang, Seok-jun Yun, and Chang-Hee Lee. “Study on the Frequency-Modulated Continuous-Wave LiDAR Mutual Interference”. In: *2019 IEEE 19th International Conference on Communication Technology (ICCT)*. ISSN: 2576-7828. Oct. 2019, pp. 1053–1056. DOI: 10.1109/ICCT46805.2019.8947067.

[42] Thomas Fersch, Robert Weigel, and Alexander Koelpin. “A CDMA Modulation Technique for Automotive Time-of-Flight LiDAR Systems”. In: *IEEE Sensors Journal* 17.11 (June 2017). Conference Name: IEEE Sensors Journal, pp. 3507–3516. ISSN: 1558-1748. DOI: 10.1109/JSEN.2017.2688126.

[43] Il-Pyeong Hwang and Chang-Hee Lee. “Mutual Interferences of a True-Random LiDAR With Other LiDAR Signals”. In: *IEEE Access* 8 (2020). Conference Name: IEEE Access, pp. 124123–124133. ISSN: 2169-3536. DOI: 10.1109/ACCESS.2020.3004891.

[44] Wenye Yin et al. “Approach for LIDAR signals with multiple returns”. EN. In: *Applied Optics* 53.30 (Oct. 2014). Publisher: Optica Publishing Group, pp. 6963–6969. ISSN: 2155-3165. DOI: 10.1364/AO.53.006963.

[45] Andreas Aßmann, Brian Stewart, and Andrew M. Wallace. "Deep Learning for LiDAR Waveforms with Multiple Returns". In: *2020 28th European Signal Processing Conference (EUSIPCO)*. ISSN: 2076-1465. Jan. 2021, pp. 1571–1575. DOI: 10.23919/Eusipco47968.2020.9287545.

[46] Robin Heinzler et al. "Weather Influence and Classification with Automotive Lidar Sensors". In: *2019 IEEE Intelligent Vehicles Symposium (IV)*. ISSN: 2642-7214. June 2019, pp. 1527–1534. DOI: 10.1109/IVS.2019.8814205.

[47] Jeff Hecht. "Lidar for Self-Driving Cars". In: *Opt. Photon. News* 29.1 (Jan. 2018). Publisher: Optica Publishing Group, pp. 26–33. DOI: 10.1364/OPN.29.1.000026.

[48] Paul F. McManamon et al. "Comparison of flash lidar detector options". In: *Optical Engineering* 56.3 (Mar. 2017). Publisher: SPIE, p. 031223. ISSN: 0091-3286, 1560-2303. DOI: 10.1117/1.OE.56.3.031223.

[49] Nanxi Li et al. "A Progress Review on Solid-State LiDAR and Nanophotonics-Based LiDAR Sensors". en. In: *Laser & Photonics Reviews* 16.11 (2022), p. 2100511. ISSN: 1863-8899. DOI: 10.1002/lpor.202100511.

[50] Christian Waldschmidt, Juergen Hasch, and Wolfgang Menzel. "Automotive Radar — From First Efforts to Future Systems". In: *IEEE Journal of Microwaves* 1.1 (Jan. 2021). Conference Name: IEEE Journal of Microwaves, pp. 135–148. ISSN: 2692-8388. DOI: 10.1109/JMW.2020.3033616.

[51] F. Norouzian et al. "Next Generation, Low-THz Automotive Radar – the potential for frequencies above 100 GHz". In: *2019 20th International Radar Symposium (IRS)*. ISSN: 2155-5753. June 2019, pp. 1–7. DOI: 10.23919/IRS.2019.8767461.

[52] M. Martínez-Vázquez. "Overview of design challenges for automotive radar MMICs". In: *2021 IEEE International Electron Devices Meeting (IEDM)*. ISSN: 2156-017X. Dec. 2021, pp. 4.1.1–4.1.3. DOI: 10.1109/IEDM19574.2021.9720688.

[53] Shinichi Yamano et al. "76GHz millimeter wave automobile radar using single chip MMIC". In: *Fujitsu Ten Technical Journal* 23 (2004).

[54] Philipp Ritter. “Toward a fully integrated automotive radar system-on-chip in 22 nm FD-SOI CMOS”. en. In: *International Journal of Microwave and Wireless Technologies* 13.6 (July 2021). Publisher: Cambridge University Press, pp. 523–531. ISSN: 1759-0787, 1759-0795. DOI: 10.1017/S1759078721000088.

[55] Ao Zhang, Farzan Erlik Nowruzi, and Robert Laganiere. “RADDet: Range-Azimuth-Doppler based Radar Object Detection for Dynamic Road Users”. English. In: IEEE Computer Society, May 2021, pp. 95–102. ISBN: 978-1-66541-413-5. DOI: 10.1109/CRV52889.2021.00021.

[56] Ziqiang Tong, Ralf Renter, and Masahiko Fujimoto. “Fast chirp FMCW radar in automotive applications”. In: *IET International Radar Conference 2015*. Oct. 2015, pp. 1–4. DOI: 10.1049/cp.2015.1362.

[57] Igal Bilik et al. “Automotive MIMO radar for urban environments”. In: *2016 IEEE Radar Conference (RadarConf)*. ISSN: 2375-5318. May 2016, pp. 1–6. DOI: 10.1109/RADAR.2016.7485215.

[58] Yoke Leen Sit et al. “2D radar imaging with velocity estimation using a MIMO OFDM-based radar for automotive applications”. In: *2013 European Radar Conference*. Oct. 2013, pp. 145–148.

[59] Claudia Vasanelli, Rahul Batra, and Christian Waldschmidt. “Optimization of a MIMO radar antenna system for automotive applications”. In: *2017 11th European Conference on Antennas and Propagation (EUCAP)*. Mar. 2017, pp. 1113–1117. DOI: 10.23919/EuCAP.2017.7928056.

[60] Martin Stolz et al. “A New Antenna Array and Signal Processing Concept for an Automotive 4D Radar”. In: *2018 15th European Radar Conference (EuRAD)*. Sept. 2018, pp. 63–66. DOI: 10.23919/EuRAD.2018.8546603.

[61] Shunqiao Sun and Yimin D. Zhang. “4D Automotive Radar Sensing for Autonomous Vehicles: A Sparsity-Oriented Approach”. In: *IEEE Journal of Selected Topics in Signal Processing* 15.4 (June 2021). Conference Name: IEEE Journal of Selected Topics in Signal Processing, pp. 879–891. ISSN: 1941-0484. DOI: 10.1109/JSTSP.2021.3079626.

[62] Gor Hakobyan and Bin Yang. “High-Performance Automotive Radar: A Review of Signal Processing Algorithms and Modulation Schemes”. In: *IEEE Signal Processing Magazine* 36.5 (Sept. 2019), pp. 32–44. ISSN: 1558-0792. DOI: 10.1109/MSP.2019.2911722.

[63] Priya Hosur, Rajashekar. Basavaraj Shettar, and Milind Potdar. “Environmental awareness around vehicle using ultrasonic sensors”. In: *2016 International Conference on Advances in Computing, Communications and Informatics (ICACCI)*. Sept. 2016, pp. 1154–1159. DOI: 10.1109/ICACCI.2016.7732200.

[64] R. H. Rasshofer and K. Gresser. “Automotive Radar and Lidar Systems for Next Generation Driver Assistance Functions”. English. In: *Advances in Radio Science* 3.B.4 (May 2005). Conference Name: Kleinheubacher Berichte 2004 - Publisher: Copernicus GmbH, pp. 205–209. ISSN: 1684-9965. DOI: 10.5194/ars-3-205-2005.

[65] Aravind B. Balasubramanian et al. “Transmitter and Receiver Enhancements for Ultrasonic Distance Sensing Systems”. In: *IEEE Sensors Journal* 22.11 (2022), pp. 10692–10698. DOI: 10.1109/JSEN.2022.3167008.

[66] Jihas Khan. “Using ADAS sensors in implementation of novel automotive features for increased safety and guidance”. In: *2016 3rd International Conference on Signal Processing and Integrated Networks (SPIN)*. IEEE, 2016, pp. 753–758. DOI: 10.1109/SPIN.2016.7566798.

[67] F. Tong, S. K. Tso, and T. Z. Xu. “A high precision ultrasonic docking system used for automatic guided vehicle”. In: *Sensors and Actuators A: Physical* 118.2 (Feb. 2005), pp. 183–189. ISSN: 0924-4247. DOI: 10.1016/j.sna.2004.06.026.

[68] Claudio Canali et al. “A temperature compensated ultrasonic sensor operating in air for distance and proximity measurements”. In: *IEEE Transactions on Industrial electronics* 4 (1982). Publisher: IEEE, pp. 336–341.

[69] Wenyuan Xu et al. “Analyzing and Enhancing the Security of Ultrasonic Sensors for Autonomous Vehicles”. In: *IEEE Internet of Things Journal* 5.6 (Dec. 2018), pp. 5015–5029. ISSN: 2327-4662. DOI: 10.1109/JIOT.2018.2867917.

[70] Mubina Toa and Akeem Whitehead. “Ultrasonic sensing basics”. In: *Dallas: Texas Instruments* (2020), pp. 53–75.

[71] Shengbo Eben Li et al. “Kalman filter-based tracking of moving objects using linear ultrasonic sensor array for road vehicles”. In: *Mechanical Systems and Signal Processing* 98 (Jan. 2018), pp. 173–189. ISSN: 0888-3270. DOI: 10.1016/j.ymssp.2017.04.041.

[72] Kenji Imou et al. “Ultrasonic Doppler Speed Sensor for Agricultural Vehicles: Effects of Pitch Angle and Measurements of Velocity Vector Components”. en. In: *Agricultural Engineering International: CIGR Journal* (2008). ISSN: 1682-1130.

[73] Tomer Gluck et al. “Spoofing Attack on Ultrasonic Distance Sensors Using a Continuous Signal”. en. In: *Sensors* 20.21 (Jan. 2020). Number: 21 Publisher: Multidisciplinary Digital Publishing Institute, p. 6157. ISSN: 1424-8220. DOI: 10.3390/s20216157.

[74] Jianzhi Lou et al. “SoundFence: Securing Ultrasonic Sensors in Vehicles Using Physical-Layer Defense”. In: *2021 18th Annual IEEE International Conference on Sensing, Communication, and Networking (SECON)*. ISSN: 2155-5494. July 2021, pp. 1–9. DOI: 10.1109/SECON52354.2021.9491590.

[75] Niels Joubert, Tyler G. R. Reid, and Fergus Noble. “Developments in Modern GNSS and Its Impact on Autonomous Vehicle Architectures”. In: *2020 IEEE Intelligent Vehicles Symposium (IV)*. ISSN: 2642-7214. Oct. 2020, pp. 2029–2036. DOI: 10.1109/IV47402.2020.9304840.

[76] Padma Bolla and Kai Borre. “Performance analysis of dual-frequency receiver using combinations of GPS L1, L5, and L2 civil signals”. en. In: *Journal of Geodesy* 93.3 (Mar. 2019), pp. 437–447. ISSN: 1432-1394. DOI: 10.1007/s00190-018-1172-9.

[77] Zhuo Zhi, Datong Liu, and Liansheng Liu. “A performance compensation method for GPS/INS integrated navigation system based on CNN–LSTM during GPS outages”. In: *Measurement* 188 (Jan. 2022), p. 110516. ISSN: 0263-2241. DOI: 10.1016/j.measurement.2021.110516.

[78] Lu Xiong et al. “IMU-Based Automated Vehicle Body Sideslip Angle and Attitude Estimation Aided by GNSS Using Parallel Adaptive Kalman Filters”. In: *IEEE Transactions on Vehicular Technology* 69.10 (Oct. 2020). Conference Name: IEEE Transactions on

Vehicular Technology, pp. 10668–10680. ISSN: 1939-9359. DOI: 10.1109/TVT.2020.2983738.

[79] Wanli Liu et al. "Design a Novel Target to Improve Positioning Accuracy of Autonomous Vehicular Navigation System in GPS Denied Environments". In: *IEEE Transactions on Industrial Informatics* 17.11 (Nov. 2021). Conference Name: IEEE Transactions on Industrial Informatics, pp. 7575–7588. ISSN: 1941-0050. DOI: 10.1109/TII.2021.3052529.

[80] Liang Chen et al. "GNSS High-Precision Augmentation for Autonomous Vehicles: Requirements, Solution, and Technical Challenges". en. In: *Remote Sensing* 15.6 (Jan. 2023). Number: 6 Publisher: Multidisciplinary Digital Publishing Institute, p. 1623. ISSN: 2072-4292. DOI: 10.3390/rs15061623.

[81] Yifang Ma et al. "Artificial intelligence applications in the development of autonomous vehicles: a survey". In: *IEEE/CAA Journal of Automatica Sinica* 7.2 (Mar. 2020). Conference Name: IEEE/CAA Journal of Automatica Sinica, pp. 315–329. ISSN: 2329-9274. DOI: 10.1109/JAS.2020.1003021.

[82] Johannes Pillmann et al. "Novel common vehicle information model (CVIM) for future automotive vehicle big data marketplaces". In: *2017 IEEE Intelligent Vehicles Symposium (IV)*. June 2017, pp. 1910–1915. DOI: 10.1109/IVS.2017.7995984.

[83] Qi Chen. "Airborne lidar data processing and information extraction". In: *Photogrammetric engineering and remote sensing* 73.2 (2007). Publisher: ASPRS AMERICAN SOCIETY FOR PHOTOGRAMMETRY AND, p. 109.

[84] Martin Isenburg. "LASzip: lossless compression of LiDAR data". In: *Photogrammetric engineering and remote sensing* 79.2 (2013). Publisher: American Society of Photogrammetry, pp. 209–217.

[85] Juan A. Béjar-Martos et al. "Strategies for the Storage of Large LiDAR Datasets—A Performance Comparison". en. In: *Remote Sensing* 14.11 (Jan. 2022). Number: 11 Publisher: Multidisciplinary Digital Publishing Institute, p. 2623. ISSN: 2072-4292. DOI: 10.3390/rs14112623.

[86] Anton Biasizzo and Franc Novak. “Hardware Accelerated Compression of LIDAR Data Using FPGA Devices”. en. In: *Sensors* 13.5 (May 2013). Number: 5 Publisher: Multidisciplinary Digital Publishing Institute, pp. 6405–6422. ISSN: 1424-8220. DOI: 10.3390/s130506405.

[87] Helge Zinner. “Automotive Ethernet and SerDes in Competition”. In: *ATZelectronics worldwide* 15.7 (2020). Publisher: Springer, pp. 40–43.

[88] Abdelmoghit Zaarane et al. “Distance measurement system for autonomous vehicles using stereo camera”. In: *Array* 5 (Mar. 2020), p. 100016. ISSN: 2590-0056. DOI: 10.1016/j.array.2020.100016.

[89] Armin Masoumian et al. “Monocular Depth Estimation Using Deep Learning: A Review”. en. In: *Sensors* 22.14 (Jan. 2022). Number: 14 Publisher: Multidisciplinary Digital Publishing Institute, p. 5353. ISSN: 1424-8220. DOI: 10.3390/s22145353.

[90] Weiping Wu, Lei Zhang, and Yan Wang. “A PVT-Robust Analog Baseband With DC Offset Cancellation for FMCW Automotive Radar”. In: *IEEE Access* 7 (2019). Conference Name: IEEE Access, pp. 43249–43257. ISSN: 2169-3536. DOI: 10.1109/ACCESS.2019.2908218.

[91] Hongsheng He, Yan Li, and Jindong Tan. “Rotational Coordinate Transformation for Visual-Inertial Sensor Fusion”. In: *Social Robotics*. Ed. by Arvin Agah et al. Cham: Springer International Publishing, 2016, pp. 431–440. ISBN: 978-3-319-47437-3.

[92] Jingwei Cao et al. “Lane Detection Algorithm for Intelligent Vehicles in Complex Road Conditions and Dynamic Environments”. en. In: *Sensors* 19.14 (Jan. 2019). Number: 14 Publisher: Multidisciplinary Digital Publishing Institute, p. 3166. ISSN: 1424-8220. DOI: 10.3390/s19143166.

[93] Amit Saxena et al. “A review of clustering techniques and developments”. In: *Neurocomputing* 267 (Dec. 2017), pp. 664–681. ISSN: 0925-2312. DOI: 10.1016/j.neucom.2017.06.053.

[94] Jorge Beltrán et al. “BirdNet: A 3D Object Detection Framework from LiDAR Information”. In: *2018 21st International Conference on Intelligent Transportation Systems*

(ITSC). ISSN: 2153-0017. Nov. 2018, pp. 3517–3523. DOI: 10.1109/ITSC.2018.8569311.

[95] Xiaomeng Cao et al. "Extended Object Tracking Using Automotive Radar". In: *2018 21st International Conference on Information Fusion (FUSION)*. July 2018, pp. 1–5. DOI: 10.23919/ICIF.2018.8455293.

[96] Mehdi Masmoudi et al. "Object Detection Learning Techniques for Autonomous Vehicle Applications". In: *2019 IEEE International Conference on Vehicular Electronics and Safety (ICVES)*. ISSN: 2643-9751. Sept. 2019, pp. 1–5. DOI: 10.1109/ICVES.2019.8906437.

[97] Babak Shahian Jahromi, Theja Tulabandhula, and Sabri Cetin. "Real-Time Hybrid Multi-Sensor Fusion Framework for Perception in Autonomous Vehicles". en. In: *Sensors* 19.20 (Jan. 2019). Number: 20 Publisher: Multidisciplinary Digital Publishing Institute, p. 4357. ISSN: 1424-8220. DOI: 10.3390/s19204357.

[98] Shengshun Duan, Qiongfeng Shi, and Jun Wu. "Multimodal Sensors and ML-Based Data Fusion for Advanced Robots". en. In: *Advanced Intelligent Systems* 4.12 (2022). _eprint: https://onlinelibrary.wiley.com/doi/pdf/10.1002/aisy.202200213, p. 2200213. ISSN: 2640-4567. DOI: 10.1002/aisy.202200213.

[99] Li Wang et al. "Multi-Modal and Multi-Scale Fusion 3D Object Detection of 4D Radar and LiDAR for Autonomous Driving". In: *IEEE Transactions on Vehicular Technology* 72.5 (May 2023). Conference Name: IEEE Transactions on Vehicular Technology, pp. 5628–5641. ISSN: 1939-9359. DOI: 10.1109/TVT.2022.3230265.

[100] Mario Bijelic et al. "Seeing Through Fog Without Seeing Fog: Deep Multimodal Sensor Fusion in Unseen Adverse Weather". In: 2020, pp. 11682–11692.

[101] Jelena Kocić, Nenad Jovičić, and Vujo Drndarević. "Sensors and Sensor Fusion in Autonomous Vehicles". In: *2018 26th Telecommunications Forum (TELFOR)*. Nov. 2018, pp. 420–425. DOI: 10.1109/TELFOR.2018.8612054.

[102] Xin Xia et al. "An automated driving systems data acquisition and analytics platform". In: *Transportation Research Part C: Emerging Technologies* 151 (June 2023), p. 104120. ISSN: 0968-090X. DOI: 10.1016/j.trc.2023.104120.

[103] Shaoshan Liu et al. “Computer Architectures for Autonomous Driving”. In: *Computer* 50.8 (2017). Conference Name: Computer, pp. 18–25. ISSN: 1558-0814. DOI: 10.1109/MC.2017.3001256.

[104] David Castells-Rufas et al. “A Survey of FPGA-Based Vision Systems for Autonomous Cars”. In: *IEEE Access* 10 (2022). Conference Name: IEEE Access, pp. 132525–132563. ISSN: 2169-3536. DOI: 10.1109/ACCESS.2022.3230282.

[105] Seyed Amin Sajadi-Alamdari, Holger Voos, and Mohamed Darouach. “Ecological Advanced Driver Assistance System for Optimal Energy Management in Electric Vehicles”. In: *IEEE Intelligent Transportation Systems Magazine* 12.4 (2020). Conference Name: IEEE Intelligent Transportation Systems Magazine, pp. 92–109. ISSN: 1941-1197. DOI: 10.1109/MITS.2018.2880261.

[106] James Fleming and William J.B. Midgley. “Energy-efficient automated driving: effect of a naturalistic eco-ACC on a following vehicle”. In: *2023 IEEE International Conference on Mechatronics (ICM)*. Mar. 2023, pp. 1–6. DOI: 10.1109/ICM54990.2023.10102074.

[107] Rolando Bautista-Montesano et al. “Longitudinal Control Strategy for Connected Electric Vehicle with Regenerative Braking in Eco-Approach and Departure”. en. In: *Applied Sciences* 13.8 (Jan. 2023). Number: 8 Publisher: Multidisciplinary Digital Publishing Institute, p. 5089. ISSN: 2076-3417. DOI: 10.3390/app13085089.

[108] Amine Taoudi et al. “Design and Optimization of a Mild Hybrid Electric Vehicle with Energy-Efficient Longitudinal Control”. en. In: *SAE International Journal of Electrified Vehicles* 10.1 (Feb. 2021), pp. 55–78. ISSN: 2691-3755. DOI: 10.4271/14-10-01-0005.

[109] T. Eichenlaub and S. Rinderknecht. “Anticipatory Longitudinal Vehicle Control using a LSTM Prediction Model”. In: *2021 IEEE International Intelligent Transportation Systems Conference (ITSC)*. Sept. 2021, pp. 447–452. DOI: 10.1109/ITSC48978.2021.9564787.

[110] Qiu Jin et al. “Power-Based Optimal Longitudinal Control for a Connected Eco-Driving System”. In: *IEEE Transactions on Intelligent Transportation Systems* 17.10 (2016), pp. 2900–2910. DOI: 10.1109/TITS.2016.2535439.

[111] Yuhan Huang et al. “Eco-driving technology for sustainable road transport: A review”. In: *Renewable and Sustainable Energy Reviews* 93 (Oct. 2018), pp. 596–609. ISSN: 1364-0321. DOI: 10.1016/j.rser.2018.05.030.

[112] Ying Zhang et al. “Energy Optimal Control of Motor Drive System for Extending Ranges of Electric Vehicles”. In: *IEEE Transactions on Industrial Electronics* 68.2 (Feb. 2021). Conference Name: IEEE Transactions on Industrial Electronics, pp. 1728–1738. ISSN: 1557-9948. DOI: 10.1109/TIE.2019.2947841.

[113] Roman Schmied et al. “Nonlinear MPC for Emission Efficient Cooperative Adaptive Cruise Control”. en. In: *IFAC-PapersOnLine*. 5th IFAC Conference on Nonlinear Model Predictive Control NMPC 2015 48.23 (Jan. 2015), pp. 160–165. ISSN: 2405-8963. DOI: 10.1016/j.ifacol.2015.11.277.

[114] Philipp Themann, Adrian Zlocki, and Lutz Eckstein. “Energy Efficient Control of Vehicle’s Longitudinal Dynamics Using V2X Communication”. en. In: *ATZ worldwide* 116.7 (July 2014), pp. 36–41. ISSN: 2192-9076. DOI: 10.1007/s38311-014-0204-1.

[115] Osman Erman Gungor et al. “One for all: Decentralized optimization of lateral position of autonomous trucks in a platoon to improve roadway infrastructure sustainability”. In: *Transportation Research Part C: Emerging Technologies* 120 (Nov. 2020), p. 102783. ISSN: 0968-090X. DOI: 10.1016/j.trc.2020.102783.

[116] Heikki Liimatainen, Oscar van Vliet, and David Aplyn. “The potential of electric trucks – An international commodity-level analysis”. In: *Applied Energy* 236 (Feb. 2019), pp. 804–814. ISSN: 0306-2619. DOI: 10.1016/j.apenergy.2018.12.017.

Conclusions

This thesis deals with a comprehensive discussion and analysis of the possible paths for the decarbonization of road transport sector. It focuses on fuels, powertrain and vehicle technology providing a technology-neutral picture of possible solutions toward the decarbonization goal. Literature, numerical and experimental studies have been carried out and used to assess the work objectives. A numerical method has been developed to compare various powertrain solutions for different vehicle classes. The developed approach is new since it adopts a physics-based model into a simulation framework, and capable to capture global trends and parameter sensitivities. Additionally, the investigation has been further extended considering, the impact of autonomous technologies on vehicles, proposing the analysis of their effects on vehicle efficiency. The main results are summarized in the following.

- Regulations are setting ever-demanding CO_2 reduction target, which requires efforts from a technology and infrastructure point of view. Regarding road transport sector, institutions have set CO_2 reduction targets of 75% for passenger cars, 70% for vans and 45% for heavy-duty vehicles by 2030. Additionally, new light-duty vehicles should have zero emissions by 2035.

- Renewable fuels can significantly reduce the environmental impact of the transport sector. Alcohols can ensure a WTW GHG reduction of up to 80-90% compared fossil fuels. Main drawbacks are cold start, engine control and stability issues. Blends of gasoline with alcohols are already deployed in many countries. HVO also offers CO_2 emissions reduction in a range of about 60-80%, and it can be used pure in CI engines offering high compatibility with all modern diesel engines. For this reason, it is particularly suited to reduce the carbon footprint. However, both alcohols and HVO are not able to comply with future reg-

ulations for which CO_2 emissions at vehicle level is not allowed. In this regard, hydrogen fuel is a viable solution and compatible for both ICE and FC based vehicles. Academia, industry and government are sustaining the development of hydrogen-ready technologies to enrich the powertrain solution portfolio for achieving the carbon-neutrality goal.

- A wider powertrain portfolio will likely be available in next future to exploit optimally available energy vectors (electricity, hydrogen, etc.) and depending on the vehicle application domain. Hydrogen-based powertrains can play an important role (ICE and FC) However, the H2-ICE technology is not well established yet, and further technological development should be achieved to start a commercial diffusion. H2-FC is a zero-emission solution, but characterized by higher cost and lower durability. On the other hand, electric vehicle are characterized by high efficiency, but the most common solution, PMSM, relies on rare earth materials. Researches are ongoing to further develop and improve efficiencies reducing the use of those materials. Then, electrical energy storage is strictly linked to lithium chemistry. Efforts are being made towards the use of more sustainable and performing materials. As sake of example, solid-state batteries are a future breakthrough, offering ultra-fast charging capability, higher durability and energy density. However, the technology is not available yet. Additionally, vehicle technologies toward a greater connectivity and autonomy are the major trends. They will respond to future requirements of shared mobility scenarios, which further reduce the environmental impact, reducing the number of circulating vehicles and improving road safety.

- A proper methodology was developed to assess comparatively various powertrain options, all complying with future regulations. The analysis are based on data gathered by the extensive literature study and activities conducted in cooperation with industrial partners. The methodology developed also allows defining vehicle parameters and boundary conditions threshold for which a solution performs better than others, as demonstrated by the sensitivity analysis on the most relevant parameters carried out. A parametric numerical model has been developed, allowing to assess various performance indicators such as TCO, GHGs emissions, energy consumption and recharging times. A comprehensive analysis on light, medium and heavy-duty vehicles showed that the optimal solutions in

each application domain strongly depends on vehicle class and mission profile. At state-of-the art technology, the battery electric vehicles are the optimal solution for short-range vehicles, while hydrogen-powered solutions generally perform better for higher-range vehicle applications. A hybrid powertrain with an electric drive and hydrogen-fueled range-extender (internal combustion engine or fuel cell) seems to be an overall promising solution.

- Driving automation systems has extensively studied and investigated numerically. Hardware architecture, data processing and management solutions have been handled with the scope to improve vehicle energy efficiency. Extensive datasets has been generated, containing quantitative and qualitative information in terms sensors, computing units, and power consumption. In terms of architecture for achieve highly reliable vehicle operation the most likely scenario is to adopt a multitude of different sensor systems trough proper sensor fusion and processing techniques. The collected data were elaborated with proper statistical distributions and used as input in a Monte Carlo simulation to estimate Vehicle energy efficiency. Main outcomes are that, autonomous vehicles consumption improvements are not obvious in comparison to conventional human-driven vehicles. In the 75% of cases analyzed the CAV result in a worsening of vehicle energy efficiency. In particular, higher vehicle consumption were detected for light-duty vehicles and of about 5% . On the other hand, HDV can benefit from DAS technology regarding vehicle efficiency due mainly to the higher power demanding powertrain.

Future outlooks

The developed methodology is valid and the result robust but margin of improvements and development are available for the comparative methodology, the analysis of driving automation systems, and the combination of the studies. In particular, regarding the methodology developed and discussed in Chapter 3, the vehicle model will be updated from a backward approach to a forward approach to better account of causality and dynamics. In particular, both approaches can be effective as they offer inverse computational requirements and accuracy characteristics, allowing the use of the best-suited ones based on the particular investigation carried out. The adoption of a forward modelling approach will also allow the development and testing of causal

control strategy and additional subsystem modeling. It would be interesting to include ageing and thermal models for fuel cells and battery packs as they can significantly influence their life expectancy with clear consequences on economic indicators. Additional KPIs will be considered to include novel aspects and expand the boundaries of the proposed holistic approach. Particular relevant will be all the environmental impact indicators such as rare materials requirements and life cycle emissions, as well as looking at life cycle assessment methodologies. Regarding the study of the driving automation system presented in Chapter 4, future works will analyze specific use cases with detailed modelling to confirm the statistical analysis carried out in this thesis. However, it should be highlighted that a comprehensive analysis of the driving automation system can not be carried out accurately without choosing the exact vehicle type configuration and application scenario. For this reason, a single vehicle class and scenario will be selected, with the most promising configuration given by the developed comparative methodology, for further assessment through detailed modelling. Future steps will improve the accuracy of the developed numerical models, limiting the investigation to the most promising powertrain solution relative to their application domain. Those activities will be developed in cooperation with various research partners such as academia and industry to support this activity by providing valuable experimental data for their validation.